Temporally periodic solitons of the parametrically driven, damped nonlinear Schrödinger equation.

Thomas van Heerden

Thesis presented for the degree of Master of Science in the Department of Mathematics and Applied Mathematics, University of Cape Town.

July 26, 2010

Plagiarism declaration

I know the meaning of plagiarism and declare that all of the work in this document, save for that which is properly acknowledged, is my own.

Abstract

The purpose of this thesis is to study the behaviour of temporally periodic solitons of the parametrically driven, damped nonlinear Schrödinger equation. Previous authors have produced an outline of the behaviour using direct numerical simulations. We adopt a different approach, obtaining periodic solutions of this partial differential equation as solutions of a two-dimensional boundary-value problem. To solve the latter we use Newtonian iteration combined with numerical continuation. This approach has the advantage in that it can find both stable and unstable solutions of the equation, not just the attractors. Direct numerical simulation can also only detect a single attractor in the case of bi- or multi-stability, and so any attractor chart produced using direct simulation may be incomplete. Since we can track multiple stable and unstable solutions we will better understand the occurring bifurcations as the damping coefficient, 'y, and driving coefficent, *h,* are changed. In particular we study the periodic solution continued from the Hopf bifurcation of the stationary soliton with $\gamma = 0.35$, $\gamma = 0.20$, $\gamma = 0.10$ and $\gamma \ll 1$ as h is increased past this point of Hopf bifurcation. For large damping (-y = 0.35) the periodic solution loses its stability at a saddle-node bifurcation and is transformed into a three-soliton complex. In the cases of intermediate damping ('y = 0.20 and $\gamma = 0.10$) the solutions undergo a series of period-doubling bifurcations. Finally, for very small damping (2y << **1)** the periodic solution undergoes a secondary Hopf bifurcation to quasi-periodic behaviour.

Acknowledgements

I would like to thank Nora Alexeeva for providing me with code to perform direct simulation of the parametrically driven, damped nonlinear Schrödinger equation. **I** would also like to thank Elena Zemlyanaya for providing me with code for numerical continuation of solutions to the parametrically driven, damped nonlinear Schrödinger equation.

Contents

Chapter 1

Introduction

In 1834 John Scott Russell made his now (in)famous observation of the wave of translation (or soliton) [71]. The importance of his observation was recognised by his peers, but unfortunately could not be immediately reconciled with contemporary theories of fluid dynamics. Nonetheless solitons, along with strange attractors, would eventually underpin a dramatic shift in analysing nonlinear differential equations: these concepts gave mathematicians and physicists in the latter half of the 20th century two completely new approaches to nonlinear systems. Previously our understanding was limited to hyperbolic nonlinear systems, and nonlinear systems whose solutions were only slight perturbations of a solution to a linear system; the second half of the century opened up entirely new areas of study.

The second half of the century also saw dramatic advances in the field of numerical analysis. As computers became faster and cheaper this burgeoning field was revolutionised. Euler's method of solving ODES was supplemented by Runge-Kutta methods; the Gauss-Newton methods of root finding and nonlinear optimisation by the Levenburg-Marquadt and Davidon-Fletcher-Powell algorithms. Previously intractable numerical problems became routine and mathematicians had another set of tools to attack the problems appearing in nonlinear dynamics.

Thus it was only from the 1950's that the importance of Russell's work was truly realised. Solitons appeared in a range of nonlinear systems, including optics [2], fluid dynamics [7, 71], and ferromagnets [43] as well in Josephson junctions [65] and other physical systems. Surprisingly, many of the properties of these solitons had already been established by Russell a hundred years earlier [71]. He knew that solitons were stable and could travel over a great distance without breaking or dispersingt. He knew also that the velocity of the soliton depended on its amplitude, and he had made some key observations about soliton-soliton interactions: he noted that two

+Picuruta Salazar surfed a tidal bore which exhibits some soliton-like properties up the Amazon river for 12.5 kilometers in 2003.

solitons would never combine, instead they passed through each other.

In this thesis we investigate the behaviour and properties of the stationary solitons of the parametrically driven, damped nonlinear Schrödinger equation (PDDNLS) as the driving and damping strength is varied. We rely heavily on the numerical tools alluded to above, and chapters 2 to 4 provide a survey of the theoretical background, historical development and implementation of the tools we use. Chapters 5 and 6 present our results and draw some conclusions. The remainder of this chapter will introduce the PDDNLS and its soliton solutions, then highlight some shortcomings in the current body of literature.

Our introduction to the PDDNLS starts with a brief introduction to the unperturbed nonlinear Schrödinger equation (NLS),

$$i\psi_t + \psi_{xx} + 2|\psi|^2 = 0, \tag{1.1}$$

where we discuss firstly the mathematical developments of the 1970s that made the study of nonlinear equations possible, and secondly the advances in optics that made solitons so important.

We then derive the PDDNLS. The derivation of the unperturbed NLS is well known, and there are many approaches. It can be derived from the small amplitude solutions to the sine-Gordon equation by the perturbation method with multiple time scales [19, 60]. Sulem [75] presents a derivation of the NLS from an arbitrary nonlinear wave equation,

$$L(\partial_t, \nabla)u + G(u) = 0, \tag{1.2}$$

where L is a linear operator and G a nonlinear function of u and its derivatives. A third derivation based on Fourier-mode coupling normally presented in plasma physics can also be found in Sulem [75], or in Zakharov [80]. We will extend the first approach to the NLS, perturbation with multiple time-scales, to the damped, driven sine-Gordon equation to recover the PDDNLS.

The chapter concludes with the introduction of the PDDNLS as a modification to the NLS. We present some common applications of the PDDNLS, and discuss the ongoing research in this area. In particular, we highlight the work of Barashenkov *et al* [4, 8, 9, 10, 11, 13, 83] whose work we extend.

1.1 The nonlinear Schrödinger equation

There are two broad areas we consider in this section. We start with an overview of the mathematical advances in the 1970s that made exact solutions to the NLS possible and discuss the concurrent technical advances in optics that elevated optical solitons to such an important level.

Exact soliton solutions to the NLS equation can be found in a number of ways. The simplest of these is to assume that the solution has the shape-preserving ansatz

$$\psi(x,t) = \Psi(x)e^{i\phi(x,t)}. \tag{1.3}$$

After substitution into (1.1) we can split into real and imaginary parts then recover

$$\psi = \alpha \operatorname{sech}(\alpha x)\, e^{i\frac{\alpha^2 t}{2}}. \tag{1.4}$$

This solution highlights a number of properties of solitons. Most importantly it it spatially localised and neither disperses nor dissipates as time progresses. There are a number of other, more complicated, methods to determine soliton solutions to the NLS that we discuss below.

The most important of these is the inverse scattering transform (IST). The procedure is analogous to the Fourier method for solving linear equations. While the Fourier method transforms the problem from the time to frequency domain, the 1ST reduces the NLS to a scattering problem. Videlicet, the NLS is reduced to a scattering problem by finding the Lax pair, the evolution of the scattering data is then determined by this system of ODES and finally the evolution of the NLS is determined from the scattering data by solving the Gelfand-Leviton-Marchenko equation. The 1ST can even find exact N-soliton solutions for $N > 1$.

This method was first proposed for the Korteweg-de Vries (KDV) equation in 1967 by Gardner, Greene, Kruskal and Miura [27]. Lax generalised their work in 1968 [52] before Zakharov and Shabat applied it to the NLS in the early 1970s [81, 82]. The method was formalised in 1974 by Ablowitz, Kaup, Newell and Segur [1]. It remains one of the workhorses of theoretical physics, although it is limited to completely integrable systems.

The NLS can also be tackled using the Bäcklund and Darboux transformations. In 1974 Lamb constructed the Bäcklund transformation for the NLS through a classical method first presented by Clairin [49, 48], and the linear structure of the AKNS system permitted the use of Darboux transformations [18, 68].

Another method proposed in the 1970s was the Hirota, or direct method, which solves PDEs after bilinearising them through appropriate transforms. It was first suggested by Hirota and Satsuma in their work on the Toda lattice [35]. For a more detailed description, interested readers may consult [34].

The NLS is the canonical example of an equation with envelope solitons, and so it has a number of applications. It's been used in modeling fluid dynamics [79], plasma physics [12] and, most importantly, nonlinear optics [2, 3]. The interpretation of b, x and t varies depending on the particular field of study. By way of example, in nonlinear optics the interpretation is that:

1. 0 is the amplitude of the light pulse in a cable,
2. x is the retarded time, i.e. the real time less the product of the distance along the cable and the group velocity. Thus the peak of the pulse is always centered at $x = 0$ as it moves along the cable, and

3. t is the distance along the cable.

Readers interested in a derivation of the NLS from Maxwell's equations may consult chapter 2 of Agrawal [2].

Fiber optic cables, and much of nonlinear optics, only became relevant in the 1950s when the introduction of dielectric cladding around the glass core of the cable dramatically reduced the signal loss [33]. The 1970s saw further improvements in production methods, and the loss rate which had dropped from - 1000 dB/km to - 10 dB/km with the introduction of cladding dropped again to - 0.1 dB/km by the end of the decade [56, 57].

Since the 1970s there's been enormous interest in fiber solitons. The first optical solitons were observed experimentally at Bell Laboratories in 1980 by Mollenauer, Stolen and Gordon [58], and the rest of the decade heralded further improvements in the generation and control of optical pulses [38, 39, 40, 55, 59]. The doped amplifiers perfected in the '80s fueled more practical research in the 90s as scientists tried to improve the speed and distance of data transmission over fiber optic cables [17, 28], and since the turn of the century most digital information transfer is through fiber optic cable.

We move now to the driven nonlinear Schrödinger equation, whose dynamics are richer and more interesting.

1.2 The parametrically driven, damped nonlinear Schrödinger equation (PDDNLS)

The PDDNLS is a natural modification of the NLS. Many real world systems exhibit some sort of dissipation which should be incorporated into our mathematical models if it is not negligible. Conversely, resonant driving is often introduced to counteract the effects of dissipation. In the case of the damped NLS two sorts of driving are commonly considered. The first is the direct driving [9, 16], and the second is parametric driving. In this dissertation we consider the second. Thus, the equation of our interest is the PDDNLS,

$$i\psi_t + \psi_{xx} + 2|\psi|^2\psi - \psi = h\psi^* - i\gamma\psi. \tag{1.5}$$

Here 'y is the damping coefficient, and h the driving strength. The asterisk represents complex conjugation. We first demonstrate how this equation arises in the description of resonantly driven nonlinear oscillatory systems.

A common phenomenon in physical systems is the self-modulation of small amplitude plane wave solutions. As the amplitude of a plane wave increases and the nonlinear effects become non-negligible, the wave may bunch into wave packets. These wave packets consist of a carrier wave, the original plane wave, modulated by an envelope. They are called **envelope solitons.** We introduce the damped, parametrically driven sine-Gordon

equation below and consider its small amplitude plane wave solutions. We will see that the resulting wave packets are governed by the PDDNLS.

Before we proceed we should note that the PDDNLS only governs the evolution of these envelope solitons under unidirectional propagation. If we allow bidirectional wave propagation the situation becomes more complicated (see [45]).

The damped, parametrically driven sine-Gordon equation is

$$\theta_{tt} + \gamma_0\theta_t + \theta_{xx} + \sin\theta - h_0\cos(2t)\sin\theta = 0. \tag{1.6}$$

We assume that the amplitude of the solutions are small, i.e.

$$\theta(x,t) = \epsilon\theta_0(X_0, X_1, \ldots, T_0, \ldots) + \epsilon^2\theta_1(X_0, X_1, \ldots, T_0, \ldots) + \ldots \tag{1.7}$$

where we have introduced new time and length scales

$$X_i = \epsilon^i x,\ T_i = \epsilon^i t. \tag{1.8}$$

It is these "slower" scales that are responsible for modulating the small amplitude solutions. Naturally, these new time and length scales mean we should introduce new derivatives, and so

$$\frac{\partial}{\partial x} = \frac{\partial X_i}{\partial x}\frac{\partial}{\partial X_i} = \epsilon^i\frac{\partial}{\partial X_i} = \epsilon^i\partial_i \tag{1.9}$$

and similarly

$$\frac{\partial}{\partial t} = \epsilon^i D_i, \tag{1.10}$$

where summation over repeated indices is implied and we have introduced D_i and ∂_i to simplify the notation. Since we have assumed that θ is small, we can also use the Taylor expansion of sine,

$$\sin\theta = \theta - (\theta^3/6) + \mathcal{O}(\theta^5). \tag{1.11}$$

Finally, we replace the damping and driving coefficients, $\gamma_0 = \epsilon^2\gamma$ and $h_0 = \epsilon^2 h$. If we substitute these expressions into equation (1.6) and sort into powers of ϵ we recover the following:

$$\begin{aligned}
\mathcal{O}(\epsilon^1) \quad &\cdot \quad D_0^2\theta_0 - \partial_0^2\theta_0 + \theta_0 = 0 \\
\mathcal{O}(\epsilon^2) \quad &\cdot \quad D_0^2\theta_1 - \partial_0^2\theta_1 + \theta_1 + 2D_0D_1\theta_0 \\
&\qquad -2\partial_0\partial_1\theta_0 = 0 \\
\mathcal{O}(\epsilon^3) \quad &\cdot \quad D_0^2\theta_2 - \partial_0^2\theta_2 + \theta_2 + 2D_0D_2\theta_0 \\
&\qquad -2\partial_0\partial_2\theta_0 + D_1^2\theta_0 - \partial_1^2\theta_0 + (1/6)\theta_0^3 \\
&\qquad +2D_0D_1\theta_1 - 2\partial_0\partial_1\theta_1 \\
&\qquad +\gamma D_0D_1\theta_0 - h\cos(2t)\theta_0 = 0
\end{aligned} \tag{1.12}$$

It will be sufficient to consider only powers of ϵ up to ϵ^3. The first equation is linear, so we can rewrite it as

$$\hat{L}\theta_0 = 0, \qquad \hat{L} = D_0^2 - \partial_0^2 + 1. \tag{1.13}$$

The solution to this equation is simply the plane wave

$$\theta_0 = A(X_1, X_2 \ldots, T_1 \ldots)e^{i(kX_0 - \omega T_0)} + \text{c.c.} \tag{1.14}$$

where k and ω are related through the dispersion relation $\omega^2 = k^2 + 1$. Here we note the importance of our earlier assumption - the plane wave represents waves moving in one direction without making any concession to possible interactions with counter-propagating waves. Note also that the amplitude is not a constant, it depends on the slow scales X_i and T_i, $i > 0$. At this stage it is useful to calculate the group velocity v_g for the solution

$$v_g = \frac{\partial \omega}{\partial k} = \frac{k}{\omega}. \tag{1.15}$$

It's also useful to introduce the notation $\sigma = kX_0 - \omega T_0$. If we substitute this solution into the second equation we find that

$$\hat{L}\theta_1 = \left(2i\omega\frac{\partial A}{\partial T_1} + 2ik\frac{\partial A}{\partial X_1}\right)e^{i\sigma} + \text{c.c.}; \tag{1.16}$$

the equation reduces to the same linear operator as before but there is now some additional driving. It is important to note that this driving is resonant, i.e. the driving frequency is the same as the frequency of solutions to the linear operator. This means that the solution will eventually blow up. To prevent this we impose the condition that the right hand side of the equation is zero, i.e.

$$\frac{\partial A}{\partial T_1} + \frac{k}{\omega}\frac{\partial A}{\partial X_1} = 0. \tag{1.17}$$

Thus the amplitude A does not depend on X_1 and T_1 independently, but only on $\xi_1 = X_1 - v_g T_1$. Having imposed this condition we can take $\theta_1 = 0$ since it satisfies the same linear operator as θ_0 and will be of the same form. Finally, we can consider the ϵ^3 equation. In particular, we consider the case when $\omega = 1$. It has the form

$$L\theta_2 = \left(\alpha e^{i\sigma} + \text{c.c.}\right) + \left(\beta e^{3i\sigma} + \text{c.c.}\right). \tag{1.18}$$

As before we will set the coefficient α of the resonant terms equal to zero:

$$-\frac{\partial^2 A}{\partial T_1^2} + \frac{\partial^2 A}{\partial X_1^2} + 2i\frac{\partial A}{\partial T_2} - \frac{1}{2}|A|^2 A + i\gamma A + \frac{1}{2}hA^* = 0. \tag{1.19}$$

We introduce the following co-ordinate transformation,

$$\xi_i = X_i - v_g T_i, \qquad \tau_i = T_i, \qquad i = 1, 2. \tag{1.20}$$

Then

$$\frac{\partial A}{\partial X_i} = \frac{\partial A}{\partial \xi_i}, \qquad \frac{\partial A}{\partial T_i} = \frac{\partial A}{\partial \tau_i} - v_g \frac{\partial A}{\partial \xi_i}. \tag{1.21}$$

Further, we know from (1.17), the condition imposed on the resonant terms in the ϵ^2 equation, that $\partial A/\partial \tau_1 = 0$. Substituting these expressions for the derivative into (1.19) and rearranging we find that

$$i\frac{\partial A}{\partial \tau_2} + \frac{1}{2}\frac{\partial^2 A}{\partial \xi_1^2} + \frac{1}{4}|A|^2 A + i\frac{\gamma}{2}A + \frac{h}{4}A^* = 0. \tag{1.22}$$

This can be reduced to its more familiar form through some careful relabeling.

1.3 Solitons of the PDDNLS

While the solitons of the NLS arise through a balance of dispersion and nonlinearity, the solitons of the PDDNLS require also the balance of loss and gain. The resulting dynamics are much richer. The starting points of our discussion are the two stationary solitons of the PDDNLS,

$$\psi_\pm = A_\pm \mathrm{sech}(A_\pm x) e^{-i\theta_\pm}. \tag{1.23}$$

The amplitudes and phases are

$$A_\pm = \sqrt{1 \pm \sqrt{h^2 - \gamma^2}}, \quad \theta_+ = \frac{1}{2}\arcsin\frac{\gamma}{h}, \quad \theta_- = \frac{\pi}{2} - \theta_+. \tag{1.24}$$

Like the solitons of the unperturbed NLS, the $\psi_\pm$ solitons are spatially translationally invariant; they can be centered at an arbitrary point x_0. This invariance means that the spectrum of the linearised operator around these solitons will always include a zero characteristic exponent, or alternatively, a unit characteristic multiplier.

The continuous spectrum of the $\psi_\pm$ solitons is also similar to the continuous spectrum of the solitons of the unperturbed NLS. In the case of the NLS the continuous spectrum is a broken vertical line centered at the origin, i.e. $|\mathrm{Im}(\mu)| > 1$ and $\mathrm{Re}(\mu) = 0$. The continuous spectrum of the $\psi_\pm$ solitons is just shifted left by the value of the damping coefficient, i.e. $|\mathrm{Im}(\mu)| > 1$ and $\mathrm{Re}(\mu) = -\gamma$.

Finally, if the ψ_+ soliton undergoes a Hopf bifurcation and births a periodic solution, this solution is temporally translationally invariant, i.e. the peak of this periodic solution can be centered at an arbitrary t_0. Thus the spectrum of the linearised operator around one of these periodic solutions will include a second zero exponent or unit multiplier.

If we consider the $\psi_\pm$ solitons as building blocks of the PDDNLS's dynamics there are a number of obvious questions.

1. In which parts of the (γ, h) parameter space are the $\psi_{\pm}$ solitons stable?

2. For values of γ and h where the solitons are unstable, what sort of stable attractors do we observe instead?

3. Can these solitons be combined to form bound states, or complexes?

   (a) If these complexes can be formed, where are they stable or unstable?

   (b) For values of γ and h where the $\psi_{\pm}$ solitons and any complexes are unstable, what attractors exist?

Some of these questions have already been partially answered, and some more answers are presented in chapter 5. As discussed in [8] the ψ_{-} soliton is always unstable, while for $h > \sqrt{1+\gamma^2}$ any localised solution will evolve into spatiotemporal chaos. Finally, when $h < \gamma$ no stationary or periodic localised attractors exist.

Thus there is a band between the curve $h = \sqrt{1+\gamma^2}$ and the straight line $h = \gamma$ where the stability of the ψ_{+} soliton and the behaviour of the PDDNLS is not immediately apparent. Bondila *et al* [13] made an attempt to classify the behaviour in this regime by direct simulation. We reproduce their attractor chart in figure 1.1 below.

In figure 1.1 curve 1 separates the stationary 0_{+} soliton from the period-1 solutions, i.e. curve 1 traces the value of the Hopf bifurcation of the 0_{+} soliton. Further, their spectral analysis found that the frequency of the period-1 solutions near the Hopf bifurcation were in good agreement with the characteristic exponent Im(μ). This result meets theoretical expectations (see theorem 2.19 in this thesis). Finally: as h increased, the difference between the frequency of the period-1 solutions and the exponent grew. This indicates anharmonic effects are responsible for the behaviour of the system.

Bondila *et al* also observed the period-doubling and quasi-periodic routes to chaos. Curve 2 marks the boundary above which the period-1 solutions underwent a sequence of period-doublings as h increases. At two points on this curve they observed strange attractors. By contrast, curve 3 marks the boundary of period-1 solutions with spatio-temporal chaos. This immediate change in behaviour is the quasi-periodic route to chaos.

Astute readers will note that the attractor chart of Bondila *et al* does not include any simulations with zero damping. For some insight into the behaviour when $\gamma = 0$ we turn to a paper by Alexeeva *et al* [4]. For the purposes of our discussion we focus mostly on section 5 from their paper. They start by deriving a reduced amplitude equation using a multi-scale expansion governing the behaviour of the PDDNLS. This analytical work suggests that the temporally periodic solution will never be asymptotically attractive, and indeed in section 5 they find two expressions (correct to

E^3) for a slowly growing and decaying attractor. They also provide direct numerical simulation confirming that small initial conditions are trapped by these attractors, and more energetic initial conditions decompose into a number of these attractors.

For all their success, direct simulation can only ever capture the behaviour of stable solutions. If, for example, we are interested in the behaviour of a particular periodic solution after it undergoes a period-doubling and has lost stability, we cannot rely on direct simulation. Any attempt to investigate its behaviour directly will instead return a result appropriate only to the stable, double-period solution that was born at the bifurcation point. In effect, the stable solutions mask the behaviour of the unstable solutions from direct simulation, and so a better tool is needed if we want to produce a complete picture (including stable and unstable behaviour) of the (-y, *h)* plane.

The tool we need is numerical continuation. It's been applied to the PDDNLS before. In 1999 Barashenkov and Zemlyanaya [10] identified some stable and unstable complexes of the PDDNLS using numerical continuation. They used a similar approach in 2001 (with Bar) and 2004 [11, 83] to show that some of these complexes, unlike the $0_{\pm}$ solitons themselves, can travel without violating the conservation of momentum.

To complete the picture of the PDDNLS's behaviour we use numerical continuation to track the behaviour of the 0_+ soliton, and the periodic solitons produced by Hopf bifurcation of the 0_+ soliton, as we change the parameters 'y and h. Chapter 2 gives an outline of bifurcation theory and explains how periodic solutions are produced by a Hopf bifurcation of the b_+ soliton. Chapter 3 discusses numerical continuation methods for following branches of solutions as the parameters controlling a system change and chapter 4 outlines two approaches for calculating the stability of those solutions. Finally, chapters 5 and 6 present the numerical results with some conclusions.

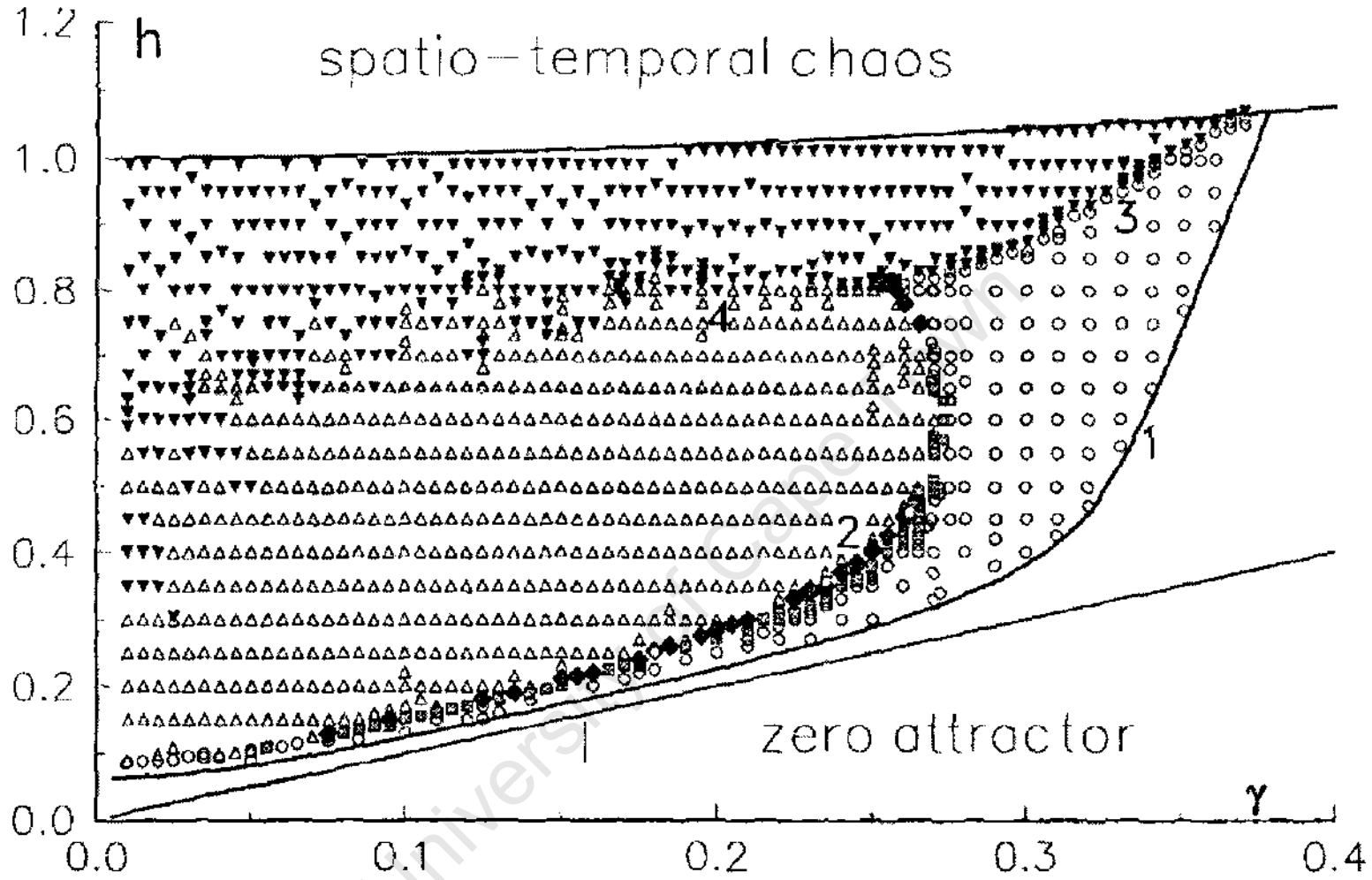

Figure 1.1: Attractor chart reproduced from Bondila *et al* [13] with their annotation. "Below the line $h = \gamma$ there are no localised solutions, and the only attractor is $\psi = 0$. Above the line $h = (1+\gamma^2)^{1/2}$, the zero solution is unstable with respect to the excitation of continuous spectrum waves. In the area between these two lines, we used empty circles to denote period-I solutions and shadowed boxes for periods-2, 4, and 8. Small white blobs indicate period-6, period-7 and period-10 solitons observed at $(\gamma = 0.262, h = 0.46)$, $(\gamma = 0.235, h = 0.355)$ and $(\gamma = 0.18, h = 0.251)$, respectively. Finally, shadowed diamonds stand for type-I and type-II strange attractors observed at $(\gamma = 0.18, h = 0.253)$ and $(\gamma = 0.26, 0.4530 < h < 0.4539)$, respectively, as well as for complex cycles. The region of stable stationary solitons is left blank; empty triangles mark the area where the only attractor is $\psi = 0$, and the domain of spatio-temporal chaos is marked by black triangles. Note an unexpectedly complex, "shark jaw" shape of the interface between the regions of spatio-temporal chaos and zero attractor."

Chapter 2

Elements of bifurcation theory

Real world phenomena are often modeled mathematically. Unfortunately, the modeling process often requires that certain factors are either approximated or completely neglected, particularly in deterministic systems like some differential equations. Thus, it is fair to ask: how good is our model? It is easy to make an empirical judgement, one can merely observe the real world and compare it to the model's behaviour.

Ideally we would like the real world and our mathematical system to coincide wherever possible. It would be undesirable if a small perturbation to our model led to drastically different behaviour, unless the same phenomena is observed in the real world, e.g. a load bearing beam which buckles as the strain increases, then suddenly snaps.

It is these critical, or bifurcation points where the behaviour of the system dramatically changes that we consider in this chapter. In section 2.1 we provide some background concepts before introducing a formal definition for the structural stability of a system and of bifurcations. Section 2.2 discusses the various bifurcations of stationary points, including the Hopf bifurcation which generates a branch of periodic solutions, or closed orbits. Section 2.3 develops some tools using the material from 2.1 and explains exactly the relationship between Hopf bifurcations of fixed points and closed orbits. Section 2.4 discusses the various bifurcations of closed orbits. The exposition presented here follows Demazure [22], Farkas [23] and Ruelle [69].

2.1 Structural stability

In this section we present two important definitions which are necessary to formalise the concept of a structurally stable system. The definitions are (1) of a manifold, and (2) of a flow. Some of the exposition may seem unnecessarily thorough for the purposes of 2.2, but section 2.3 will build on

this work.

Definition 2.1. *A **Banach space** is a normed vector space which is complete with respect to the metric induced by the norm.*

The most familiar Banach space is just $\mathbb{R}^n$. Later definitions will refer to Banach spaces in general, but all the examples we consider will use $\mathbb{R}^n$ or a subset $V \subset \mathbb{R}^n$. We now introduce some topological terms.

Definition 2.2. *A topological space W is **Hausdorff** if for every two distinct points w_1, w_2 in W there exist disjoint neighborhoods W_1, W_2 of those points, i.e. $w_1 \in W_1$ and $w_2 \in W_2$ and $W_1 \cap W_2 = \emptyset$.*

Definition 2.3. *A topological space W is **paracompact** if every open cover has an open locally finite refinement, i.e. any point $w_1 \in W$ has a neighborhood W_1 that intersects with only finitely many sets in the refinement of the cover.*

A manifold is a topological space, M, which behaves locally like a Banach space, B. Intuitively, we would like to find a space M, and a collection of maps from M into B such that M is covered by the domain of these maps, and that the maps agree whenever they intersect. We formalise this below.

Definition 2.4. *Let B be a Banach space, and M a Hausdorff, paracompact topological space. The triplet (U, φ, B) comprised of an open subset U of M, a Banach space and a homeomorphism $\varphi : U \to B$ is called a **chart**. A family of charts $(U_\alpha, \varphi_\alpha, B_\alpha)$ such that M is covered by U_α and $\varphi_\beta \circ \varphi_\alpha^{-1}$ is C^r wherever the composition is defined is a C^r **atlas**. Two C^r atlases are equivalent if their union is a C^r atlas. The space M and the equivalence class of a C^r atlas is a C^r **manifold**.*

If $r \geq 1$ then M is a differentiable manifold. If $E_\alpha = E$ for all α then the manifold is of type E with dimension $d = \dim(E)$. As mentioned above, we will only be considering well-behaved manifolds, i.e $r \geq 1$ and $E_\alpha = \mathbb{R}^n$ and so the manifold is differentiable and of type $\mathbb{R}^n$ with dimension n.

Consider a point $u \in U_p \cap U_q$. This point will have two different coordinate representations in $\mathbb{R}^n$, the first in $\varphi_p(U_p)$, i.e. $\varphi_p : u \mapsto u_p = (u_p^1, u_p^2, \ldots, u_p^n)$ and the second similarly in $\varphi_q(U_q)$. The derivatives of $\varphi_q \circ \varphi_p^{-1}$ form a Jacobian matrix, $J_{ij} = [\partial u_q^i / \partial u_p^j]$, and it simply captures the change in coordinates as we move between $\varphi_p(U_p)$ and $\varphi_q(U_q)$.

Definition 2.5. *A manifold is **orientable** if there exists an atlas $(U_\alpha, \varphi_\alpha, B_\alpha)$ such that the Jacobian matrix has positive determinant for all $\varphi_\beta \circ \varphi_\alpha^{-1}$ where $U_\alpha \cap U_\beta \neq \emptyset$.*

The second definition we need is of a flow. We often use the notation $\mathbf{v}(t)$ for solutions to systems of differential equations, and while we informally treat these solutions as continuous functions of t, this is not strictly correct. They are in fact flows, or group actions on a set.

Definition 2.6. *A **flow** on a set V is a function $\phi : \mathbb{R} \times V \to V$ such that*

1. $\phi(0, \mathbf{v}) \mapsto \mathbf{v}$ *for all* $\mathbf{v} \in V$.

2. $\phi(t, \phi(s, \mathbf{v})) = \phi(s + t, \mathbf{v})$.

We are going to be working with flows not on arbitrary sets, but on manifolds, and so we can impose a further condition which ensures the flow is continuous.

3. $\phi \in C^1$ *and for a fixed* t, $\phi(t, \cdot)$ *maps* V *diffeomorphically into itself* .

There are a number of closely related terms we define now. For a given $\mathbf{v_0}$ in V the set $\{\phi(t, \mathbf{v_0}) \in V : t \in \mathbb{R}\}$ is called its **path** or **trajectory** and the function $\phi(\cdot, \mathbf{v_0})$ its **motion**. If the path is a singleton set, or the motion a constant function, then the point $\mathbf{v_0}$ is called a **fixed** or **equilibrium point**.

If there exists a point $\mathbf{v}_p$ such that there exists $T > 0$ with $\phi(T, \mathbf{v}_p) = \mathbf{v}_p$ then $\mathbf{v}_p$ is a **periodic point** with period T. Its motion is a periodic function. This follows easily from 2 above.

As alluded earlier, flows are generated by autonomous systems of differential equations,

$$\dot{\mathbf{v}} = F(\mathbf{v}) \tag{2.1}$$

where $F : V \to \mathbb{R}^n$ is smooth, and $V \subset \mathbb{R}^n$. For any point $(t_0, \mathbf{v}_0) \in \mathbb{R} \times V$ we know by the existence and uniqueness theorems that a single solution passes through this point. We denote it $\mathbf{V}(t; (t_0, \mathbf{v}_0))$.

We now define a function $\phi_F : \mathbb{R} \times V \to V$ by $\phi_F(t - t_0, \mathbf{v}_0) = \mathbf{V}(t; (t_0, \mathbf{v}_0))$. We will show that the function ϕ_F is a flow. Before we proceed, please note that the uniqueness of solutions and the autonomy of (2.1) make the choice of t_0 arbitrary, and so we consider only the case where $t_0 = 0$.

Clearly 2.6.1 holds since $\phi_F(0, \mathbf{v}_0) = \mathbf{V}(0; (0, \mathbf{v}_0)) = \mathbf{v}_0$. To show 2.6.2 pick any $s \in \mathbb{R}$. Then for any $\mathbf{v}_0 \in V$ set $t = 0$. We find that

1. $\phi_F(t + s, \mathbf{v}_0) = \phi_F(s, \mathbf{v}_0) = \mathbf{V}(0; (0, \mathbf{v}_0))$.

2. $\phi_F(t, \phi_F(s, \mathbf{v}_0)) = \phi_F(0, \phi_F(s, \mathbf{v}_0)) = \phi_F(s, \mathbf{v}_0)) = \mathbf{V}(0; (0, \mathbf{v}_0))$.

The two expressions agree for one value of t, and so by the uniqueness of solutions to initial value problems they must agree for all values of t. Finally, 2.6.3 must hold since the family of solutions to (2.1) is continuous with respect to both time and the initial conditions. Interested readers may consult any introductory text to systems of differential equations for a proof.

We are done with the introductory material and can now formalise the idea of structural stability mentioned at the beginning of the chapter. Two concepts are going to be crucial. The first is the distance between our mathematical systems so that we can talk meaningfully about making "small

perturbations" to them. The second is of equivalence between the resulting behaviour, i.e. flows, of those systems so we can distinguish "drastically different" behaviour.

Let M be a compact, orientable C^2 manifold of type $\mathbb{R}^n$ embedded in $\mathbb{R}^m$ (this embedding is always possible, see Whitney [78]). Then consider two smooth functions $F : M \to \mathbb{R}^n$ and $G : M \to \mathbb{R}^n$ (i.e. $F, G \in C^1(M, \mathbb{R}^n)$) generating flows on M by

$$\dot{\mathbf{v}} = F(\mathbf{v}) \quad \text{and} \quad \dot{\mathbf{v}} = G(\mathbf{v}). \tag{2.2}$$

Definition 2.7. *Denote by J_F and J_G the Jacobian matrices of the systems F and G respectively. Then the C^1-**distance** between the two systems F and G is given by*

$$\operatorname{dist}(F, G) = \max_{\mathbf{v} \in M} ||F(\mathbf{v}) - G(\mathbf{v})||_2 + \max_{\mathbf{v} \in M} ||J_F(\mathbf{v}) - J_G(\mathbf{v})||_2. \tag{2.3}$$

Note that the maximum is obtained on M since the manifold is compact. Having defined a distance between systems we now define an equivalence relation between flows.

Definition 2.8. *Two flows are equivalent if there is a self-homeomorphism on M mapping the paths of the first flow onto the paths of the second that preserves the direction of motion along paths.*

Finally we can define structural stability. We consider all the systems "near" our original system (with respect to the C^1-distance we've introduced) and if the flows generated by all those systems are equivalent the system is structurally stable.

Definition 2.9. *A system, F, is **structurally stable** if there exists a neighborhood of F in $C^1(M, \mathbb{R}^n)$ such that the flow it generates is equivalent to the flows generated by all the systems in that neighborhood.*

We have established a definition for structural stability, and now there is one obvious, outstanding question. How do we determine whether a system is structurally stable? Unfortunately, there are no easy answers. Andronov and Pontriagin [6], and Peixoto [62, 63] provided a characterisation of stable systems in two dimensions, but no similar characterisation exists for higher dimensions and so we need to simplify the problem before we can proceed.

The first step is to introduce a parameterized system

$$\dot{\mathbf{v}} = F(\mathbf{v}; \zeta) \tag{2.4}$$

and then instead of considering arbitrary perturbations to the system, rather just consider the changing behaviour as the parameter ζ changes. From here there are two approaches.

1. We can look for the critical values of ζ where the structural stability (as defined above) is lost. This is the catastrophe theory of Rene Thom [76] which gives a complete classification for gradient systems when the dimension of the parameter space is less than or equal to five, i.e.

$$\dot{\mathbf{v}} = -\nabla \tilde{F}(\mathbf{v};\zeta) \quad \text{and} \quad \zeta \in \mathbb{R}^m, m \leq 5. \tag{2.5}$$

2. We can look for values of ζ where certain fundamental properties of the system change. These include the existence, number and stability of fixed points and closed orbits. It is these bifurcation points where the properties of the system change drastically that we consider in the sections below.

2.2 Bifurcations of fixed points

The first set of bifurcations we consider are of fixed points to our system. The last of these bifurcations, the Hopf bifurcation, leads to a branch of periodic solutions, or closed orbits. We will discuss bifurcations of these closed orbits in section 2.4.

2.2.1 Saddle-node bifurcation

The first bifurcation we discuss is the **saddle-node bifurcation**. As ζ changes and the system passes through a saddle-node bifurcation, two new fixed points appear simultaneously and then split. One of these is stable (the node) and the other is unstable (the saddle). Conversely, should the system pass through the bifurcation in the other direction, we would observe the collision and subsequent disappearance of a stable fixed point and an unstable fixed point. This is a generic phenomena, and is observed in systems of all dimensions, see Gale and Sotomayor [26].

Example 2.10. *Consider the one-dimensional system*

$$\dot{v} = -v^2 + \zeta, \qquad v, \zeta \in \mathbb{R}. \tag{2.6}$$

While $\zeta < 0$ the right hand side is always negative and so there are no fixed points. At $\zeta = 0$ we see that $\dot{v} = 0$ for $v = 0$ and so a fixed point appears. As ζ increases this fixed point splits into two, $v_{1,2} = \pm\sqrt{\zeta}$. See figure 2.1. The fixed points on the upper branch are nodes, those on the lower branch are saddles.

2.2.2 Pitchfork bifurcation

The second bifurcation we discuss is the **pitchfork bifurcation** which occurs generically in systems satisfying certain conditions, e.g. oddness of

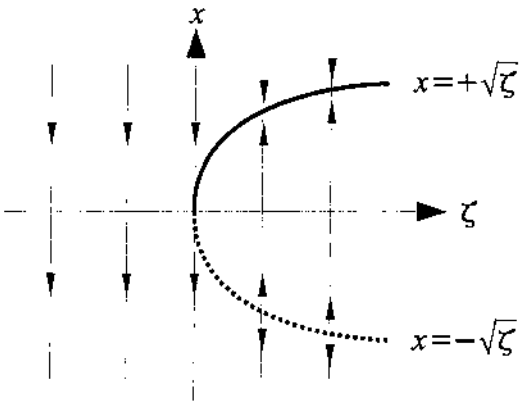

Figure 2.1: Saddle-node bifurcation in the x, (-plane of example 2.10. The solid curve indicates a stable fixed point, while the dashed curve indicates an unstable fixd point.

the right hand side [30]. As (changes and the system passes through a pitchfork bifurcation, the stability of one of its fixed points changes and two additional fixed points branch off from that original fixed point. These additional fixed points have the same stability as the original fixed point. There are two types of pitchfork bifurcations, super- and subcritical pitchforks. If the additional fixed points arise as (increases it is a supercritical pitchfork, conversely, if they arise as (decreases it is a subcritical pitchfork.

Example 2.11. *Consider the one-dimensional system*

$$\dot{v} = -v^3 + \zeta v, \qquad v, \zeta \in \mathbb{R}. \tag{2.7}$$

Clearly the right hand side is always zero when $v = 0$. *This is the fixed point that will change stability as we pass through the pitchfork bifurcation. While* $(< 0$ *there are no other fixed points since the two terms in the right hand side are either both positive or both negative for* $v \neq 0$. *Once* $(> 0$ *two additional fixed points appear at* $\pm\sqrt{(}$. *The characteristic pitchfork shape of this bifurcation is clear in figure 2.2.*

2.2.3 Hopf bifurcation

The final bifurcation we discuss is the **Hopf bifurcation.** In this section will provide the same sort of non-technical description and example as we did for the saddle-node and pitchfork bifurcations, but in 2.3 we will provide a more formal exposition which includes a statement of the Hopf bifurcation theorem, 2.19, and an outline of its proof using the central manifold theorem, 2.18.

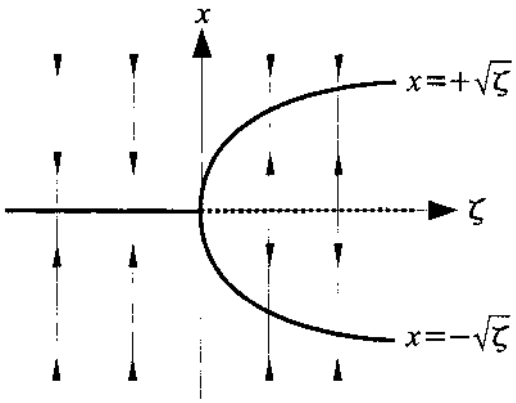

Figure 2.2: Pitchfork bifurcation in the x, ($-plane of example 2.11. The solid curve indicates a stable fixed point, while the dashed curve indicates an unstable fixd point.

In many real world systems, e.g. civil and electrical engineering or ecological systems, we observe a stable equilibrium which begins to oscillate as one of the factors controlling its behaviour changes. It is this change from a stable fixed point to a stable closed orbit that characterises Hopf bifurcations.

In our mathematical models, as (changes and the system moves through a Hopf bifurcation, we observe a complex conjugate pair of eigenvalues pass from the left hand half-plane to the right hand half-plane. It is these eigenvalues of the linearized system that change the stability of the system and are responsible for the periodic branch of solutions that appears.

Example 2.12. *Consider the system*

$$\begin{aligned} \dot{v} &= w - v(v^2 + w^2 - \zeta) \\ \dot{w} &= -v - w(v^2 + w^2 - \zeta). \end{aligned} \tag{2.8}$$

The origin is always an equilibrium point. If we linearise the system around the origin we find that

$$\frac{d}{dt}\begin{pmatrix} v \\ w \end{pmatrix} = \begin{pmatrix} \zeta & 1 \\ -1 & \zeta \end{pmatrix}\begin{pmatrix} v \\ w \end{pmatrix}. \tag{2.9}$$

We can now easily determine the eigenvalues of the system,

$$\mu_{1,2} = \zeta \pm i. \tag{2.10}$$

Clearly the eigenvalues will pass from the left hand half-plane to the right hand half-plane as a complex conjugate pair at $\zeta = 0$. It's useful to convert

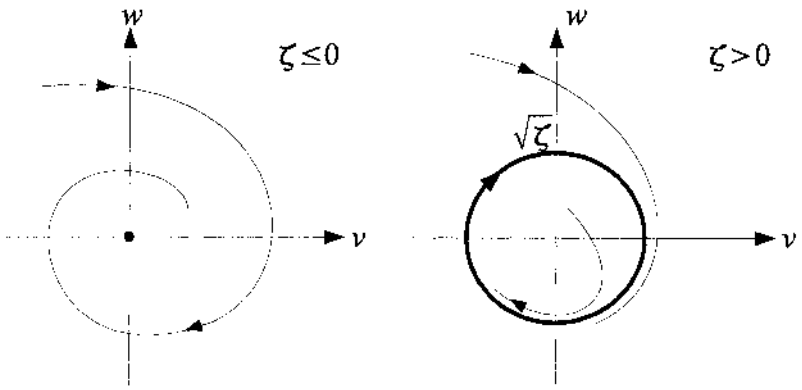

Figure 2.3: Hopf bifurcation of the system in 2.12 as (passes through zero. The single fixed point at the origin (left) is transformed into a closed orbit, a circle with radius ₙg (right).

the system to polar equations so that we can accurately picture its behaviour at this point. Let

$$v = r\cos\theta \quad \text{and} \quad w = r\sin\theta \tag{2.11}$$

then the system is reduced to

$$\begin{aligned} \dot{r} &= -r(r^2 - \zeta) \\ \dot{\theta} &= -1. \end{aligned} \tag{2.12}$$

Now it's obvious that for (< 0 *all the trajectories spiral inwards towards the origin. However, when (* > 0 we *see that ii-* = 0 *for r =* ₙ*g and so the trajectories far from the origin will instead spiral inwards to a closed orbit with radius* ₙ*g while trajectories near the origin will spiral outwards to this orbit. Figure 2.3 makes this change of behaviour clear.*

2.3 From fixed points to closed orbits

The aim of this section is to state the Hopf bifurcation theorem (HBT), outline a proof and then explain its consequences. We will not use the theorem explicitly in our work. It is necessary however, that we understand it. The Hopf bifurcation theorem guarantees the existence of the periodic solutions we plan to study, and further it suggests a value for their period. This suggested value is useful in our numerical analysis where a good initial guess for the period can make our numerical continuation faster.

The material presented here is quite dry, so we have included an outline of this section with a brief explanation of everything we've covered. Readers who tackle the entire section anyway will notice that there are no proofs.

These omissions are in the interest of readability, but we have indicated where the proofs may be found should you be interested.

1. We start by examining a linearised system, and show that it can be decomposed into three independent subsystems: the stable, unstable and central. A simple example is included to illustrate the point.

2. This idea of decomposition is expanded, and we see that it can be extended to nonlinear systems. We use this nonlinear decomposition and the definition of a locally invariant manifold to define the stable, unstable and center manifolds.

3. We introduce the central manifold theorem, and the Hopf bifurcation theorem. We outline a proof of the HBT that relies on the central manifold theorem, and check that the formal definitions of the HBT agree with the informal explanation of the Hopf bifurcation in section 2.2.3 above.

Consider a system

$$\dot{\mathbf{v}} = A\mathbf{v} + \mathbf{g}(\mathbf{v}) \tag{2.13}$$

where the matrix A is $n \times n$ and constant and the function $\mathbf{g} \in C^k(\mathbb{R}^n)$ with $k \geq 2$. We assume without loss of generality that the origin is an equilibrium point, i.e. $\mathbf{g}(\mathbf{0}) = \mathbf{0}$ and further that $J_g(\mathbf{0}) = \mathbf{0}$. (Recall that J_g is just the Jacobian of g.) Denote the flow generated by the system by $\phi(t, \mathbf{v})$.

In addition, we note the following. The matrix A will have n eigenvalues that can be split into three distinct types. There are $s \geq 0$ stable eigenvalues with strictly negative real part, $u \geq 0$ unstable eigenvalues with strictly positive real part and $c \geq 0$ eigenvalues with zero real part. We take account of the multiplicity of eigenvalues so that $s + u + c = n$. Each set of eigenvectors corresponding to these eigenvalues will span a subspace of $\mathbb{R}^n$, denoted $\mathbb{R}^s, \mathbb{R}^u, \mathbb{R}^c$ respectively , and their direct sum is the entire space,

$$\mathbb{R}^n = \mathbb{R}^s \oplus \mathbb{R}^u \oplus \mathbb{R}^c. \tag{2.14}$$

If we linearise the system (2.13) around a solution $\mathbf{v}$ we find that

$$\dot{\mathbf{w}} = [A + J_g(\mathbf{v})]\,\mathbf{w}. \tag{2.15}$$

In particular we can consider linearising about the equilibrium point, the origin. Then $\mathbf{v} = \mathbf{0}$ and so $J_g(\mathbf{v}) = \mathbf{0}$ and we find simply that

$$\dot{\mathbf{w}} = A\mathbf{w}. \tag{2.16}$$

Then the solution $\phi(t, \mathbf{v})$ can be expressed simply as $\phi(t, \mathbf{v}) = e^{At}\mathbf{v} + G(t, \mathbf{v})$ where $G(t, \mathbf{v}) \in C^k(\mathbb{R}^n)$ satisfies $G(t, \mathbf{0}) = \mathbf{0}$ and $J_G(t, \mathbf{0}) = \mathbf{0}$. Consider

now what happens if we introduce a regular linear coordinate change to the linearised system (2.16), i.e.

$$\dot{\tilde{\mathbf{w}}} = \tilde{A}\tilde{\mathbf{w}} \tag{2.17}$$

such that

$$\tilde{A} = \begin{pmatrix} S & 0 & 0 \\ 0 & U & 0 \\ 0 & 0 & C \end{pmatrix}. \tag{2.18}$$

Here S, U and C are $s \times s$, $u \times u$ and $c \times c$ matrices whose eigenvalues either have strictly negative, strictly positive or zero real part. Then if we consider the projection of this linearised system (2.16) onto the eigenspaces $\mathbb{R}^s, \mathbb{R}^u, \mathbb{R}^c$ we find that it decomposes into three independent systems

$$\dot{\tilde{\mathbf{w}}}^s = S\tilde{\mathbf{w}}^s \quad \text{and} \quad \dot{\tilde{\mathbf{w}}}^u = U\tilde{\mathbf{w}}^u \quad \text{and} \quad \dot{\tilde{\mathbf{w}}}^c = C\tilde{\mathbf{w}}^c \tag{2.19}$$

where $\tilde{\mathbf{w}} \in \mathbb{R}^n$ is the direct sum of its components, $\tilde{\mathbf{w}} = \tilde{\mathbf{w}}^s \oplus \tilde{\mathbf{w}}^u \oplus \tilde{\mathbf{w}}^c$. $\mathbb{R}^s$ is called the **stable subspace** of the system: all the solutions it contains decay exponentially. $\mathbb{R}^u$ is called the **unstable subspace** of the system: all the nonzero solutions it contains grow exponentially. $\mathbb{R}^c$ is called the **centre subspace** of the system: the solutions it contains are either bounded and non-trivial, or they grow non-exponentially to infinity.

Example 2.13. *The previous passage may be hard to digest. We include an example to explain exactly what is implied. Consider the system*

$$\dot{\mathbf{v}} = \begin{pmatrix} 0 & -1 & -1 \\ 1 & 0 & 1 \\ -1 & 1 & 0 \end{pmatrix} \mathbf{v} + \mathbf{g}(\mathbf{v}). \tag{2.20}$$

The nonlinearity $\mathbf{g}$ *satisfies the conditions above. Clearly the origin is a fixed point. If we linearise about the origin we will recover the following system*

$$\dot{\mathbf{w}} = \begin{pmatrix} 0 & -1 & -1 \\ 1 & 0 & 1 \\ -1 & 1 & 0 \end{pmatrix} \mathbf{w}. \tag{2.21}$$

We stop to note that the eigenvalues and eigenvectors of this matrix are

$$(\lambda_1, \lambda_2, \lambda_3) = (-1, 1, 0), \qquad W = \left(\begin{array}{c|c|c} \mathbf{w}_1 & \mathbf{w}_2 & \mathbf{w}_3 \end{array}\right) = \left(\begin{array}{c|c|c} 0 & -1 & 1 \\ -1 & 0 & 1 \\ 1 & 1 & -1 \end{array}\right). \tag{2.22}$$

If we introduce a new vector $\tilde{\mathbf{w}} = (\tilde{w}^s, \tilde{w}^u, \tilde{w}^c)^T$ *defined by*

$$\tilde{\mathbf{w}} = W^{-1}\mathbf{w}, \tag{2.23}$$

then our system (2.21) can be rewritten

$$\begin{aligned} \dot{\mathbf{w}} &= A\mathbf{w} && (2.24)\\ W\dot{\tilde{\mathbf{w}}} &= AW\tilde{\mathbf{w}} && (2.25)\\ \dot{\tilde{\mathbf{w}}} &= W^{-1}AW\tilde{\mathbf{w}} && (2.26)\\ \dot{\tilde{\mathbf{w}}} &= \begin{pmatrix} -1 & 0 & 0 \\ 0 & 1 & 0 \\ 0 & 0 & 0 \end{pmatrix}\tilde{\mathbf{w}}. && (2.27) \end{aligned}$$

This is easy to solve,

$$\tilde{\mathbf{w}} = \begin{pmatrix} Ae^{-t} \\ Be^{t} \\ C \end{pmatrix} \tag{2.28}$$

and the solution to our original system can be determined by transforming back,

$$\mathbf{w} = \begin{pmatrix} -Be^{t} + C \\ -Ae^{-t} + C \\ Ae^{-t} + Be^{t} - C \end{pmatrix}. \tag{2.29}$$

We write the coefficients A, B and C in terms of the initial value $\mathbf{w}(0) = (w_1, w_2, w_3)^T$,

$$\begin{aligned} A &= w_1 + w_3 \\ B &= w_2 + w_3 \\ C &= w_1 + w_2 + w_3. \end{aligned} \tag{2.30}$$

Consider the solutions that arise when the initial value $\mathbf{w}(0)$ is one of the eigenvectors $\mathbf{w}_i$. If we take $\mathbf{w}_1$ we find that $A = 1, B = 0, C = 0$, and so the resulting solution is just

$$\mathbf{w}(t) = \begin{pmatrix} 0 \\ -e^{-t} \\ e^{-t} \end{pmatrix}. \tag{2.31}$$

In fact, any solution with initial condition on $\mathbb{R}^s$ will decay exponentially. Similarly, the solutions with initial condition on $\mathbb{R}^u$ will grow exponentially, and solutions with initial condition on $\mathbb{R}^c$ will remain constant.

So we have seen that the linearised system can easily be solved by exploiting its underlying structure. In the example above the stable, unstable and centre subspaces ($\mathbb{R}^s, \mathbb{R}^u, \mathbb{R}^c$) were just the one-dimensional eigenspaces. We would like to know whether the nonlinear system has a similar structure, and whether we can exploit it. It does, and we reproduce the result below. See [31] or [42] for proof.

Theorem 2.14. *Given the system (2.13) there exists a neighborhood V_0 of the origin of $\mathbb{R}^n$ and a regular coordinate transformation $r : V_0 \to \tilde{V}_0$ of this*

neighborhood onto a second neighborhood $\tilde{V}_0$ of the origin such that $r(0) = 0$, the flow $\phi(t, \mathbf{v})$ is transformed to the flow $\psi(t, \tilde{\mathbf{v}}) = (r \circ \phi \circ r^{-1})(t, \tilde{\mathbf{v}})$[†] which has the form

$$\psi(t, \tilde{\mathbf{v}}) = \begin{pmatrix} e^{St} & 0 & 0 \\ 0 & e^{Ut} & 0 \\ 0 & 0 & e^{Ct} \end{pmatrix} \tilde{\mathbf{v}} + \tilde{G}(t, \tilde{\mathbf{v}}). \tag{2.32}$$

The $s \times s$ matrix e^{St} has eigenvalues with modulus less than 1 for all t. The $u \times u$ matrix e^{Ut} has eigenvalues with modulus greater than 1 for all t. The $c \times c$ matrix e^{Ct} has eigenvalues with modulus equal to 1 for all t. The vector function $\tilde{G}(t, \tilde{\mathbf{v}})$ is the direct sum of three vector functions $\tilde{G}^s(t, \tilde{\mathbf{v}}), \tilde{G}^u(t, \tilde{\mathbf{v}}), \tilde{G}^c(t, \tilde{\mathbf{v}})$ with dimension s, u and c respectively. Further

$$\begin{array}{l} \tilde{G}^u(t, (\tilde{\mathbf{v}}^s, 0, 0)) = 0 \quad \text{and} \quad \tilde{G}^c(t, (\tilde{\mathbf{v}}^s, 0, 0)) = 0 \\ \tilde{G}^s(t, (0, \tilde{\mathbf{v}}^u, 0)) = 0 \quad \text{and} \quad \tilde{G}^c(t, (0, \tilde{\mathbf{v}}^u, 0)) = 0 \end{array} \tag{2.33}$$

where $\tilde{\mathbf{v}} = \tilde{\mathbf{v}}^s \oplus \tilde{\mathbf{v}}^u \oplus \tilde{\mathbf{v}}^c$. The same coordinate transformation reduces our system to

$$\begin{array}{rcl} \dot{\tilde{\mathbf{v}}}^s & = & S\tilde{\mathbf{v}}^s + \tilde{g}^s(\tilde{\mathbf{v}}^s, \tilde{\mathbf{v}}^u, \tilde{\mathbf{v}}^c), \\ \dot{\tilde{\mathbf{v}}}^u & = & U\tilde{\mathbf{v}}^u + \tilde{g}^u(\tilde{\mathbf{v}}^s, \tilde{\mathbf{v}}^u, \tilde{\mathbf{v}}^c), \\ \dot{\tilde{\mathbf{v}}}^c & = & C\tilde{\mathbf{v}}^c + \tilde{g}^c(\tilde{\mathbf{v}}^s, \tilde{\mathbf{v}}^u, \tilde{\mathbf{v}}^c). \end{array} \tag{2.34}$$

S, U, C are $s \times s$, $u \times u$ and $c \times c$ matrices respectively with strictly negative, strictly positive or zero real parts of their eigenvalues respectively. The functions $\tilde{g}$ satisfy

$$\begin{array}{l} \tilde{g}^u(\tilde{\mathbf{v}}^s, 0, 0) = 0 \quad \text{and} \quad \tilde{g}^c(\tilde{\mathbf{v}}^s, 0, 0) = 0 \\ \tilde{g}^s(0, \tilde{\mathbf{v}}^u, 0) = 0 \quad \text{and} \quad \tilde{g}^c(0, \tilde{\mathbf{v}}^u, 0) = 0 \end{array} \tag{2.35}$$

and their direct sum is the original function $\tilde{g}$, i.e. $\tilde{g}(\tilde{\mathbf{v}}) = (\tilde{g}^s \oplus \tilde{g}^u \oplus \tilde{g}^c)(\tilde{\mathbf{v}})$.

This decomposition is similar to the one we have discussed in the example above. However, since we are now considering the entire system, including its nonlinearity, the decomposition is no longer as simple as the one we've already seen. Instead of decomposing onto the three subspaces $\mathbb{R}^s$, $\mathbb{R}^u$ and $\mathbb{R}^c$ we have decomposed the nonlinear system onto three invariant manifolds, M_s, M_u and M_c.

Definition 2.15. *A **local invariant manifold** of the system (2.13) or of the flow $\phi(t, \mathbf{v})$, is a differentiable manifold M passing through the origin such that there exists an ϵ such that $\forall \mathbf{v} \in M$, $|\phi(t, \mathbf{v})| < \epsilon \Rightarrow \phi(t, \mathbf{v}) \in M$.*

[†]This is an abuse of notation. We should really introduce a new transformation $\hat{r} = I \times r : \mathbb{R} \times V_0 \to \mathbb{R} \times \tilde{V}_0$ to account for the time.

Definition 2.16. *The locally invariant manifolds*

$$\begin{aligned} M_s &= \{\mathbf{v} \in V_0; \mathbf{v} = r^{-1}(\tilde{\mathbf{v}}^s, 0, 0), (\tilde{\mathbf{v}}^s, 0, 0) \in \tilde{V}_0\} \\ M_u &= \{\mathbf{v} \in V_0; \mathbf{v} = r^{-1}(0, \tilde{\mathbf{v}}^u, 0), (0, \tilde{\mathbf{v}}^u, 0) \in \tilde{V}_0\} \end{aligned} \tag{2.36}$$

are called the ***stable*** *and* ***unstable manifolds of the equilibrium point.***

Consider an initial point $(\tilde{\mathbf{v}}_0^s, 0, 0) \in \tilde{V}_0$. Let $\tilde{\mathbf{v}}_t = \psi(t, (\tilde{\mathbf{v}}_0^s, 0, 0))$. From (2.32) and (2.33) we see that for all time $\tilde{\mathbf{v}}_t = (\tilde{\mathbf{v}}_t^s, 0, 0)$. It follows immediately that M_s is a locally invariant manifold. Further, from the condition on the eigenvalues of the matrix e^{St} we know that this solution will tend exponentially to zero, and so the solution $\mathbf{v}_t = \phi(t, r^{-1}(\tilde{\mathbf{v}}_0)) = r^{-1}(\psi(t, \tilde{\mathbf{v}}_0))$ will also decay. Similar analysis holds for the unstable manifold, but we will find that the solutions tend to infinity.

If $c = 0$, i.e. the system is hyperbolic, then our analysis is complete. Every solution that tends to zero as $t \to \pm\infty$ must locally be contained in M_s or M_u respectively. If, however, $c \neq 0$ we can define a third locally invariant manifold, the centre manifold of the system. Again, we present the result without proof, see [77] for details.

Theorem 2.17. *Given the system 2.13 there exists a neighborhood $V_0 \subset \mathbb{R}^n$ of the origin and a mapping $h : \mathbb{R}^c \to \mathbb{R}^s \oplus \mathbb{R}^u$, $h \in C^k(\mathbb{R}^c)$, $h(0) = 0$ and $J_h(0) = 0$ such that the set*

$$M_c = \{\mathbf{v}_c \oplus h(\mathbf{v}_c) \in \mathbb{R}^n; \mathbf{v}_c \in \mathbb{R}^c\} \tag{2.37}$$

is a locally invariant manifold of the system in V_0 and if for $\mathbf{v} \in V_0$, $\phi(t, \mathbf{v}) \in V_0$ for all t then $\mathbf{v} \in M_h$. M_h is the ***local centre manifold*** *of the system.*

In the same way that solutions on M_s and M_u tend to the origin as $t \to \pm\infty$, solutions that are bounded for all time, i.e. they stay near the origin, must be contained in M_c. One last point to note about the centre manifold is that it is not necessarily unique, [77]. Finally we are in a position to state the centre manifold theorem. Again, see [77] for a proof. Recall that we are interested in bifurcations where the behaviour of the system changes, and so we consider the case where the system is initially stable, i.e. $u = 0$.

Theorem 2.18. ***Centre manifold theorem.*** *Given a system (2.13) where the matrix A has eigenvalues such that $s > 0$, $c > 0$, $u = 0$. Let M_c be a local centre manifold of the system. Then there exists a neighborhood $V_0 \subset \mathbb{R}^n$ of the origin and an α with $0 < \alpha < \min_{1 \leq i \leq s} |\mathrm{Re}[\mu_i]|$ where μ_i are the eigenvalues of A with negative real part such that*

1. *if $\mathbf{v} \in M_c \cap V_0$, and $\phi(t, \mathbf{v}) \in V_0$, then $\phi(t, \mathbf{v}) \in M_c$.*
2. *if $\mathbf{v} \in V_0$, and for $t \in (-\infty, 0]$ we have $\phi(t, \mathbf{v}) \in V$, then $\mathbf{v} \in M_c$.*

3. *if* $\mathbf{v} \in V_0$, *and the closure of the positive semitrajectory of* $\mathbf{v}$ *is contained in* V_0, *then there exists a* $t_0 \geq 0$ *and an* $\mathbf{m} \in M_c \cap V_0$ *such that*

$$\sup_{t \geq t_0} \exp(\alpha t)|\phi(t, \mathbf{v}) - \phi(t - t_0, \mathbf{m})| < \infty \tag{2.38}$$

In the theorem above proposition 2.18.1 just restates that the manifold is locally invariant in the neighborhood V_0. Proposition 2.18.2 states that any solution which remained near the origin in the past has an initial value on the centre manifold. This is obvious, since there is no unstable manifold and any initial value on the stable manifold would grow exponentially as $t \to -\infty$. Finally proposition 2.18.3 states that any solution which remains near the origin will tend to a solution with an initial condition on the centre manifold, and the distance between these two solutions will decrease exponentially. Put simply, the manifold M_c is locally attractive. This theorem is important in the proof of the Hopf bifurcation theorem which we state below with a rough outline of its proof.

Theorem 2.19. ***Hopf bifurcation theorem*** *[36]. Given a system*

$$\dot{\mathbf{v}} = f(\mathbf{v}; \zeta) \tag{2.39}$$

where $f \in C^{k+1}(\mathbb{R}^n \times \mathbb{R})$, $k \geq 4$ *and* $f(0; \zeta) = 0$. *Consider the case when for small* $|\zeta|$ *the Jacobian matrix* $J_f(0; \zeta)$ *has a pair of complex conjugate eigenvalues* $\alpha \pm i\beta$ *with* $\alpha(0) = 0$ *and* $d\alpha/d\zeta(0) > 0$ *and all its other eigenvalues have strictly negative real part. Then*

1. *there exists a* $\delta > 0$ *and a function* $\zeta \in C^{k-2}((-\delta, +\delta), \mathbb{R})$ *such that for* $\epsilon \in (0, +\delta)$ *the system* $\dot{\mathbf{v}} = f(\dot{\mathbf{v}}; \zeta(\epsilon))$ *has a periodic solution* $p(t, \epsilon)$ *with period* $T(\epsilon) > 0$, $T \in C^{k-2}(\mathbb{R})$, $\zeta(0) = 0$, $T(0) = 2\pi/\beta(0)$, $p(t, 0) = 0$ *and the amplitude of this periodic solution is proportional to* $\sqrt{\epsilon}$.

2. *the origin* $(\mathbf{v}, \zeta)$ *has a neighbourhood* $V \subset \mathbb{R}^n \times \mathbb{R}$ *that does not contain any periodic orbits except those belonging to the family* $p(t, \epsilon)$.

3. *if the origin* $\mathbf{v} = 0$ *is an asymptotically stable (or unstable) equilibrium of the system* $\dot{\mathbf{v}} = f(\mathbf{v}, 0)$, *then* $\zeta(\epsilon) > 0$ *(or* $\zeta(\epsilon) < 0$*) for* $\epsilon \neq 0$ *and the periodic solution* $p(t, \epsilon)$ *is stable (or unstable).*

Before we outline a proof for this theorem we should endeavour to understand it and check that it describes the situation introduced in section 2.2.3.

Indeed, we see that it describes a periodic solution in proposition 2.19.1 that appears when the parameter ζ moves through zero, and gives a value for its period, T. (Note that setting the bifurcation point to zero and the fixed point of the system to the origin can be done without a loss of generality; we can always transform to a new parameter $\zeta' = \zeta - \zeta_0$ and variable $\mathbf{v}' = \mathbf{v} - \mathbf{v}_0$

to meet these requirements.) Further, proposition 2.19.2 states that this is the only periodic solution near the bifurcation point and 2.19.3 states that the periodic solution that appears inherits the stability of the stationary solution. Theorem 2.19 has formalised the naive description of section 2.2.3, and we now understand rigorously the transition from fixed points to closed orbits.

The Hopf bifurcation theorem is important to our work. It guarantees the existence of the temporally periodic solitons we would like to investigate, and gives us an initial value for the period, T. We use this value as our initial guess when we solve the PDDNLS as a two-dimensional boundary value problem through Newtonian iteration.

To conclude this section we outline a proof for theorem 2.19. Interested readers may refer back to [23] for details. The first part of the proof is to prove the Hopf bifurcation theorem in the two-dimensional case. In the second part of the proof the system is recast in the form

$$\dot{\mathbf{v}} = J_f(\mathbf{v};\zeta)\mathbf{v} + g(\mathbf{v};\zeta) \tag{2.40}$$

with some conditions on the value and continuity of g and its derivatives at the fixed and bifurcation points. At $\zeta = 0$ the matrix $J_f(0;\zeta)$ has a pair of complex conjugate eigenvalues $\mu_{1,2} = \alpha \pm i\beta$ and $n-2$ eigenvalues with strictly negative real part. The eigenspace spanned by the two eigenvectors corresponding to $\mu_{1,2}$ is $\mathbb{R}^c = \mathbb{R}^2$.

While ζ is fixed at zero, the system has a two dimensional centre manifold M_2 whose tangent spaces is just $\mathbb{R}^c$, and this is the space to which we would like to reduce this problem. Unfortunately, it is not a centre manifold if we allow ζ to change. To remedy this, the equation

$$\dot{\zeta} = 0 \tag{2.41}$$

is appended to the original system and a three dimensional centre manifold M_3 of the new system is introduced. The properties of the centre manifold discussed above are used to simplify the system, after which it is projected back onto M_3 and reduced to

$$\dot{\zeta} = 0, \quad \frac{d}{dt}\begin{pmatrix} v_1 \\ v_2 \end{pmatrix} = \begin{pmatrix} \alpha(\zeta) & -\beta(\zeta) \\ \beta(\zeta) & \alpha(\zeta) \end{pmatrix}\begin{pmatrix} v_1 \\ v_2 \end{pmatrix} + \begin{pmatrix} G_1(v_1, v_2, \zeta) \\ G_2(v_1, v_2, \zeta) \end{pmatrix}. \tag{2.42}$$

Finally, ζ is discarded as a variable and treated only as a parameter. We recover a two-dimensional system, and this case has been dealt with in the first part of the proof.

2.4 Bifurcations of closed orbits

In section 2.3 we introduced the Hopf bifurcation theorem which explains how periodic solutions, i.e. closed orbits of the flow, are generated when

the system passes through a Hopf bifurcation point. Like the fixed points in section 2.2, these closed orbits can undergo bifurcations of their own. We will discuss three types of bifurcations of periodic solutions: saddle-node, period-doubling and Hopf bifurcations of periodic solutions.

Before we discuss the bifurcations we reiterate the distinction between the eigenvalues ,μi of the operator, and the corresponding multipliers Ai = exp[μ_iT]. Assuming the solution is initially stable, it will lose its stability when one of its eigenvalues passes into the positive half-plane, or equivalently, when one of the multipliers passes through the unit circle.

2.4.1 Saddle-node bifurcation of cycles

The **saddle-node bifurcation** is characterised by a single multiplier passing through the unit circle via the point (1, 0) on the complex plane. It's analogous to the saddle-node bifurcation of fixed points described in section 2.2.1. As (is changed and the system undergoes a saddle-node bifurcation a pair of closed orbits appear simultaneously, then split into a stable orbit and unstable orbit. Conversely, if the system passes through the bifurcation point in the other direction we observe the collision, and subsequent disappearance, of a stable and unstable closed orbit.

Note that in this thesis we will never observe the sudden appearance of a pair of closed orbits. Rather, we will follow a particular periodic solution as the driving strength b (which plays the part of () changes and any saddle-node bifurcations will indicate that the branch we're following has turned and doubled back on itself. By way of graphical explanation, in figure 2.4 we would follow the parabola through its turning point rather than moving along the (axis until the turning point of the parabola appears. See chapter 3 for a discussion of numerical continuation, and chapter 5 for some examples.

2.4.2 Period-doubling bifurcation

The **period-doubling bifurcation** is characterised by a single multiplier passing through the unit circle via the point (-1, 0) on the complex plane. As (is changed and a closed orbit (with period T) undergoes a period-doubling bifurcation it loses its stability, and a new closed orbit with period 2T appears. Again, chapter 5 includes some examples of period-doubling.

The period-doubling bifurcation is important in the transition of a system to chaos as the parameters controlling its behaviour change. We discuss briefly Feigenbaum's work on the logistic map [24] by means of introduction to period-doubling, chaos and its universality.

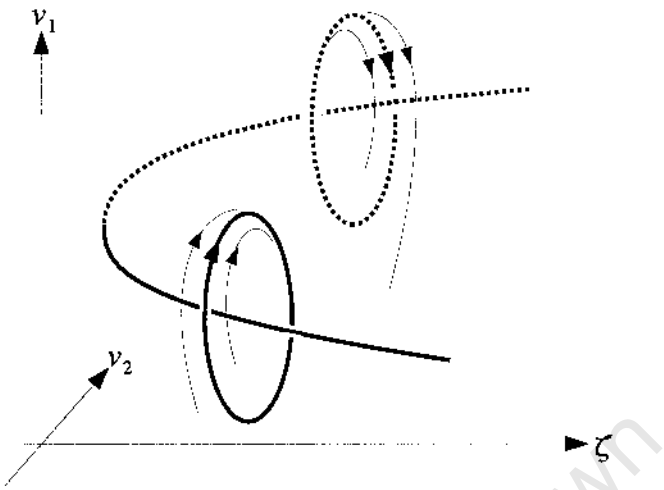

Figure 2.4: Generic saddle-node bifurcation of a closed orbit. The thick solid and dashed circles represent a stable and unstable closed orbit, while the thick solid and dashed line represents the branch of periodic solutions in $(\mathbf{v}, \zeta)$ space.

The logistic map: the period-doubling route to chaos

The logistic map is the one-dimensional, one parameter map

$$x_{n+1} = rx_n(1 - x_n), \qquad r > 0. \tag{2.43}$$

If we consider the case when $x_{n+1} = x_n$ we find two fixed points, $\bar{x}_0 = 0$ and $\bar{x}_r = 1 - (1/r)$. We will consider how the behaviour changes as r increases.

While $0 < r < 1$, $\bar{x}_0$ is stable, and all initial conditions (except $x_0 = \bar{x}_r$) tend to it. Once $r \geq 1$ we can immediately simplify the problem by considering only initial conditions in the interval $[0, 1]$. If x_i is ever negative, then $x_{i+1} - x_i$ will also be negative, and so the solution will tend to $-\infty$. Conversely, if $x_i > 1$ then $x_{i+1} < 0$ and so the solution will tend to $-\infty$ as well.

As r increases we observe the following behaviour, some examples are included in figure 2.5. Note that the choice of initial condition, as long as it lies in the interval $[0, 1]$, is qualitatively irrelevant to the behaviour.

1. For $1 < r \leq 2$ the solution converges directly to the fixed point $\bar{x}_r$.

2. For $2 < r < 3$ the solution oscillates around the fixed point $\bar{x}_r$ before converging linearly to it.

3. For $r = 3$ the solution oscillates around $\bar{x}_r$ before converging sublinearly to it.

4. For $3 < r < (3.45 \sim)$ the solution converges to a two point closed orbit around $\bar{x}_r$, i.e. $x_0 \mapsto x_1 \mapsto \cdots \mapsto x_p \mapsto x_q \mapsto x_p \mapsto x_q \mapsto \cdots$ where $x_p < \bar{x}_r < x_q$.

5. For $(3.45 \sim) < r < (3.54 \sim)$ the solution converges to a four point closed orbit around $\bar{x}_r$, i.e. $x_0 \mapsto x_1 \mapsto \cdots \mapsto x_p \mapsto x_q \mapsto x_s \mapsto x_t \mapsto x_p \mapsto x_q \mapsto x_s \mapsto x_t \mapsto \cdots$ where two of the points are smaller than $\bar{x}_r$ and two are greater than it.

6. For $(3.54 \sim) < r < (3.57 \sim)$ the solution converges to a closed orbit around $\bar{x}_r$ with an increasing number of points, first an eight point closed orbit, then a sixteen point closed orbit etc.

7. For $(3.57 \sim) < r < 4$ the system is chaotic. There are some intervals of r for which the system returns to an ordered, closed orbit before undergoing a series of period-doubling bifurcations and then returning to chaos.

8. For $4 \leq r$ any initial condition is almost everywhere divergent, i.e. most initial conditions x_0 will eventually bounce out of the interval $[0, 1]$ and x_n will tend to $-\infty$ as discussed above. Further, the initial conditions that do not diverge but instead behave chaotically form a set with measure zero [46].

This is the seminal example of the period-doubling route to chaos discussed by Feigenbaum. In his work he made a series of further observations. If we label the values of r where the two, four, eight, sixteen...point closed orbits appear by $r_1, r_2, r_3, \ldots$ then the ratio of distances between successive period-doubling bifurcations tends to a constant, i.e.

$$\lim_{i \to \infty} \frac{r_i - r_{i-1}}{r_{i+1} - r_i} = \delta = 4.66920\ldots. \tag{2.44}$$

In addition, if we consider the series of period-doubling bifurcations that restore chaos when 3.57 < r, e.g. when r = 3.839 and there is a three point closed orbit, then the ratio of distances between these successive period-doubling bifurcations tends to this same constant. He also proposed that the same holds for the period-doubling route to chaos in any one-dimensional map with a quadratic maximum. In 1982 his conjectures were proved by Oscar E. Lanford **III** using a computer-assisted proof [51].

2.4.3 Hopf bifurcation of cycles

The **Hopf bifurcation** is characterised by a complex conjugate pair of multipliers passing through the unit circle. As (changes and a closed orbit undergoes a Hopf bifurcation, this periodic solution becomes unstable, and a stable quasiperiodic solution is born. This situation is quite difficult to

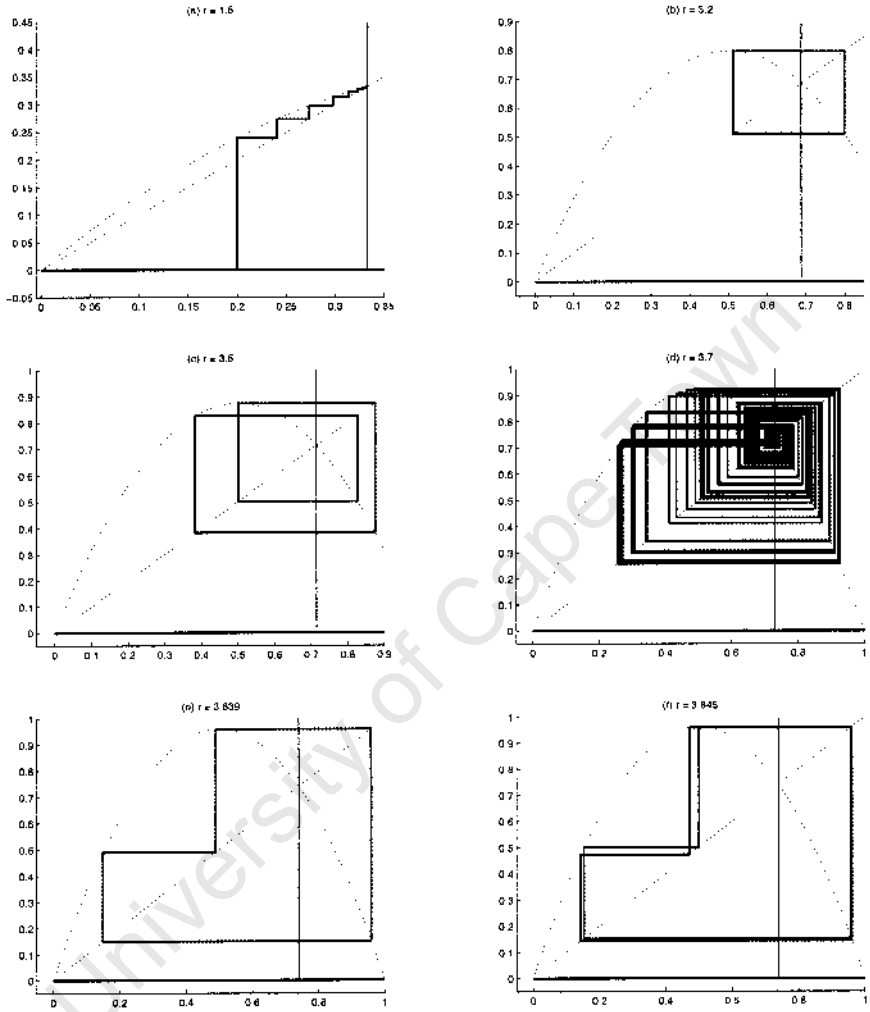

Figure 2.5: Behaviour of the logistic map as the parameter r changes: (a) shows the initial value $x = 0.2$ converging to a fixed point, (b) shows a closed orbit around the fixed point, (c) shows the closed orbit after the first period-doubling, (d) shows the chaotic behaviour of the system, (e) shows a periodic orbit with three points that arises at $h = 3.839$ and (f) shows its period doubling to a six point closed orbit. In plots (b) - (f) the first 10000 iterations were discarded to remove transient behaviour.

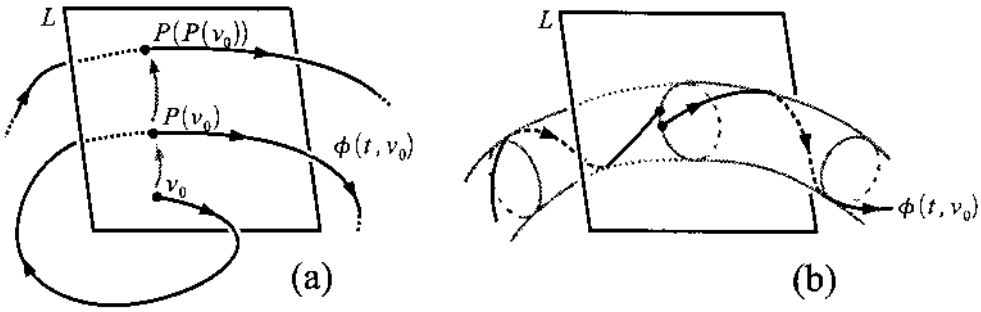

Figure 2.6: The Poincaré map: (a) shows the general action of the map, (b) shows the closed orbit in L and the quasiperiodic motion of the solution after the Hopf bifurcation.

visualise. One of the tools we can use to better understand the behaviour is the Poincaré map.

Definition 2.20. *Consider an n-dimensional autonomous system of differential equations*

$$\dot{\mathbf{v}} = f(\mathbf{v}; \zeta) \tag{2.45}$$

*which generates a flow 0(t, v). Let v_o be the initial condition, and L be an n — **1** dimensional hyperplane containing v_o and transversal to its path. Assume that there exists r(v_o) such that 0(7,* vo) E *L. Then by the continuity of the flow with respect to initial conditions there exists a neighborhood V C L of v_o such that*

$$P : V \to L, \qquad P(\mathbf{v}) = \phi(\tau(\mathbf{v}), \mathbf{v}) \tag{2.46}$$

*is well-defined. This is the **Poincaré map.***

The action of this map is illustrated on the figure 2.6.a. Note that if the motion of vo is a periodic function, then P(vo) = vo, i.e. we will observe only a single point on *L.* If the system underwent a period-doubling bifurcation of the type described above, we would observe two points on ***L.*** Continued doublings would introduce additional points.

Conversely, as (changes and the original system undergoes a Hopf bifurcation of its periodic solution, we observe that the fixed point of the Poincare map undergoes a Hopf bifurcation of its own. (For a detailed discussion please see [54) Unlike the single-, double-, quadruple- etc... period solutions above which pass through a finite number of points on ***L,*** our solution now passes through a continuous closed orbit in ***L,*** see figure 2.6.b.

We can think of our periodic solution with period T_1 being modulated by a second periodic function with period T2 such that the fraction T_1/T_2 is irrational. In this way the trajectory will wrap itself around a hyper-torus

in Rn and form a dense set on its surface. The Ruelle-Takens theory [70] views this bifurcation from a stable periodic solution onto the surface of a torus as the start of turbulence in a system.

Chaos, turbulence and strange attractors

We have already discussed the first mechanism that may lead our system to chaos: the period-doubling route to chaos, or Feigenbaum cascade. There is a second mechanism we discuss now, the quasi-periodic route of Ruelle-Takens.

Turbulent behaviour in physical systems, e.g. in fluid dynamics, has previously been described by Hopf [37] and Landau [50]. They assume that the behaviour is described by a quasi-periodic flow

$$v(t) = \mathbf{f}(\omega_1 t, \ldots, \omega_k t) \tag{2.47}$$

where **f** is periodic in each of its arguments with period **1** and w_i are not rationally related. Further, as the control parameter (is increased the system undergoes a series of Hopf bifurcations and k increases, leading to more complicated behaviour. In practice the behaviour alternates between this fully quasi-periodic motion and simpler quasi-periodic, or even periodic, motion as frequency locking of the arguments occurs intermittently [64].

This approach to turbulent behaviour is problematic. These quasi-periodic functions do not occur generically, unlike the turbulence itself which is observed in many physical systems. After Lorenz's work on chaos [53] which introduced the strange attractor, Ruelle and Takens [70] proposed an alternative mechanism to explain turbulent behaviour. In their model, chaos is explained by the appearance of a strange attractor after a *finite* number of Hopf bifurcations.

We can summarise our findings as follows. We consider a system

$$\dot{\mathbf{v}} = F(\mathbf{v}; \zeta). \tag{2.48}$$

As the parameter (is changed, the behaviour of the system changes. Firstly, its fixed points may undergo a number of bifurcations: saddle-node, pitch-fork and Hopf. The Hopf bifurcations are the most relevant to our discussion, since at these points a branch of periodic orbits appears. Secondly, these periodic orbits may undergo bifurcations of there own as (changes: saddle-node, period-doubling and Hopf. Thirdly, the system may transition to chaos through an *infinite* series of period-doubling bifurcations or a *finite* series of Hopf bifurcations.

We proceed now to chapter 3 on numerical continuation where we discuss how to trace these branches of periodic solutions, and then to chapter 4 where we discuss various methods of determining the eigenvalues of the PDDNLS and identifying these bifurcations.

Chapter 3

Continuation methods

In this chapter we discuss continuation methods. We will provide a general exposition which highlights the sort of problems they can solve while also explaining specifically how periodic solutions to the PDDNLS can be derived from its stationary soliton solutions v+ by applying these continuation methods.

Continuation methods are tools to determine a solution of the nonlinear, algebraic systems of equations

$$\mathrm{F}(\mathrm{y}) = \mathbf{0}. \tag{3.1}$$

For the remainder of our discussion we assume that the map F(y) : Rn is smooth, i.e. it is continuous and its derivatives are continuous.

If a good initial guess is available, it is easy to determine a stationary point iteratively by approximating the Jacobian of F and using a Newton-like method. More commonly, there is no a *priori* knowledge of the solution and we need a smarter way of choosing our initial guess. The general idea is to start with a known solution yG of a related (preferably simpler) smooth map G(y) : Rn --- Rn, and then to deform this map back to F while updating the solution.

Definition 3.1. A ***homotopy*** *from G to* F *is* a *smooth map*

$$H(\mathbf{y}, \xi) : \mathbb{R}^n \times \mathbb{R} \rightarrow \mathbb{R}^n \tag{3.2}$$

such that there exist $\xi_{\mathrm{F}}, \xi_{\mathrm{G}} \in \mathbb{R}$ *satisfying*

$$H(\mathbf{y}, \xi_{\mathrm{G}}) = G(\mathbf{y}) \quad \text{and} \quad H(\mathbf{y}, \xi_{\mathrm{F}}) = F(\mathbf{y}). \tag{3.3}$$

There are a number of systematic ways to introduce a homotopy, the simplest is just the **convex homotopy** defined by

$$H(\mathbf{y}, \xi) = \xi F(\mathbf{y}) + (1 - \xi) G(\mathbf{y}). \tag{3.4}$$

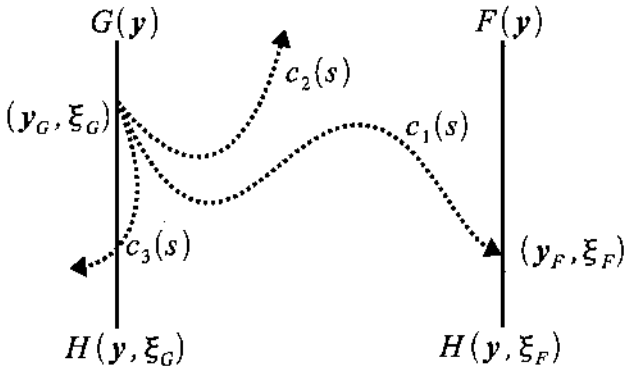

Figure 3.1: Possible options for the curve $c(s)$.

Whatever choice we make for the homotopy, we are looking for a curve $c(s) : \mathbb{R} \to \mathbb{R}^n \times \mathbb{R}$ which runs from our starting point $(\mathbf{y}_G, \xi_G)$ to a point $(\mathbf{y}_F, \xi_F)$ such that

$$H(\mathbf{y}, \xi) = 0 \tag{3.5}$$

for all $(\mathbf{y}, \xi)$ lying on the curve $c(s)$. Figure 3.1 shows some possible options for this curve. Some problems are immediately apparent.

1. How do we know a curve $c(s)$ passing through $(\mathbf{y}_G, \xi_G)$ with $H(c(s)) = 0$ exists?

2. If this curve exists, how do we know whether it reaches a point $(\mathbf{y}_F, \xi_F)$ instead of doubling back on itself or tending to infinity?

3. If this curve exists and reaches a point $(\mathbf{y}_F, \xi_F)$, how do we trace it?

The third question is the easiest to answer. There are two main approaches to tracing this curve $c(s)$: predictor-corrector (PC) continuation methods and piecewise-linear (PL) continuation methods. The bulk of this chapter will be spent discussing PC methods (see section 3.1) and the various ways to implement them.

The remaining two questions are trickier. The implicit function theorem guarantees the existence of the curve near $(\mathbf{y}_G, \xi_G)$ when it is a regular zero point of H. In the general case guaranteeing that $c(s)$ intersects $(\mathbf{y}_F, \xi_F)$ in finite length is much more difficult. We'll consider the specific case of the PDDNLS below, but interested readers may consult chapter 11 of Allgower and Georg [5] for a broader analysis.

In our case we can reduce the PDDNLS with periodic temporal boundary conditions and infinite spatial boundary conditions to a system of nonlinear equations by discretizing x and t over the domain $[-L, L] \times [0, T]$ and replacing the derivatives with finite difference formulae. It is necessary to choose

L sufficiently large to prevent any interaction between the boundaries and the spatially localised solitons. We discretize space over J points, and time over K points. The main difference in our specific case is that we have an additional parameter, the period T, which varies as ξ changes.

Now $H(\mathbf{y}, T, \xi) : \mathbb{R}^{2JK} \times \mathbb{R}^2 \to \mathbb{R}^{2JK}$ is just the discretized PDDNLS with a fixed value of the damping γ and the starting point $(\mathbf{y}_G, T_G, \xi_G)$ is defined by

1. $\xi_G = h_{HB}(\gamma)$. Here $h_{HB}(\gamma)$ is the point of Hopf bifurcation.
2. $\mathbf{y}_G$ is the corresponding discretization of the well known ψ_+ soliton for the particular values of γ and h_{HB}. We've split this into real and imaginary parts which introduces the factor of 2 in $\mathbb{R}^{2JK}$.
3. An initial guess for the additional parameter T can be determined using the Hopf bifurcation theorem. If we return to section 2.3 we see that the period of the solution at the Hopf bifurcation point is given by $T = \frac{2\pi}{\beta}$, where $\pm\beta$ is the imaginary component of the complex conjugate pair of characteristic exponents that pass into the positive half-plane.

The role of e is played by the driving strength h. Further, some of the problems listed on the previous page are not relevant to our system. We're not interested in finding a solution at a particular value of h, but just in the shape of the curve after the Hopf bifurcation point. Thus, if the curve doubles back on itself or tends to infinity we'll just follow it as long as is necessary, or possible, and record that behaviour as our result.

Finally, we elected to use natural parameterization and so instead of considering y, h and T as functions of s, the arclength, we instead consider y(h) and $T(h)$. Subsection 3.1.3 includes more detail.

3.1 Predictor-corrector methods

The simplest class of continuation methods are the PC methods we discuss in this section. The core idea is to trace the curve $c(s)$ iteratively while alternating between predicting the next value and then correcting this initial guess. In this sense it is similar to the predictor-corrector methods used to solve differential equation, particularly initial value problems, but there is one important difference. Since the curve $c(s)$ satisfies $\mathrm{H}(\mathrm{y},) = 0$ the correction step can exploit the same local contraction properties responsible for the convergence of Newton-like methods near the roots of nonlinear equations.

We need to formalise this core idea before we proceed to a more rigorous discussion of PC methods. Pick $\epsilon > 0$ as our tolerance. Then let $(\mathbf{y}_n, \xi_n)$ be a solution to $|H(\mathbf{y}, \xi) < \epsilon|$ with $\xi_n \in [\xi_G, \xi_F]$. Denote the next guess

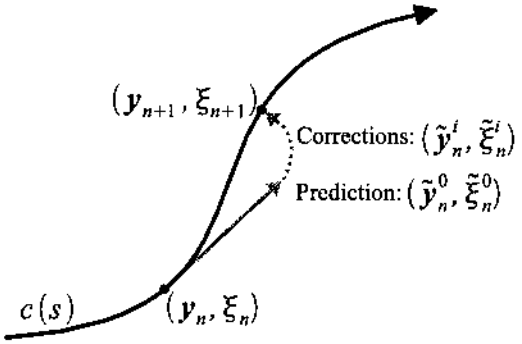

Figure 3.2: One iteration of a general PC method.

$(\tilde{\mathbf{y}}_n^0, \tilde{\xi}_n^0)$ and its subsequent corrections $(\tilde{\mathbf{y}}_n^1, \tilde{\xi}_n^1), (\tilde{\mathbf{y}}_n^2, \tilde{\xi}_n^2)$ etc... The first of these corrections satisfying $H(\tilde{\mathbf{y}}_n^m, \tilde{\xi}_n^m) < \epsilon$ is taken as the next step along the curve $c(s)$, i.e. $(\mathbf{y}_{n+1}, \xi_{n+1}) = (\tilde{\mathbf{y}}_n^m, \tilde{\xi}_n^m)$. We include pseudo-code for a general PC method below as well a graphical illustration of one iteration in figure 3.2.

Pseudo-code for a general PC method

`subroutine` H	*system*
`subroutine predict`	*predictor*
`subroutine correct`	*corrector*
$(\mathbf{y}_0, \xi_0) = (\mathbf{y}_G, \xi_G)$	*starting point*
$\epsilon > 0$	*tolerance*
$n = 0$	
`while` $\xi_n < \xi_F$	*continue to desired value*
$\quad m = 0$	
$\quad (\tilde{\mathbf{y}}_n^m, \tilde{\xi}_n^m) =$ `predict` $[(\mathbf{y}_n, \xi_n)]$	*predict the next step*
$\quad$ `while` $\|H[(\tilde{\mathbf{y}}_n^m, \tilde{\xi}_n^m)]\| < \epsilon$	*check tolerance*
$\quad\quad (\tilde{\mathbf{y}}_n^{m+1}, \tilde{\xi}_n^{m+1}) =$ `correct` $[(\tilde{\mathbf{y}}_n^m, \tilde{\xi}_n^m)]$	*correct guess*
$\quad\quad m = m + 1$	
$\quad (\mathbf{y}_{n+1}, \xi_{n+1}) = (\tilde{\mathbf{y}}_n^{m-1}, \tilde{\xi}_n^{m-1})$	*accept corrected guess*
$\quad n = n + 1$	

We have broadly outlined the method and can now proceed to some specifics. We will start by discussing various options for the predict and correct subroutines in the pseudo-code above (sections 3.1.1-3.1.2). This is followed by an explicit discussion of two concepts implicit in those subroutines: the parameterization of the problem and the step size of the predictor (sections 3.1.3-3.1.4).

3.1.1 Predictors

Predictors can be classified broadly into two sets of methods: ODE-type methods which rely on the value of $H(\mathbf{y}_n, \xi_n)$ and its derivatives, and polynomial extrapolation which needs only the solution values $(\mathbf{y}_i, \xi_i)$.

ODE-type methods

The $n \times (n+1)$ Jacobian matrix, $J(\mathbf{y}, \xi)$, of the system $H(\mathbf{y}, \xi)$ is composed of its partial derivatives

$$J = \left(\begin{array}{ccc|c} \partial_{y_1} h_1 & \dots & \partial_{y_n} h_1 & \partial_\xi h_1 \\ \vdots & & \vdots & \vdots \\ \partial_{y_1} h_n & \dots & \partial_{y_n} h_n & \partial_\xi h_n \end{array} \right). \tag{3.6}$$

For brevity we introduce the notation $J = (H_\mathbf{y} | H_\xi)$.

The simplest approach to continuation problems, **natural parameter continuation**, was first introduced by Davidenko [20]. If we take derivatives on both sides of (3.5) the result can be neatly expressed as

$$H_\mathbf{y} d\mathbf{y} + H_\xi d\xi = 0 \tag{3.7}$$

which means the problem can be reformulated as an initial value problem (IVP)

$$\begin{aligned} \mathbf{y}_\xi &= -(H_\mathbf{y})^{-1} H_\xi \\ \mathbf{y}(\xi_0) &= \mathbf{y}_0. \end{aligned} \tag{3.8}$$

This method has two advantages. Firstly, it's quite intuitive - the curve $c(s)$ is just traced out as the solution to our ODE, and secondly, it's easy to solve. There is one obvious shortcoming though: the method fails at turning points when the matrix $H_\mathbf{y}$ becomes singular.

The second approach we could adopt is the **tangent predictor**, used by Keller [41] and Rheinbolt [66]. Consider the tangent vector to our curve $c(s)$ in $\mathbb{R}^{n+1}$ defined by

$$\mathbf{t} = \left(\begin{array}{c} dy_1 \\ dy_2 \\ \vdots \\ dy_n \\ d\xi \end{array} \right). \tag{3.9}$$

We can rewrite (3.7) simply as $(H_\mathbf{y} | H_\xi)\mathbf{t} = 0$. This does not uniquely define the tangent vector though, so we need to introduce a normalisation. Let $\mathbf{e}_i$ by the i-th unit vector, i.e. all it's components are zero except for the i-th which is one. It's sufficient now to set

$$(\mathbf{e}_i)^T \mathbf{t} = 1 \tag{3.10}$$

and to append this condition to (3.7). Then the tangent vector is the unique solution to the linear system

$$\begin{pmatrix} H_{\mathbf{y}} | H_{\xi} \\ \hline (\mathbf{e}_i)^T \end{pmatrix} \mathbf{t} = \mathbf{e}_{n+1}. \tag{3.11}$$

Having calculated the tangent to the curve, we use it to predict the next point, i.e.

$$(\tilde{\mathbf{y}}_n^0, \tilde{\xi}_n^0) = (\mathbf{y}_n, \xi_n) + \sigma_n \mathbf{t}(\mathbf{y}_n, \xi_n). \tag{3.12}$$

This method will work as long as the path in $\mathbb{R}^{n+1}$ is regular, i.e. the Jacobian of the matrix in (3.11) is invertible, and it can follow the curve around turning points. The choice of the step length σ_n will be discussed in 3.1.4, and some more complicated methods, e.g. (pseudo-)arclength continuation, will be introduced when we deal with parameterizations in section 3.1.3.

Polynomial extrapolation

In contrast to the ODE-type methods above, polynomial extrapolation only requires the values of previous solutions $(\mathbf{y}_i, \xi_i)$ to (3.5) rather than any derivatives. The general idea is to fit a polynomial to the already calculated solutions $(\mathbf{y}_0, \xi_0), (\mathbf{y}_1, \xi_1), \ldots (\mathbf{y}_n, \xi_n)$ and extrapolate to predict $(\tilde{\mathbf{y}}_n^0, \tilde{\xi}_n^0)$.

It's possible to to construct this polynomial as a function of any of y_i or ξ, but for simplicity we assume that we continue in ξ. Lagrange's polynomial formula is

$$\mathbf{L}(\xi) = \sum_{i=0}^{n} \mathbf{y}_i \prod_{j=0, j\neq i}^{n} \frac{\xi - \xi_j}{\xi_i - \xi_j}. \tag{3.13}$$

The prediction is then just $(\tilde{\mathbf{y}}_n^0, \tilde{\xi}_n^0) = (\mathbf{L}(\xi_n + \delta\xi_n), \xi_n + \delta\xi_n)$. The choice of step size $\delta\xi_n$ will be discussed in more depth in section 3.1.4.

While we can, in theory, use a polynomial of degree n to make this prediction there are generally only two values used in practise. The first is the trivial case where the only data point available is the starting point and so the initial guess is just $(\tilde{\mathbf{y}}_0^0, \tilde{\xi}_0^0) = (\mathbf{y}_0, \xi_0 + \delta\xi_0)$.

The second case is the **secant predictor** shown in figure 3.3 below. This is just a polynomial extrapolation using two points, i.e. the prediction lies on a straight line connecting the previous two solutions.

$$(\tilde{\mathbf{y}}_n^0, \tilde{\xi}_n^0) = (\mathbf{y}_n, \xi_n) + (\delta\xi_n \times \frac{\mathbf{y}_n - \mathbf{y}_{n-1}}{\xi_n - \xi_{n-1}}, \delta\xi_n) \tag{3.14}$$

While higher order methods are sometimes used, see Haselgrove [32], it's normally more efficient to make a faster, worse prediction than a slower and slightly better one since the correction step enjoys strong contractive properties and converges superlinearly.

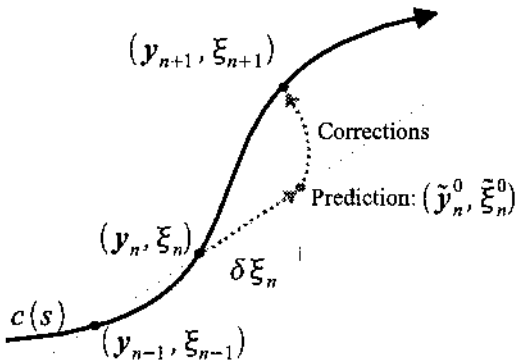

Figure 3.3: The secant predictor.

3.1.2 Correctors

The correction step consists of finding a solution $(\mathbf{y}_{n+1}, \xi_{n+1})$ to a nonlinear system of equations

$$H(\mathbf{y}, \xi) = 0 \tag{3.15}$$

when a good initial approximation $(\tilde{\mathbf{y}}_n^0, \tilde{\xi}_n^0)$ is available. This problem can be solved effectively by Newton or quasi-Newton methods which enjoy quadratic or superlinear convergence. (Please see Ortega and Rheinboldt [61] for a more thorough discussion of convergence properties and error analysis.)

At this stage we need to make a clear distinction between two possible sorts of systems that we will need to solve. The first is the sort we have already dealt with: $H(\mathbf{y}, \xi) : \mathbb{R}^n \times \mathbb{R} \to \mathbb{R}^n$, i.e. the system is underdetermined; there are $n+1$ unknowns $(y_1, \ldots, y_n, \xi)$ but only n equations. This becomes more pronounced in multiparameter problems, like solving the PDDDNLS, where there may be $n+k$ unknowns and only n equations.

The second sort of system will arise when we discuss parameterizations in 3.1.3. In some systems it's useful to introduce a parameterizing equation and the resulting system is, e.g.

$$H_{\text{EX.}}(\mathbf{y}(\rho), \xi(\rho)) = \begin{pmatrix} H(\mathbf{y}(\rho), \xi(\rho)) \\ P(\mathbf{y}(\rho), \xi(\rho)) \end{pmatrix} = 0. \tag{3.16}$$

The extended system $H_{\text{EX.}}(\mathbf{y}, \xi) : \mathbb{R}^n \times \mathbb{R} \to \mathbb{R}^n \times \mathbb{R}$ is no longer underdetermined and, more importantly, its Jacobian is square.

Denote the Jacobian of this extended system as $J_{\text{EX.}}$. Then the solution is easily determined by Newton's method,

$$(\tilde{\mathbf{y}}_n^{n+1}, \tilde{\xi}_n^{n+1}) = (\tilde{\mathbf{y}}_n^n, \tilde{\xi}_n^n) - \left[J_{\text{EX.}}(\tilde{\mathbf{y}}_n^n, \tilde{\xi}_n^n)\right]^{-1} H(\tilde{\mathbf{y}}_n^n, \tilde{\xi}_n^n). \tag{3.17}$$

This naive implementation of Newton's method should be modified before we can use it as a corrector.

1. Calculating the Jacobian matrices J or J_{EX} is numerically expensive. It is often preferable to calculate it only once at the initial guess and then update it at each step and use an approximation in equation (3.17). The first of these quasi-Newton algorithms was the Davidon-Fletcher-Powell (DFP) formula [21] but it has been replaced by the "good" Broyden [14] and Broyden-Fletcher-Goldfarb-Shanno (BFGS) methods [15, 25, 29, 74].

2. The Jacobian may not be invertible. In fact, it may not even be square. In these cases it is sufficient to replace the inverse $[J]^{-1}$ with the Moore-Penrose pseudoinverse $[J]^{+}$, i.e.

$$(\tilde{\mathbf{y}}_n^{n+1}, \tilde{\xi}_n^{n+1}) = (\tilde{\mathbf{y}}_n^n, \tilde{\xi}_n^n) - \left[J(\tilde{\mathbf{y}}_n^n, \tilde{\xi}_n^n)\right]^{+} H(\tilde{\mathbf{y}}_n^n, \tilde{\xi}_n^n). \tag{3.18}$$

   Please see chapter three of Allgower and Georg [5] for more detail.

3.1.3 Parameterizations

When we are tracing out the implicit curve $c(s)$ in $\mathbb{R}^{n+1}$ it's useful to have some way of recording our progress along the curve; some way of quantifying the difference between the previous, current and next iteration. To do this we may introduce a parameterization to the system, $P(\mathbf{y}, \xi, \rho) = 0$. We chose to use the natural parameterization explained below for the PDDNLS.

We will discuss three broad approaches to parameterizing the system:

1. **natural parameterization**, which is by the continuation parameter ξ.

2. **local parameterization**, which is by a component y_i of $\mathbf{y}$.

3. **arclength** and **pseudo-arclength parameterization**, which is by the distance along the curve, s.

Natural parameterization is the simplest to understand, and easiest to implement. We order our points just by the distance traveled along the ξ-axis. Specifically, we set $\rho = \xi$ and $P(\mathbf{y}, \xi) = \xi - \xi_k$. Here ξ_k is the suggested next value of ξ provided by the step length algorithm.

Local parameterization is similarly quite easy to understand and implement. Here we order our points (at least locally) by the distance traveled along one of the y_i-axes. In this case $P(\mathbf{y}, \xi, \rho) = y_k - \rho$. Again, ρ is picked by the step length algorithm as the next desired value of y_k, e.g.

$$\rho = y_{k,n} + \sigma_n(y_{k,n} - y_{k,n-1}). \tag{3.19}$$

Local parameterization has the advantage that turning points in ξ can be followed, since the y_i-axes are all perpendicular to the ξ-axis. Further, at

each iteration the value of k can be modified should it be necessary. It is this flexibility of choice that is responsible for the local in its name.

The final, and most useful, method we discuss is **arclength parameterization**. We parameterize $\mathbf{y}$ and ξ by distance along the curve $c(s)$. Consider $\mathbf{y} = \mathbf{y}(s)$ and $\xi = \xi(s)$. Then equation (3.7) becomes

$$F_{\mathbf{y}} \frac{d\mathbf{y}}{ds} + F_{\xi} \frac{d\xi}{ds} = 0 \tag{3.20}$$

with the additional condition $P(\mathbf{y}, \xi, \rho = s)$,

$$\left(\frac{dy_1}{ds}\right)^2 + \ldots + \left(\frac{dy_n}{ds}\right)^2 + \left(\frac{d\xi}{ds}\right)^2 = 1 \tag{3.21}$$

Multiplying equation (3.21) by ds^2 and approximating the one-forms dy_i etc... by differences yields the classic arclength parameterization

$$P(\mathbf{y}, \xi, s) = \sum_{i=1}^{n} [y_i - y_i(s_n)]^2 + [\xi - \xi(s_n)]^2 - (s - s_n)^2 \tag{3.22}$$

proposed in [41, 44, 47]. Here s_n is the distance along the curve corresponding to the last good solution and s is the distance along the curve of the next solution, as predicted by the step length algorithm.

A modification to (3.22) was proposed by [41]. A weighting factor $0 < \zeta < 1$ is introduced which controls the importance of $\mathbf{y}$ relative to ξ. This **pseudo-arclength** parameterization is

$$P(\mathbf{y}, \xi, s) = \zeta \sum_{i=1}^{n} [y_i - y_i(s_n)]^2 + (1 - \zeta)[\xi - \xi(s_n)]^2 - (s - s_n)^2. \tag{3.23}$$

An alternative pseudo-arclength parameterization can be derived from the Taylor series expansion

$$[(\mathbf{y}(s), \xi(s)) - (\mathbf{y}(s_n), \xi(s_n))] = (s - s_n)[\frac{d}{ds}(\mathbf{y}, \xi)]_{s=s_n} + \mathcal{O}\left(|s - s_n|^2\right), \tag{3.24}$$

namely

$$P(\mathbf{y}, \xi, s) = \zeta \sum_{i=1}^{n} (y_i - y_i(s_n)) \frac{dy_i(s_n)}{ds} + (1 - \zeta)(\xi - \xi(s_n)) \frac{d\xi(s_n)}{ds} - (s - s_n). \tag{3.25}$$

This second formulation has the advantage that it is linear in the differences $\Delta\mathbf{y}$, $\Delta\xi$ and Δs.

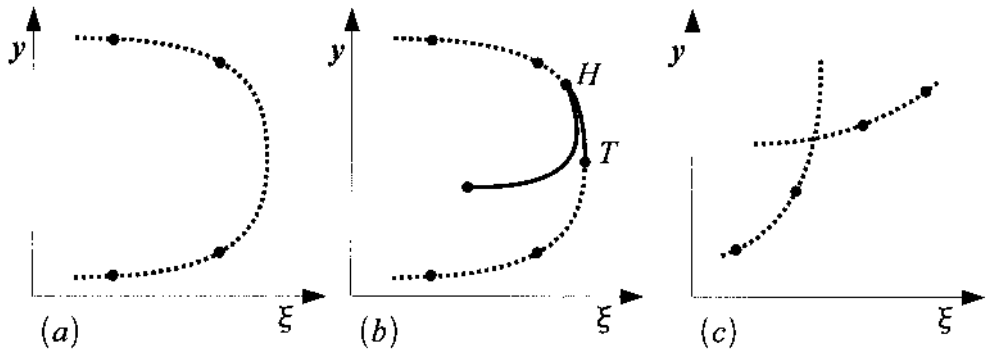

Figure 3.4: Problems with large step sizes. In (a) four large steps have been taken around the curve. At all four points the solution is unstable. In (b) two smaller steps are added, revealing a short interval of stable solutions between the turning point T and a Hopf bifurcation H. In addition a short branch of stable periodic solutions emanates from the original branch. In (c) the large steps jump from one branch to the next without resolving their intersection.

3.1.4 Step control

The step size between the current and next iteration is important to the accuracy and efficiency of any PC continuation strategy, regardless of the particular type of predictor, corrector or parameterization chosen. As with all numerical analysis, there is a tradeoff between

1. small steps which will be accurate, but are unnecessary and waste computation time on straight sections of *c(s)*.

2. big steps which can move through straight sections of *c(s)* cheaply, but may not resolve all the detail of *c(s)* or waste computation time if the initial guess is too far from the curve to be quickly corrected.

Some of the problems with large step sizes are graphically illustrated in figure 3.4. The solution is to adapt the step size between iterations and avoid unnecessary computation.

Seydel [72, 73] has shown that for quasi-Newton correctors, maximum efficiency of the PC method is obtained when the corrector takes a specific number of steps, $N_{opt}(\dot{E})$, which is related to the desired tolerance, E. It's then simply a matter of adjusting the next step size upward if the corrector took less than N_{opt} and downwards if it took more. Put simply, we choose an initial step size, øo, choose some bounds on the step size, *(o ,,, a*),* denote the number of steps taken by the corrector N_n and update using

$$\tilde{\sigma}_{n+1} = \sigma_n \left(\frac{N_n}{N_{\text{opt}}} \right), \tag{3.26}$$

$$\sigma_{n+1} = \begin{cases} \sigma^* & \text{if } \tilde{\sigma}_{n+1} > \sigma^* \\ \sigma_* & \text{if } \tilde{\sigma}_{n+1} < \sigma_* \\ \tilde{\sigma}_{n+1} & \text{otherwise} \end{cases} . \tag{3.27}$$

We have just seen how continuation methods can be used to follow a branch of solutions. Chapter 2 outlined various bifurcations that can occur as we follow these branches, and chapter 4 explains how we can find the eigenvalues of solutions on these branches, and thus identify the bifurcations when they occur.

Chapter 4

Approaches to determining stability

In this chapter we will demonstrate two methods to determine the stability of the solutions that we calculated by continuing the stationary $1/4$ soliton of the PDDNLS. We present an exposition of the Floquet theory in section. 4.1. In section 4.2 we restate the problem and linearise the PDDNLS, making some simplifications that are justified by the Floquet theory. The last two sections, 4.3 and 4.4, highlight two different methods to determine the stability of the linearised system.

4.1 Floquet theory

We start by establishing definitions for some background terms, and then show some preliminary results before we move onto the most important part of this section: the proofs of theorems 4.10 and 4.12. We start by defining a linear, homogenous, first-order system of differential equations with periodic coefficients.

Definition 4.1. *The general form for a* ***linear, homogenous, first-order system of differential equations of order*** n *is*

$$\dot{\mathbf{v}}(t) = A(t)\mathbf{v}(t) \tag{4.1}$$

where $\mathbf{v}$ *is a* $n \times 1$ *column vector, the overdot represents differentiation with respect to time,* A *is an* $n \times n$ *matrix and* $t \in \mathcal{T} = [t_0, t_1]$.

We assume that the vector $\mathbf{v}$ and matrix A are complex-valued.

Definition 4.2. *The system of equations (4.1) has* ***periodic coefficients*** *(with period* T*) if it satisfies the following:*

$$A(t+T) = A(t) \tag{4.2}$$

for every t in the interval T and *if T is minimal, i.e. there is no* $0 < T < T$ *such that the previous conditions hold for T.*

Since the system in (4.1) is linear we know that (1) the zero function, (2) a scalar multiple of a solution, and (3) the sum of two solutions are all solutions themselves. Thus the set of solutions to (4.1) form a vector space over the field of complex numbers once equipped with addition and scalar multiplication. We denote this space V.

We would like to understand the behaviour of solutions to these sorts of systems beyond the properties we have outlined above. Our first, naive assumption may be that a system with periodic coefficients would have periodic solutions, but this is not true. While the solution v(t) will exhibit some behaviour that repeats with the time-scale *T*, in general v(t *T) v(t)* bar a few special cases.

Consider a simple, one-dimensional problem:

$$\mathbf{v}_t(t) = (1 + \cos t)\mathbf{v}. \tag{4.3}$$

The general solution is

$$\mathbf{v}_{\text{gn}}(t) = c_1 \exp[t + \sin t] \tag{4.4}$$

and for any initial condition $\mathbf{v}(0) \neq 0$, $c_1 \neq 0$ and assuming $\mathcal{T} = [0, \infty)$ as $t \to \infty$, $|\mathbf{v}(t)| \to \infty$ precluding the possibility of periodicity. We plot the solution satisfying $\mathbf{v}(0) = 1$ below.

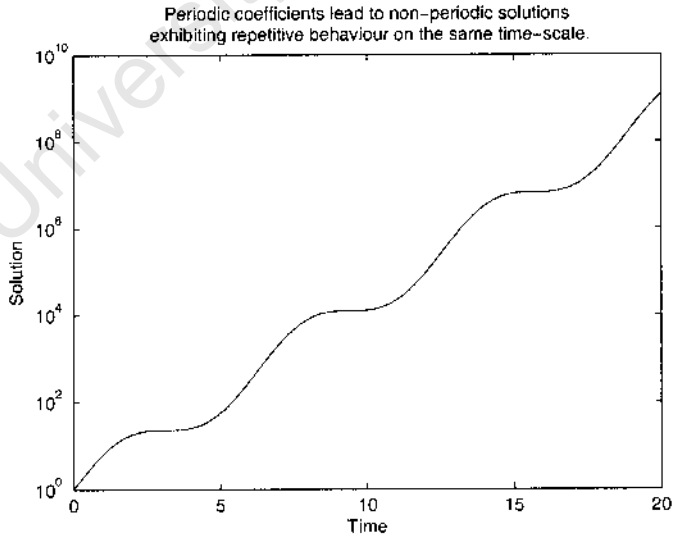

While the solution is clearly not periodic, it's obvious that there is some behaviour (in this case the speeding and slowing of the solution's growth)

which repeats on the same time-scale as the periodic coefficients. It is this behaviour which is captured in the theorems (4.10) and ((4.12). The proof of these theorems needs the notion of linear (in)dependence for a set of vector-valued functions.

Definition 4.3. *A set, S, of vector-valued functions, i.e.*

$$S = \{\mathbf{v}_m(t) : m \in M\} \tag{4.5}$$

*is **linearly dependent** on an interval $\mathcal{T} = [t_0, t_1]$ if there exists a set, C, of scalar constants not all zero, i.e.*

$$C = \{c_m : \exists\ m' \text{ s.t. } c_{m'}^2 \neq 0\}, \tag{4.6}$$

such that

$$\sum_{m \in M} c_m \mathbf{v}_m(t) = \mathbf{0} \tag{4.7}$$

*for all values of $t \in \mathcal{T}$. If a set is not linearly dependent, it is **linearly independent** (on that interval).*

By using the existence and uniqueness theorem for solutions to a system of differential equations we can map from $\mathbb{C}^n$ to $\mathbb{V}$. Given an element $\mathbf{w} \in \mathbb{C}^n$ the corresponding element in $\mathbb{V}$ is just the solution satisfying the initial condition $\mathbf{v}(t_0) = \mathbf{w}$. Conversely, we can map from $\mathbb{V}$ back to $\mathbb{C}^n$ by taking $\mathbf{w} = \mathbf{v}(t_0)$. This mapping, along with the definition of linear independence just provided, make it easy to show that the dimension of the space $\mathbb{V}$ is just n.

We move now to define the (principal) fundamental matrix and Wronskian.

Definition 4.4. *Given n solutions to (4.1), i.e. $\mathbf{v}_1(t), \mathbf{v}_2(t), \ldots, \mathbf{v}_n(t)$, we can form a solution matrix V whose m-th column is the solution $\mathbf{v}_m(t)$,*

$$V(t) = (\mathbf{v}_1(t)|\cdots|\mathbf{v}_n(t))\,. \tag{4.8}$$

Note, this matrix satisfies

$$V_t = AV. \tag{4.9}$$

*If the set of solutions comprising the solution matrix is linearly independent we call it a **fundamental matrix**, and if there exists $t_* \in \mathcal{T}$ such that $V(t_*) = I$ we further call it **principal**.*

Definition 4.5. *The **Wronskian**, $W(t)$, of a solution matrix, $V(t)$ is*

$$W(t) = \det[V(t)]. \tag{4.10}$$

The Wronskian has a number of useful properties that we will prove. The first of these is provided immediately below, but the second requires some preliminary work. Note that the first proof exploits the same sort of mapping we discussed above.

Theorem 4.6. *If there exists $t_* \in \mathcal{T}$ such that $W(t_*) = 0$ then the set of solutions $\mathbf{v}_1(t), \mathbf{v}_2(t), \ldots, \mathbf{v}_n(t)$ is linearly dependent and $W(t) = 0$ for all $t \in \mathcal{T}$. Conversely, if there exists $t_* \in \mathcal{T}$ such that $W(t_*) \neq 0$ then the set of solutions is linearly independent and the Wronskian is non-zero on the entire interval.*

Before we can proceed to the next property of the Wronskian we need to show a preliminary result: Jacobi's formula for the derivative of a determinant. The statement of the formula requires the definition of the adjugate, which is not immediately obvious.

Definition 4.7. *The (p, q) minor of a matrix J is the determinant of the matrix formed by omitting the p-th row and q-th column of J. The (p, q) cofactor of J is the (p, q) minor scaled by $(-1)^{p+q}$. The cofactor matrix is a matrix whose (p, q) entry is the (p, q) cofactor. The **adjugate** of J is the transpose of the cofactor matrix of J. Denote it* $\mathrm{adj}[J]$.

Theorem 4.8. ***Jacobi's Formula.***

$$\frac{d}{dt}\det[J] = \mathrm{tr}\left[\mathrm{adj}[J]\frac{d}{dt}J\right] \tag{4.11}$$

Proof. Denote the entries of the matrix J as $j_{p,q}$ and the entries of its adjugate as $a_{p,q}$. Then the determinant is just

$$\det[J] = \sum_p (j_{p,q}) \times (a_{q,p}). \tag{4.12}$$

Note that we could have summed over q instead. Each element appears linearly, so it's easy to determine the partial derivatives if we recall that the elements $a_{q,p}$ depend on the minor of J with the p-th row and q-th column removed,

$$\frac{\partial}{\partial j_{p,q}}\det[J] = a_{q,p}. \tag{4.13}$$

By expressing the total derivative with respect to time as the sum of the partials

$$\frac{d}{dt}\det[J] = \sum_{p,q}\left(\frac{\partial}{\partial j_{p,q}}\det[J]\right)\left(\frac{d}{dt}j_{p,q}\right) \tag{4.14}$$

we can easily recover

$$\frac{d}{dt}\det[J] = \sum_{p,q} a_{q,p}\left(\frac{d}{dt}j_{p,q}\right). \tag{4.15}$$

In the above expression the summation over q calculates the diagonal entries of the matrix multiplication $\text{adj}[J] \times \frac{dJ}{dt}$ and so the summation over p is just the trace of the product. Thus

$$\frac{d}{dt}\det[J] = \text{tr}\left[\text{adj}[J]\frac{dJ}{dt}\right]. \tag{4.16}$$

□

Having shown Jacobi's formula we are ready to prove the next property of the Wronskian. This property, also known as Liouville's formula, relates the evolution of the Wronskian to the coefficient matrix A from (4.1).

Theorem 4.9. ***Liouville's formula.***

$$W(t_b) = W(t_a)\exp\left[\int_{t_a}^{t_b} \text{tr}[A(s)]\ ds\right] \text{ for all } t_a, t_b \in \mathcal{T} \tag{4.17}$$

Proof. If $W(t) = 0$ for any value of $t \in \mathcal{T}$ then it is zero over the entire interval and so (4.17) is immediately satisfied. Assume then that $W(t) \neq 0$ on the interval and note that this implies the matrix V is invertible.

From Jacobi's formula (4.11) we know that

$$\frac{dW}{dt} = \text{tr}\left[\text{adj}[V]\frac{dV}{dt}\right]. \tag{4.18}$$

Substituting the expression for V_t from (4.9) we see that

$$\frac{dW}{dt} = \text{tr}\left[\text{adj}[V]AV\right]. \tag{4.19}$$

We can swap the order of multiplication within the trace function, so we rearrange and substitute $\text{adj}[V] = \det[V]V^{-1}$:

$$\frac{dW}{dt} = \text{tr}\left[\det[V]AVV^{-1}\right] \tag{4.20}$$

$$\frac{dW}{dt} = W\text{tr}[A]. \tag{4.21}$$

We can recover (4.17) by integrating. □

We're finally ready to tackle the two theorems we will need in sections 4.3 and 4.4. We state them below with proof.

Theorem 4.10. *Given a fundamental matrix $V(t)$ for the system (4.1), there exists a non-singular constant matrix B such that*

$$V(t+T) = V(t)B \tag{4.22}$$

and further

$$\det[B] = \exp\left[\int_0^T \text{tr}[A(s)]\ ds\right]. \tag{4.23}$$

Proof. The first part of the proof relies on (4.9) and the periodicity of A. Let $U(t) = V(t+T)$. Then

$$\begin{aligned} U_t(t) &= V_t(t+T) \\ &= A(t+T)V(t+T) \\ &= A(t)U(t) \end{aligned} \tag{4.24}$$

and so $U(t)$ is also a fundamental matrix. Since both matrices are full rank the columns of U must just be constant, time-independent linear combinations of the columns of V and so $U(t) = V(t)B$ for some non-singular constant matrix B, which in turn implies $V(t+T) = V(t)B$.

The second part of the proof uses (4.17). Note that we have two expressions for $W(t+T)$. The first is derived from Liouville's formula,

$$W(t+T) = W(t)\exp\left[\int_t^{t+T} \mathrm{tr}[A(s)]ds\right] \tag{4.25}$$

while the second comes from taking the determinant on both sides of (4.22),

$$W(t+T) = W(t)\det[B]. \tag{4.26}$$

Equating these obviously implies that

$$\det[B] = \exp\left[\int_t^{t+T} \mathrm{tr}[A(s)]ds\right] \tag{4.27}$$

and so the result is proved since the integration covers a complete period and it's immaterial whether we start at t or 0. □

The repetitive yet non-periodic behaviour of the system is captured by the matrix B. More specifically, its eigenvalues determine whether the solutions are stable or not.

Definition 4.11. *The eigenvalues $\lambda_1, \lambda_2, \ldots, \lambda_n$ of B are called* ***characteristic multipliers*** *for the system (4.1). Each characteristic multiplier has an associated* ***characteristic exponent*** *$\mu_1, \mu_2, \ldots, \mu_n$ defined by*

$$\lambda_m = e^{\mu_m T}, \quad m \in \{1, 2, \ldots, n\} \tag{4.28}$$

It is important to note two things:

1. each characteristic exponent μ_m is chosen from a family of equivalent exponents $\mu_{m,k} = \mu_m + 2\pi ik/T$ where $k \in \mathbb{Z}$. The choice makes no difference since the shift up or down the imaginary axis disappears after exponentiation.

2. the characteristic multipliers (and hence exponents) do not depend on the choice of matrix $V(t)$. Suppose we have two matrices $V(t)$ and $\hat{V}(t)$ with corresponding B and $\hat{B}$. Since both matrices are fundamental, their columns are linear combinations of each other and so $V(t) = \hat{V}(t)C$ for a non-singular constant matrix C. Then

$$V(t) = V(t+T)B \tag{4.29}$$

yields

$$\hat{V}(t) = \hat{V}(t+T)CBC^{-1} \tag{4.30}$$

after substitution. Comparison with

$$\hat{V}(t) = \hat{V}(t+T)\hat{B} \tag{4.31}$$

shows that

$$\hat{B} = CBC^{-1} \tag{4.32}$$

and so the two matrices have the same eigenvalues.

Theorem 4.12. *For every characteristic multiplier λ of (4.1) and corresponding characteristic exponential μ there exists a solution $\mathbf{v}(t)$ such that*

$$\mathbf{v}(t+T) = \lambda\mathbf{v}(t) \tag{4.33}$$

and there exists a periodic function $\mathbf{p}(t)$

$$\mathbf{v}(t) = e^{\mu t}\mathbf{p}(t). \tag{4.34}$$

Both of these conditions hold for all $t \in \mathcal{T}$.

Proof. Given a multiplier λ_m, consider the corresponding eigenvector $\mathbf{b}_m$ of B, i.e.

$$B\mathbf{b}_m = \lambda\mathbf{b}_m. \tag{4.35}$$

Construct a solution

$$\mathbf{v}_m(t) = V(t)\mathbf{b}_m. \tag{4.36}$$

Now we see that

$$\mathbf{v}_m(t+T) = V(t+T)\mathbf{b}_m = V(t)B\mathbf{b}_m = V(t)\lambda_m\mathbf{b}_m = \lambda_m\mathbf{v}_m(t). \tag{4.37}$$

To show the second part of the theorem, define the function $\mathbf{p}_m(t) = \mathbf{v}_m e^{-\mu_m t}$. Then

$$\mathbf{p}_m(t+T) = \mathbf{v}_m(t+T)e^{-\mu_m(t+T)} = \lambda e^{-\mu T}\mathbf{v}_m(t)e^{-\mu t} = \mathbf{p}_m(t). \tag{4.38}$$

Please note that μ_m can be shifted by $2\pi ik/T$ as pointed out above, but it will make no difference since the exponentiation masks this shift. □

4.2 Linearising the PDDNLS

In this thesis we are investigating the PDDNLS,

$$i\psi_t + \psi_{xx} + 2|\psi|^2\psi - \psi = h\psi^* - i\gamma\psi. \tag{4.39}$$

Specifically, we are investigating the behaviour of its stationary ψ_+ soliton solution,

$$\psi_+ = A_+\text{sech}(A_+x)e^{-i\theta_+}, \tag{4.40}$$

which undergoes a Hopf bifurcation as the driving parameter h is increased. Some work has already been done on this problem: Bondila *et al* [13] have produced an attractor chart by direct simulation (it is reproduced in chapter 5), but it has some shortcomings and so we outlined three questions in the introduction.

1. In which parts of the (γ, h) parameter space are the $\psi_\pm$ solitons stable?
2. For values of γ and h where the solitons are unstable, what sort of stable attractors do we observe instead?
3. Can these solitons be combined to form bound states, or complexes?

Numerical continuation can find periodic solutions to the PDDNLS. To answer these questions completely, however, we require the eigenvalue spectrum of the operator we obtain by linearising the PDDNLS around one of these periodic solutions.

Before we start we should note that numerical continuation will not find a continuous solution $\psi(x,t)$ for $(x,t) \in [-\infty,\infty] \times [0,T]$, but can only find the value of ψ at discrete points in $[-L,L] \times [0,T]$. We will address this point in more detail later.

To linearise the PDDNLS around one of its periodic solutions, ψ_0, we substitute $\psi = \psi_0 + \delta\psi$ into equation (1.5). If we make this subsitution we find that

$$i\delta\psi_t + \delta\psi_{xx} + 4|\psi_0|^2 + 2\psi_0^2\delta\psi^* - \delta\psi = h\delta\psi^* - i\gamma\delta\psi \tag{4.41}$$

after higher order $\delta\psi$ terms are neglected. We split the equation into its real and imaginary parts, $\delta\psi = u + iv$ and $\psi_0 = \mathcal{R} + i\mathcal{I}$ and recover

$$\begin{array}{rcl} -v_t + u_{xx} + (6\mathcal{R}^2 + 2\mathcal{I}^2)u + 4\mathcal{R}\mathcal{I}v - u &=& hu + \gamma v \\ u_t + v_{xx} + (2\mathcal{R}^2 + 6\mathcal{I}^2)v + 4\mathcal{R}\mathcal{I}u - v &=& -hv - \gamma u \end{array}. \tag{4.42}$$

We introduce a vector $\mathbf{w} = (u,v)^T$ and rewrite the equation in matrix form

$$\mathbf{w}_t = -H(x,t)\mathbf{w}, \tag{4.43}$$

where the matrix $H(x,t)$ is defined as

$$H = \begin{pmatrix} 4\mathcal{R}\mathcal{I} + \gamma & \partial_x^2 + 2\mathcal{R}^2 + 6\mathcal{I}^2 - 1 + h \\ -\partial_x^2 - 6\mathcal{R}^2 - 2\mathcal{I}^2 + 1 + h & -4\mathcal{R}\mathcal{I} + \gamma \end{pmatrix}. \quad (4.44)$$

Once we've recast the equation it is clear that (4.43) has nearly the same form as (4.1) since the time dependance of the matrix H is introduced through the real and imaginary parts of ψ_0 which are periodic for some value T. All that remains is to discretise in the spatial dimension and so to remove the differential operators from the matrix H. In both sections below we discretise the spatial dimension by expanding in spatial Fourier series, but in 4.4 we expand in temporal Fourier series at the same time and so this is the latest point of commonality.

4.3 Analysis through the monodromy matrix

The first method to determine the stability of the solutions picks up immediately after the Floquet theory and linearisation we have just discussed. We will replace $\mathbf{w} = (u, v)^T$ from (4.43) with its spatial Fourier expansion, i.e.

$$\mathbf{w} = \sum_{n=-N}^{N} \mathbf{w}_n e^{-i\nu_n x} \quad (4.45)$$

where $\nu_n = \pi n/L$ and $\mathbf{w}_n = (u_n, v_n)^T$. This will transform our PDE to a larger system of ODEs. It's important to note that:

1. this system of ODEs will have periodic coefficients since we linearised around a periodic solution ψ_0.
2. since the coefficients are periodic the behaviour of the solutions to this new system of ODEs will by governed by the Floquet theory.
3. the solutions to this system of ODEs will approximate the solution to the PDE. The accuracy of the approximation depends on N, the number of terms in the Fourier expansion.

We substitute the Fourier expansion for $\mathbf{w}$ back into (4.43) and then use the orthogonality of exponentials to recover

$$\partial_t \mathbf{w}_{n'} = \sum_{n=-N}^{N} H_{n',n} \mathbf{w}_n. \quad (4.46)$$

$$H_{n',n} = \frac{1}{2L} \int_{-L}^{L} e^{\frac{i\pi}{L}(n'-n)x} \begin{pmatrix} 4\mathcal{R}\mathcal{I} + \gamma & \nu_n^2 + 2\mathcal{R}^2 + 6\mathcal{I}^2 - 1 + h \\ -\nu_n^2 - 6\mathcal{R}^2 - 2\mathcal{I}^2 + 1 + h & -4\mathcal{R}\mathcal{I} + \gamma \end{pmatrix} dx. \quad (4.47)$$

By introducing a vector

$$\vec{\mathbf{w}} = \begin{pmatrix} u_{-N} \\ v_{-N} \\ u_{-N+1} \\ v_{-N+1} \\ \vdots \\ u_{+N} \\ v_{+N} \end{pmatrix} \tag{4.48}$$

and a matrix

$$\hat{H} = \begin{pmatrix} H_{-N,-N} & H_{-N,-N+1} & \cdots & H_{-N,+N} \\ H_{-N+1,-N} & & & \vdots \\ \vdots & & & \vdots \\ H_{+N,-N} & \cdots & \cdots & H_{+N,+N} \end{pmatrix} \tag{4.49}$$

we can recast (4.46) and (4.47) in a much simpler form

$$\vec{\mathbf{w}}_t = \hat{H}(t)\vec{\mathbf{w}}. \tag{4.50}$$

Finally we see that equation (4.50) is of the same form as (4.1), and so its solutions will also be the product of a periodic function and an exponential. Further, these solutions approximate the solutions of (4.43), and so approximate their characteristic exponentials and stability.

If we review theorems 4.10 and 4.12 it's obvious how we can solve this problem: it is only necessary to determine the eigenvalues of a matrix B. The matrix B can be calculated by solving (4.50) 4N + 2 times with initial conditions corresponding to the columns of the identity matrix, i.e. W(0) = I.

The final step is to calculate the eigenvalues of B, a complex (4N + 2) x (4N + 2) matrix, but this is a standard problem and many routines exist to solve it.

Notes on implementation

There are two areas where the implementation merits discussion - both areas arise because the solution we obtain numerically is known on a discrete mesh covering the domain [0, *T] x [—L, L]* rather than continuously on [0, T] x

The first is the numerical integration of the real and imaginary parts of the solution after they have been multiplied by an exponential. There are many different approaches to quadrature but we are constrained in our choices by some factors. We know only the value of the function, not its derivatives, and we know those values only at evenly spaced points over the range of integration. Because of these constraints we have to integrate

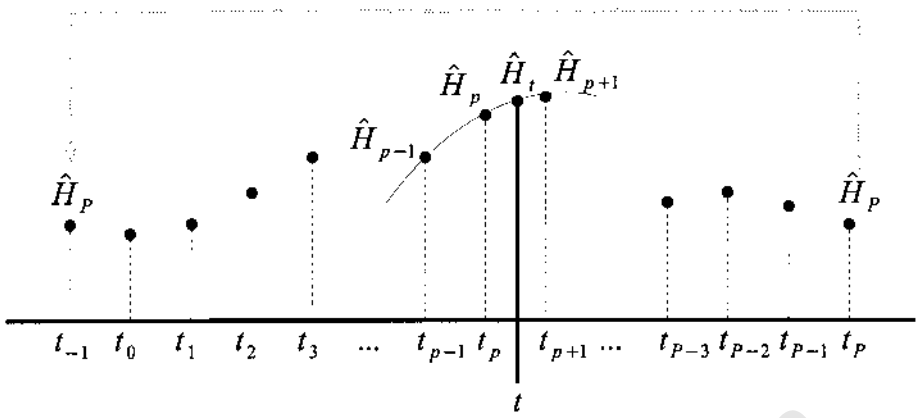

Figure 4.1: Numerical continuation only provides values for the solution at to, t_i . . . *tp* so must interpolate to find values of *H(t)* between these points. We don't have an explicit value for H_1, but since the solution is periodic we can just duplicate ***Hp.***

using one of the Newton-Cotes' rules; we used Simpson's rule. This is not a problem though, since we expect our solution to be reasonably well-behaved, and the numerical continuation returns values on a relatively fine grid: 0.05 while our solutions have a spatial profile roughly resembling sech(x)

The second area is the solution of the differential equation. We don't know the values of the matrix ***H*** at every point in time, but we used an ODE solver with an adaptive step size. This often meant that the solver would need values of ***H*** between two known values. In these cases we used quadratic interpolation to determine the necessary value of ***H.*** Denote the points on the grid to, t1 . . . *tp* and $H(t_p) = H_p$ for convenience. Then for $t_v < t <$ tp+i

$$\hat{H}(t) = \frac{1}{(\Delta t)^2}\left[\hat{H}_{p-1}(t-t_p)(t-t_{p+1}) - \hat{H}_p(t-t_{p-1})(t-t_{p+1}) + \hat{H}_p(t-t_{p-1})(t-t_p)\right]. \tag{4.51}$$

For $p = 0$ we wrap around to find $\hat{H}_{-1}$. Figure 4.1 illustrates this.

Testing

This method was tested on two different problems. Before we describe the tests and the results we repeat the terminology introduced in section 4.1 for clarity. The eigenvalues of the matrix ***B*** are the characteristic multipliers of the system, not their characteristic exponents. Thus in this thesis we will use the term eigenvalue and the symbol A to refer to the multipliers of the system not the exponents, which we denote by p,.

Firstly, we determined the stability of the soliton solution

$$\psi_0 = Ae^{iA^2t}\text{sech}(Ax) \tag{4.52}$$

to the unperturbed nonlinear Schrödinger equation,

$$i\psi_t + \psi_{xx} + 2|\psi|^2\psi = 0. \tag{4.53}$$

The soliton has a well known spectrum: the exponents
axis above i and below —i with four exponents at zero that arise from its translational invariance and U(1) symmetry. We recovered the corresponding spectrum of multipliers, A, with the correct multiplicity of the discrete multipliers at 1, i.e. there were four discrete multipliers at 1. We have not included the results from this test.

The second test was to analyse the stability of the stationary $0_{\pm}$ solitons to the PDDNLS. We recall from chapter 1 that these solitons are given by

$$\psi_{\pm} = A_{\pm}e^{-i\theta_{\pm}}\text{sech}(A_{\pm}x). \tag{4.54}$$

Note that these solutions are stationary, but that it's necessary we make a choice for their "period". We have chosen $T = 1$ for the pictures below. Since A = exp[μT] this makes no difference to the stability of the solution, but it will change the arguments of A_i as they pass through the unit circle. If we chose T corresponding to the periodic solution that appears at the bifurcation point, the discrete eigenvalues would all pass through the unit circle along the real axis.

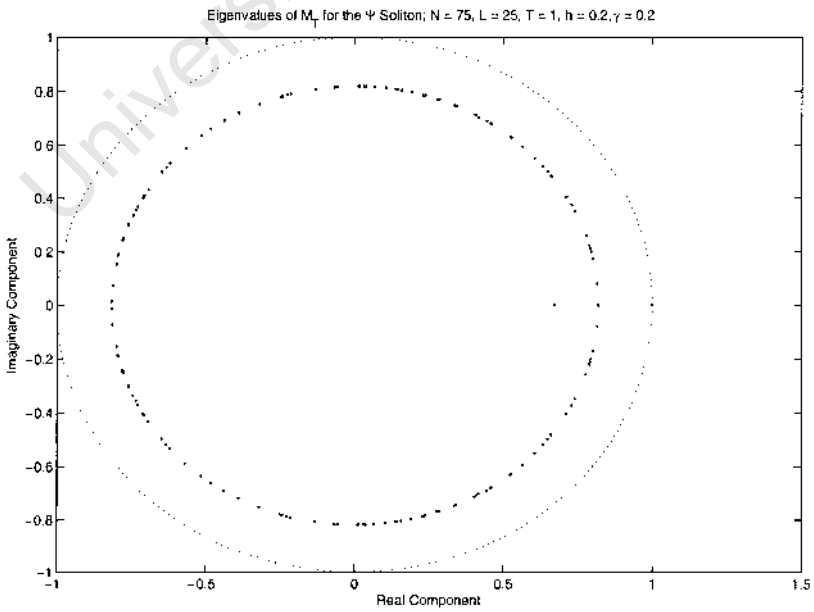

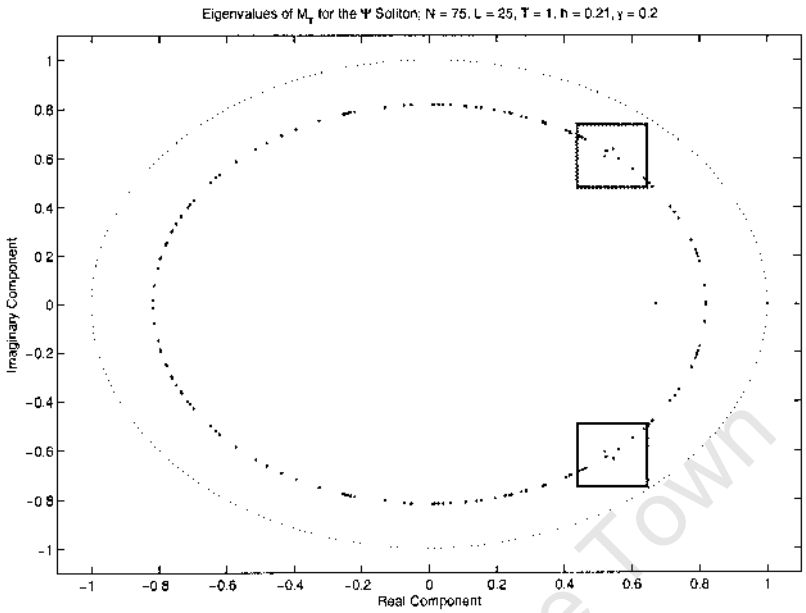

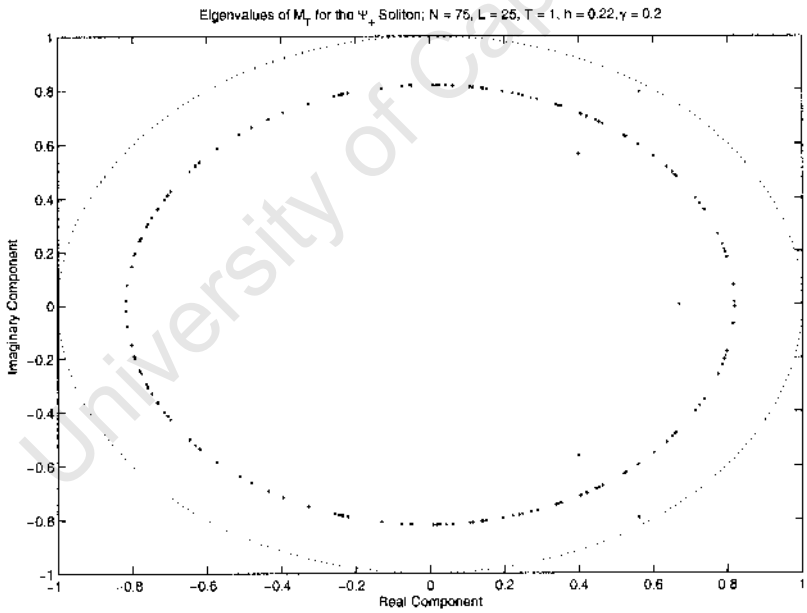

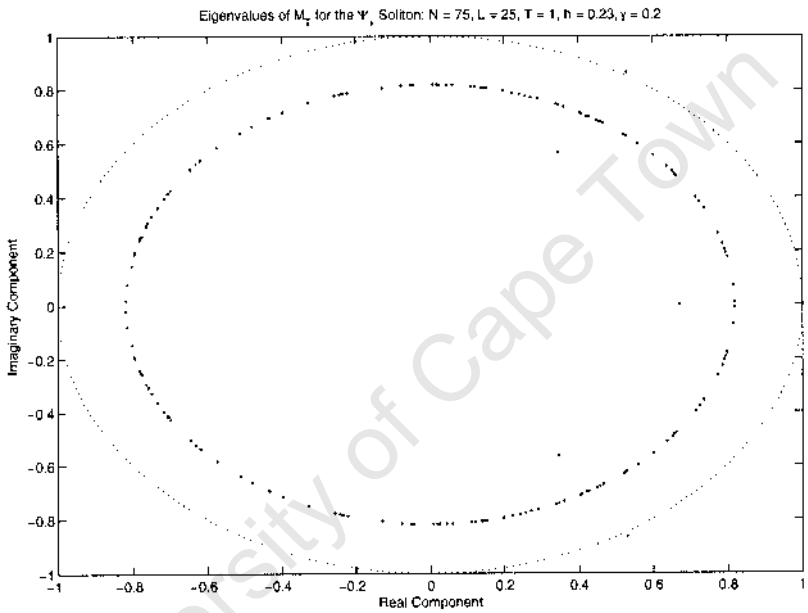

Figure 4.2: Testing the code on the $7/>_{+}$ soliton. In all four pictures $\acute{Y} = 0.20$ while h increases from 0.20 to 0.23 in steps of 0.01. As h is increased two complex conjugate pairs of eigenvalues detach from the continuous spectrum (inside the box) and move outward passing through the unit circle. This agrees with the known results, see [13].

Shortcomings

The main shortcoming of our method is that it cannot be both fast and accurate. Consider the parameter N, the number of modes in the Fourier expansion. We want this to be as large as possible so that we can resolve all the detail of the solutions 0_o, but as we increase N the computation becomes quite slow.

This slowdown arises because both the number of variables in the system of differential equations and the number of times that system needs to be solved are given by 4N + 2. Not only is the system becoming larger, it must also be solved a greater number of times. This is further compounded if the period of 00 grows and the linear system must be solved on a longer interval $[0, T]$.

We could increase the resolution by decreasing the width of the interval $[—L, L]$ rather than increasing N, but this requires that solution decays quickly to zero. It is not a reliable answer to this problem.

The inaccuracy manifests itself in two ways. The first is misplacement of the discrete eigenvalues; they may either simply be shifted from their true position or qualitative changes may occur, e.g. the two unit eigenvalues may be transformed into a complex conjugate pair with a small imaginary part. This can be addressed by increasing N and redoing the analysis.

The second type of inaccuracy is a thickening of the continuous spectrum. Ideally the spectrum should have no thickness; all the continuous eigenvalues should lie exactly on a circle of radius exp[-ÝT]. In some cases the eigenvalues appear in pairs lying slightly inside and outside the circle giving the continuous spectrum an apparent thickness. This thickening is not inherently worrying, but it does indicate that the discrete eigenvalues may be inaccurate.

4.4 Analysis through two-dimensional Fourier expansion

We have outlined one method of determining the stability of a periodic solution above. Unfortunately, if we want to accurately determine the eigenvalue spectrum it takes a long time to run. This long run time motivates us to consider a second approach.

In section 4.3 we presented a method of calculating the stability of the linearised **PDDNLS.** The method we present here is developed differently; it is applied first to a simpler problem.

1. We apply our second method not to the PDDNLS, but to a simpler problem, the unperturbed NLS and its spatially homogenous solution = A exp [2iA²t]. During this presentation we point out where errors

may arise, how we can detect them, and hence how we can correct them.

2. We extend our method to the PDDNLS, taking into account the error-correction strategies we developed for the simpler problem.

4.4.1 The unperturbed NLS and its spatially homogenous solutions

We start by considering a problem which has only a trivial dependence on the spatial dimension. We are going to examine the NLS

$$i\psi_t + \psi_{xx} + 2|\psi|^2\psi = 0, \tag{4.55}$$

and its x-independent solution

$$\psi_0 = Ae^{2iA^2t}. \tag{4.56}$$

We have chosen this problem because it is simple enough that we can first calculate the results analytically, and then compare those results against the results we obtain numerically.

Analytical results for the unperturbed NLS

The first step is to linearise the equation and to split into real and imaginary parts as we did in section 4.2 for the PDDNLS. First we perturb equation (4.55) about the solution ψ_0, i.e. we let $\psi = \psi_0 + \delta\psi$. This gives the following

$$i\delta\psi_t + \delta\psi_{xx} + 4|\psi_0|^2\delta\psi + 2\psi_0^2\delta\psi^* = 0. \tag{4.57}$$

At this stage we can simplify the equation by introducing a new variable $\delta\phi = \delta\psi \times \exp\{2iA^2t\}$. Substitution into the above yields

$$i\delta\phi_t + \delta\phi_{xx} + 2A^2\left(\delta\phi + \delta\phi^*\right) = 0, \tag{4.58}$$

which is an equation with constant coefficients, and now splitting $\delta\phi$ into real and imaginary parts, $\delta\phi = P + iQ$, is fairly straightforward. We find that

$$\begin{aligned} -Q_t + P_{xx} + 4A^2P &= 0, \\ P_t + Q_{xx} &= 0. \end{aligned} \tag{4.59}$$

We separate the space and time dependent parts of P and Q:

$$P = p(x)e^{\mu t} \quad \text{and} \quad Q = q(x)e^{\mu t}, \tag{4.60}$$

and then substitute again:

$$\begin{aligned} p_{xx} + 4A^2p &= \mu q, \\ -q_{xx} &= \mu p. \end{aligned} \tag{4.61}$$

The final step is to expand p and q as Fourier series in space, i.e.

$$p(x) = \sum_{n=-\infty}^{\infty} p_n e^{-i\nu_n x} \quad \text{and} \quad q(x) = \sum_{n=-\infty}^{\infty} q_n, e^{-i\nu_n x} \tag{4.62}$$

where $\nu_n = \pi n/L$, which leads to

$$\begin{aligned} (4A^2 - \nu_n^2)p_n &= \mu q_n, \\ \nu_n^2 q_n &= \mu p_n. \end{aligned} \tag{4.63}$$

This can be rewritten in matrix form as

$$\begin{pmatrix} 4A^2 - \nu_n^2 & -\mu \\ -\mu & \nu_n^2 \end{pmatrix} \begin{pmatrix} p_n \\ q_n \end{pmatrix} = 0. \tag{4.64}$$

If we set the determinant of the matrix to zero we find an expression for the values of μ which determine the long term behaviour of the perturbation $\delta\phi$ and hence the stability of the solution ψ. This expression is

$$\mu^2 = \nu_n^2(4A^2 - \nu_n^2). \tag{4.65}$$

At this stage it is useful to note that the period of the solution ψ_0 is π/A^2, and the variables $\delta\psi$ and $\delta\phi$ are related by an exponential with the same period. Thus in equation (4.60) we can replace μ with $\mu \pm 2iA^2k, k \in \mathbb{N}$ and the shift will be unnoticed once we transform from $\delta\phi$ to $\delta\psi$.

Numerical analysis of the unperturbed NLS

We return to our analysis at (4.57), i.e.

$$i\delta\psi_t + \delta\psi_{xx} + 4|\psi_0|^2\delta\psi + 2\psi_0^2\delta\psi^* = 0. \tag{4.66}$$

As above we expand in real and imaginary parts. Let $\delta\psi = u + iv$ and $\psi_0 = \mathcal{R} + i\mathcal{I}$. While we know the real and imaginary parts of ψ_0 explicitly in this case, we choose to keep the work as general as possible so that it's easier to extend from our simplified problem to the PDDNLS (which includes damping, driving and a non-trivial spatial dependence). Substituting these two expressions gives us the following equations:

$$\begin{aligned} -v_t + u_{xx} + 6\mathcal{R}^2u + 2\mathcal{I}^2u + 4\mathcal{R}\mathcal{I}v &= 0, \\ u_t + v_{xx} + 2\mathcal{R}^2v + 6\mathcal{I}^2v + 4\mathcal{R}\mathcal{I}u &= 0. \end{aligned} \tag{4.67}$$

Given that the real and imaginary parts of the solution ψ_0 are periodic, we know from Floquet theory that we can write $u = e^{\mu t}r$ and $v = e^{\mu t}s$, where $r(x,t)$ and $s(x,t)$ are both $T-$periodic. We can rewrite the equations above as

$$\begin{pmatrix} 0 & 1 \\ -1 & 0 \end{pmatrix} \begin{pmatrix} -\partial_x^2 - 6\mathcal{R}^2 - 2\mathcal{I}^2 & \partial_t - 4\mathcal{R}\mathcal{I} \\ -\partial_t - 4\mathcal{R}\mathcal{I} & -\partial_x^2 - 2\mathcal{R}^2 - 6\mathcal{I}^2 \end{pmatrix} \begin{pmatrix} r \\ s \end{pmatrix} = \mu \begin{pmatrix} r \\ s \end{pmatrix}. \tag{4.68}$$

We expand the functions r and s in two dimensional Fourier series, i.e.

$$r = \sum_{m,n=-\infty}^{+\infty} \hat{r}_{m,n} e^{-i\nu_n x} e^{-i\omega_m t} \quad \text{and} \quad s = \sum_{m,n=-\infty}^{+\infty} \hat{s}_{m,n} e^{-i\nu_n x} e^{-i\omega_m t} \tag{4.69}$$

where we define $\nu_n = \pi n/L$ and $\omega_m = 2\pi m/T$ with L and T being the spatial length and temporal period respectively. Substitution gives

$$\sum_{m,n=-\infty}^{+\infty} \begin{pmatrix} 0 & 1 \\ -1 & 0 \end{pmatrix} \begin{pmatrix} \nu_n^2 - 6\mathcal{R}^2 - 2\mathcal{I}^2 & -i\omega_m - 4\mathcal{R}\mathcal{I} \\ i\omega_m - 4\mathcal{R}\mathcal{I} & \nu_n^2 - 2\mathcal{R}^2 - 6\mathcal{I}^2 \end{pmatrix} \begin{pmatrix} \hat{r}_{m,n} \\ \hat{s}_{m,n} \end{pmatrix} e^{-i\nu_n x} e^{-i\omega_m t}$$
$$= \mu \sum_{m,n=-\infty}^{+\infty} \begin{pmatrix} \hat{r}_{m,n} \\ \hat{s}_{m,n} \end{pmatrix} e^{-i\nu_n x} e^{-i\omega_m t}. \tag{4.70}$$

We now truncate the infinite sums at some finite values, i.e. we take $m \in \mathcal{M} = \{-M/2, \ldots, -1, 0, 1, \ldots, M/2-1\}$ and $n \in \mathcal{N} = \{-N/2, \ldots, N/2-1\}$. Once we've done that we can multiply through by $\exp[i\omega_{m'}t + i\nu_{m'}x]$ (where m' and $n' \in \mathcal{M}, \mathcal{N}$) and integrate over the entire spatio-temporal domain, $[-L, L] \times [0, T]$.

The result is the system of equations below:

$$\begin{aligned} a_{m,m',n,n'}\hat{r}_{m,n} - \nu_{n'}^2 \hat{r}_{m',n'} + b_{m,m',n,n'}\hat{s}_{m,n} + i\omega_{m'}\hat{s}_{m',n'} &= \mu \hat{s}_{m',n'} \\ c_{m,m',n,n'}\hat{r}_{m,n} + i\omega_{m'}\hat{r}_{m',n'} + d_{m,m',n,n'}\hat{s}_{m,n} + \nu_{n'}^2 \hat{s}_{m',n'} &= \mu \hat{r}_{m',n'} \end{aligned}. \tag{4.71}$$

The coefficients a, b, c, d are integrals of the product of the potentials and exponentials, i.e.

$$\begin{aligned} a_{m,m',n,n'} &= \frac{1}{TL} \int_{T,L} \left(6\mathcal{R}^2 + 2\mathcal{I}^2\right) e^{i(\omega_{m'} - \omega_m)t + i(\nu_{n'} - \nu_n)x} \, dt \, dx \\ b_{m,m',n,n'} &= \frac{1}{TL} \int_{T,L} \left(4\mathcal{R}\mathcal{I}\right) e^{i(\omega_{m'} - \omega_m)t + i(\nu_{n'} - \nu_n)x} \, dt \, dx \\ c_{m,m',n,n'} &= -b_{m,m',n,n'} \\ d_{m,m',n,n'} &= -\frac{1}{TL} \int_{T,L} \left(2\mathcal{R}^2 + 6\mathcal{I}^2\right) e^{i(\omega_{m'} - \omega_m)t + i(\nu_{n'} - \nu_n)x} \, dt \, dx. \end{aligned}$$

We can resolve this rank-four (m, m', n, n') system of equations into a useful two dimensional matrix by introducing a vector $\mathbf{r}$ whose components are the coefficients $\hat{r}_{m,n}$ and $\hat{s}_{m,n}$. We need to make a choice about the arrangement of the coefficients in this vector and then apply it consistently. We have opted to list all of the $\hat{r}_{m,n}$ then all of the $\hat{s}_{m,n}$ and we order them by holding n constant while cycling through all the values of m and then increasing n,

i.e.

$$\mathbf{r} = \begin{pmatrix} \hat{r}_{-M/2,-N/2} \\ \hat{r}_{-M/2+1,-N/2} \\ \vdots \\ \hat{r}_{M/2-1,-N/2} \\ \hat{r}_{-M/2,-N/2+1} \\ \vdots \\ \hat{r}_{M/2-1,N/2-1} \\ \hat{s}_{-M/2,-N/2} \\ \vdots \\ \hat{s}_{M/2-1,N/2-1} \end{pmatrix}. \tag{4.72}$$

Once we've rearranged the coefficients, the four-dimensional system of equations can be rewritten as a matrix eigenvalue problem,

$$A\mathbf{r} = \mu\mathbf{r}. \tag{4.73}$$

Note that the matrix A has the following neat structure: A is divided into four equally sized sub-matrices, i.e.

$$A = \begin{pmatrix} A_{\text{top, left}} & A_{\text{top, right}} \\ A_{\text{bottom, left}} & A_{\text{bottom, right}} \end{pmatrix}. \tag{4.74}$$

The top two correspond to the first line of equation (4.71) while the bottom two correspond to the second line. The two sub-matrices on the left correspond to the coefficients $\hat{r}_{m,n}$ while those on the right correspond to $\hat{s}_{m,n}$. To determine the values of $\hat{\mu}$ all we need to do now is compute A and then determine its eigenvalues. The first part is easy: the linear terms lie on the main diagonals of the submatrices and the nonlinear (potential) terms can be quickly evaluated using the fast Fourier transform. The second part is also easy: a number of routines exist to determine the eigenvalues of a matrix.

Errors arising in the numerical analysis of the NLS

As we mentioned at the beginning of section 4.4, the results of this method are subject to numerical error. We will explain where the error arises and how we can compensate.

We resume at equation (4.70). The error arises in the next step of our analysis when we truncate the infinite sums. Consider what happens to the top equation if we multiply through by $\exp[i\omega_{m'}t + i\nu_{m'}x]$ and integrate over the entire spatio-temporal domain when $n' \in \mathcal{N}$ but $m' \notin \mathcal{M}$.

$$L\delta_{n,n'}\int_0^T [6\mathcal{R}^2+2\mathcal{I}^2]e^{-i\omega_{m-m'}t}\hat{r}_{m,n}dt + L\delta_{n,n'}\int_0^T [4\mathcal{R}\mathcal{I}]e^{-i\omega_{m-m'}t}\hat{s}_{m,n}dt = 0. \tag{4.75}$$

Recalling that the solution ψ_0 is Ae^{2iA^2t} we can replace $\mathcal{R}$ with $A\cos(\omega_1 t)$ and $\mathcal{I}$ with $A\sin(\omega_1 t)$ where $\omega_1 = 2A^2$.

$$\begin{aligned} &2A^2 L\delta_{n,n'} \int_0^T [1 + 2\cos^2(w_1 t)] e^{-i\omega_{m-m'}t} \hat{r}_{m,n} dt \\ &+2A^2 L\delta_{n,n'} \int_0^T [2\sin(w_1 t)\cos(w_1 t)] e^{-i\omega_{m-m'}t} \hat{s}_{m,n} dt = 0. \end{aligned} \tag{4.76}$$

This can be simplified by using the trigonometric identities $2\sin\theta\cos\theta = \sin 2\theta$ and $2\cos^2\theta = 1 + \cos 2\theta$ (any constants introduced by these trigonometric substitutions can be ignored since they are multiplied by exponentials with purely imaginary arguments whose oscillations coincide with the range of integration):

$$\begin{aligned} &2A^2 L\delta_{n,n'} \int_{I'} \cos(\omega_2 t) e^{-i\omega_{m-m'}t} \hat{r}_{m,n} dt \\ &+2A^2 L\delta_{n,n'} \int_T \sin(\omega_2 t) e^{-i\omega_{m-m'}t} \hat{s}_{m,n} dt = 0. \end{aligned} \tag{4.77}$$

We can now evaluate the integrals. Recalling that $e^{-i\omega_{m-m'}t} = \cos(\omega_{m-m'}t) - i\sin(\omega_{m-m'}t)$ we see that

$$\delta_{n,n'}\delta_{2,m-m'}\hat{r}_{m,n} \pm i\delta_{n,n'}\delta_{\pm 2,m-m'}\hat{s}_{m,n} = 0, \tag{4.78}$$

where summation over repeated indices is implied. We can derive a similar constraint using the second line of (4.70). These constraints have not yet been considered when we calculate the eigenvalues p, in equation (4.73). Some of the eigenvectors that we calculate do satisfy the constraints, but the majority do not, and it is this majority that produce the erroneous scatter of eigenvalues in figure 4.3 below. Clearly we should make some allowances for these constraints. Two methods were considered.

1. We can use the equations (4.78) to express some values of either 13,,, or 4,,, in terms of each other and then to eliminate them from our system of equations. This corresponds to removing columns from the matrix A and then adjusting its rows.

2. We can use the equations to winnow out the inaccurate eigenvalues. After calculating the eigenvalues and corresponding eigenvectors of the full matrix A, we can check which eigenvectors satisfy (4.78) and discard those that do not.

The first method works, but cannot be easily extended to the complete problem: it was only because we were working with a simplified problem that the constraints were so neat. In equation (4.75) we could replace the real and imaginary parts of the solution with either sine or cosine, and so derive a simple relation between some of the elements of the eigenvector. In turn this allows us to easily modify the matrix A. The solutions to the PDDNLS are far more complex; integrals in (4.75) would be two-dimensional and the

resulting constraints would almost certainly not allow a quick modification to the matrix A.

The second method provides the correct result, and can be easily generalised to the PDDNLS.

4.4.2 The PDDNLS and its spatially inhomogenous solutions

The stability analysis for the PDDNLS is easily extended from the above numerical analysis for the toy problem; we only need to make one set of changes. The additional terms in the PDDNLS are on the right hand side of the equation

$$i\psi_t + \psi_{xx} + 2|\psi|^2\psi = h\psi^* - i\gamma\psi + \psi \tag{4.79}$$

and will obviously modify the system of equations (4.67) and hence the matrix A in (4.73). In the interest of brevity we will not repeat all the analysis here; fortunately it is sufficiently straightforward that we can jump to the conclusion.

The net result is that the main diagonals of the four submatrices that make up A are modified either by $-\gamma$ (the top left and bottom right submatrices) or $-h \pm 1$ (the top right, $+$, and bottom left, $-$).

There is one final, implicit, change: the nonlinear (off-diagonal) terms depend on the solution to (4.79) which is now unfortunately not as simple as $\psi_0 = Ae^{2iA^2t}$ and thus must now be determined numerically.

Having made these changes and determined the solution numerically, i.e. by continuation in the parameter h of the known soliton solutions, we still need to implement one of the methods discussed above to deal with the error introduced when we truncate the infinite series. As mentioned above, it is the second method that can most easily be generalised to the PDDNLS*.

The outputs from our code are the eigenvalues, μ_i, and associated eigenvectors, $\mathbf{v}_i$, of the matrix equation (4.73). To winnow the correct eigenvalues from the chaff, we need to calculate a set of constraints. We do this analogously to the work in equations (4.75) to (4.78). The most important change is that because our solution is no longer a simple function the resulting constraints are not as simple.

We pick $n' \in \mathcal{N}$ but $m' \notin \mathcal{M}$ and multiply the top equation of (4.70) through by $\exp[i\omega_{m'}t + i\nu_{m'}x]$ and integrate over the entire spatio-temporal domain. The result is an equation constraining the coefficients $\hat{p}_{m,n}$ and $\hat{q}_{m,n}$;

$$\delta_{n,n'}\alpha_{m,m'}\hat{p}_{m,n} + \delta_{n,n'}\beta_{m,m'}\hat{q}_{m,n} = 0. \tag{4.80}$$

Clearly each value of m' will yield a new equation and since the coefficients $\alpha_{m,m'}$ and $\beta_{m,m'}$ depend on the solution that we only know numerically, the

*In the remainder of this section we will refer to equations from section 4.4.1, which dealt with the NLS. It is to be understood that we mean the corresponding equations after modification to account for the additional terms in the PDDNLS.

constraints are not going to be as neat as those we derived in the simplified problem. Finally, we note (as for the simplified problem) that the procedure should be repeated with the bottom equation of (4.70).

If we recall the arrangement of the vector $\mathbf{r}$ from (4.72) we can finally outline the complete process for determining whether a multiplier μ_i with corresponding eigenvector $\mathbf{v}_i$ is faithful or spurious.

1. Choose a value for the first parameter, $K \in \mathbb{N}$. This parameter determines how many of the constraints we will use when we make our assessment.

2. Then, for every m' such that $M/2 - 1 < m' < M/2 - 1 + K$ or $-M/2 - K > m' > -M/2$:

   (a) and for every $n' \in \mathcal{N}$ calculate the equations (4.80) for the top and bottom equation of (4.70).

   (b) Append the coefficients of these equations as new rows of a matrix C.

3. Choose a second parameter, $\epsilon > 0$. This is a tolerance.

4. Then for every μ_i, if $||C\mathbf{v}_i|| > \epsilon$ discard the eigenvalue as spurious.

We present our some numerical results below to highlight this error correction method. Before we discuss the results we repeat the terminology from section 4.1 for clarity. The term eigenvalue and the symbol λ refer to a characteristic multiplier, not an exponent.

Figure 4.3 is a reproduction of the characteristic multipliers for the PDDNLS linearised around a periodic solution determined by numerical continuation. The parameter values are $\gamma = 0.2$ and $h = 0.235$. There are two components to the picture.

Firstly, there are correct eigenvalues whose positions are indicated by solid circles on the diagram. These eigenvalues agree with the results we obtained using the first method on this solution, and also with our theoretical expectations. There is a continuous spectrum of eigenvalues lying on the circle $\exp[-\gamma T]$. There are also six discrete eigenvalues. All six have zero imaginary part. Two of these eigenvalues lie near the point $(1, 0)$, and correspond to the two zero multipliers.

Secondly, there are a number of spurious eigenvalues, indicated by empty squares. We know that these eigenvalues are spurious because they don't agree with the results of our first method, don't agree with our theoretical expectations and, most importantly, because of the error-detection methods we developed when we applied the second method to spatially homogenous solutions of the NLS.

If we had not developed the error-detection methods by first implementing our method on a simpler problem, and had no other methods with which

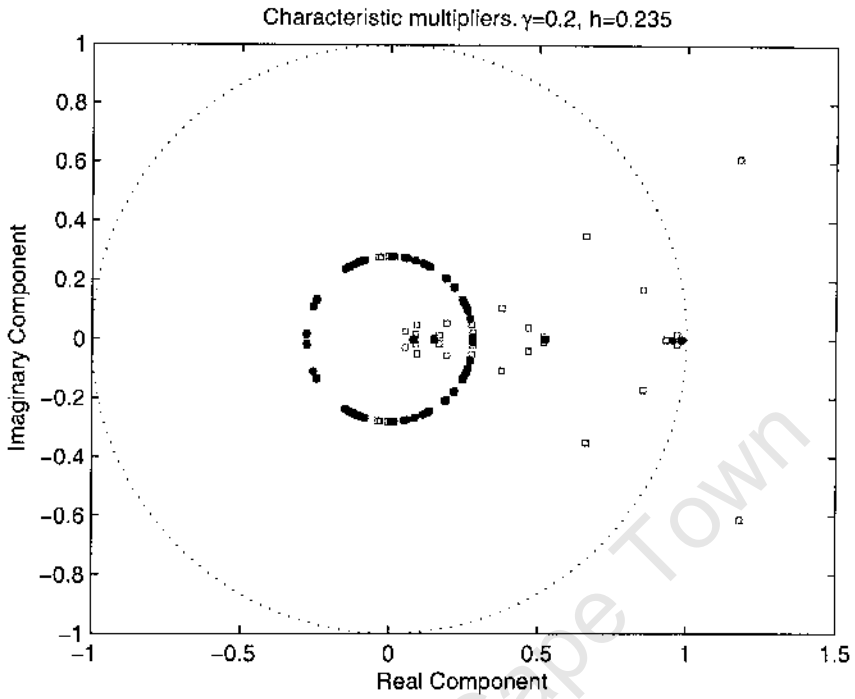

Figure 4.3: The blue dots above are eigenvalues that fall in the correct position, while the red squares represent additional eigenvalues that are scattered over the complex plane.

to check our results, we would incorrectly conclude that this solution is unstable as we would not be able to differentiate between the correct and spurious eigenvalues.

In theory then, the two parameters K and c control the number of eigenvalues that are kept and the number that are discarded, and we can tweak these parameters when h and -y change to ensure that we retain only faithful eigenvalues. Unfortunately, in practice we find that as h increases and we move away from the Hopf bifurcation point all the eigenvalues become spurious. In this situation we can only retain eigenvalues if we increase our tolerance dramatically. This is unacceptable; if we increase our tolerance to retain eigenvalues we can no longer trust their accuracy.

This inaccuracy is due to insufficiently large values of M and N, i.e. there is detail that we can not resolve. To address this problem we would like to increase these parameters, but we cannot as we run into hardware limitations. The memory used to store a (2 x M x N) x (2 x M x N) complex, double precision matrix increases dramatically as the parameters increase.

By illustration, consider $M = N = 50$. The vector r has 2x M x N entries - the factor of 2 arises from splitting JO into real and imaginary parts

and there are $M \; x \; N$ coefficients in the two-dimensional Fourier expansion.

The resulting matrix A is then 5000 x 5000, i.e. there are 25,000,000 entries each using 16 bytes (8 bytes each for the real and imaginary component). This is a total of 400,000,000 bytes, or 400MB, just for the storage of the matrix. A modest increase to $M = N = 60$ more than doubles the memory required.

Further, as the size of the matrix increases, more memory and processor cycles are required to calculate its eigenvalues. The net result is that this method cannot be implemented in its current state on a system with 32 bit architecture.

Thus we are forced to use our method presented in 4.3. While it is slow, it produces accurate results everywhere, not just near the Hopf bifurcation.

Chapter 5

Continuation and stability of the temporally periodic solitons of the PDDNLS

In this thesis we are investigating the PDDNLS

$$i\psi_t + \psi_{xx} + 2|\psi|^2\psi - \psi = h\psi^* - i\gamma\psi. \tag{5.1}$$

We are interested in the behaviour of its soliton solutions

$$\psi_\pm = A_\pm \mathrm{sech}(A_\pm x)e^{-i\theta_\pm}. \tag{5.2}$$

The three questions we asked in the introduction were:

1. In which parts of the ('y, *h)* parameter space are the 7/)+ solitons stable?
2. For values of *7* and *h* where the solitons are unstable, what sort of stable attractors do we observe instead?
3. Can these solitons be combined to form bound states, or complexes?

As we discussed in the introduction, some of these questions have already been answered. The *0_* soliton is always unstable, while the VL$_F$ soliton is stable in a region which must be contained in the area bounded by the curve $h = -V1 + 7^2$ and the straight line $h = 7$.

Figure 5.1 below is reproduced from Bondila *et al* [13]. It was constructed by direct simulation of the 0_+ soliton across the (7, *h)* plane. What we notice from figure 1.1 is that for fixed damping strength 7, the 7I>+ soliton undergoes a Hopf bifurcation as the driving strength *h* is increased.

As the driving strength increases further the system eventually devolves into some sort of spatio-temporal chaos. The route it takes to chaos depends on the damping strength, and so what we present in this section is a more thorough investigation of the behaviour of the 0_+ soliton after the

Hopf bifurcation point. In section 5.1 we consider the cases with damping coefficient $7 = 0.35$. This is representative of behaviour above the tri-critical point ('$y_e = 0.25$, $h = 0.81$) in figure 5.1. In sections 5.2 and 5.3 we consider $7 = 0.20$ and $7 = 0.10$ respectively. These are representative of behaviour below the tri-critical point. In section 5.4 we explain why there is no periodic solution if the damping is removed, i.e. $7 = 0.00$ [4].

Before the results of the continuation and stability analysis are presented it is prudent to make some comments about the conventions we have adopted. Firstly, the "spectra" described below refer to characteristic multipliers not exponents, i.e. A rather than μ. When a continuation diagram has more than one branch (as a result of period-doubling bifurcations) we denote by A' the eigenvalues of the first doubling, A" the eigenvalues of the second doubling etc.

Secondly, the spectra are neatly divided into two parts: a continuous spectrum which lies on a circle centered on the origin in the complex plane, with radius exp[-ÝT], and a few discrete eigenvalues off the circle. These discrete eigenvalues always occur in pairs - an eigenvalue outside the continuous spectrum circle and its counterpart mirrored inside the circle. We will only describe the behaviour of the exterior eigenvalues since the interior eigenvalues just mirror their movements, and it is only the exterior eigenvalues that can pass through the unit circle and influence the stability of the solution.

Finally, a note on continuation diagrams. The stable parts of the branches are drawn in solid black line, while the unstable parts are drawn in a dashed line. Further, any reference to an "upper" or "lower" branch refers to the branch with longer or shorter period. We will use these conventions throughout this chapter.

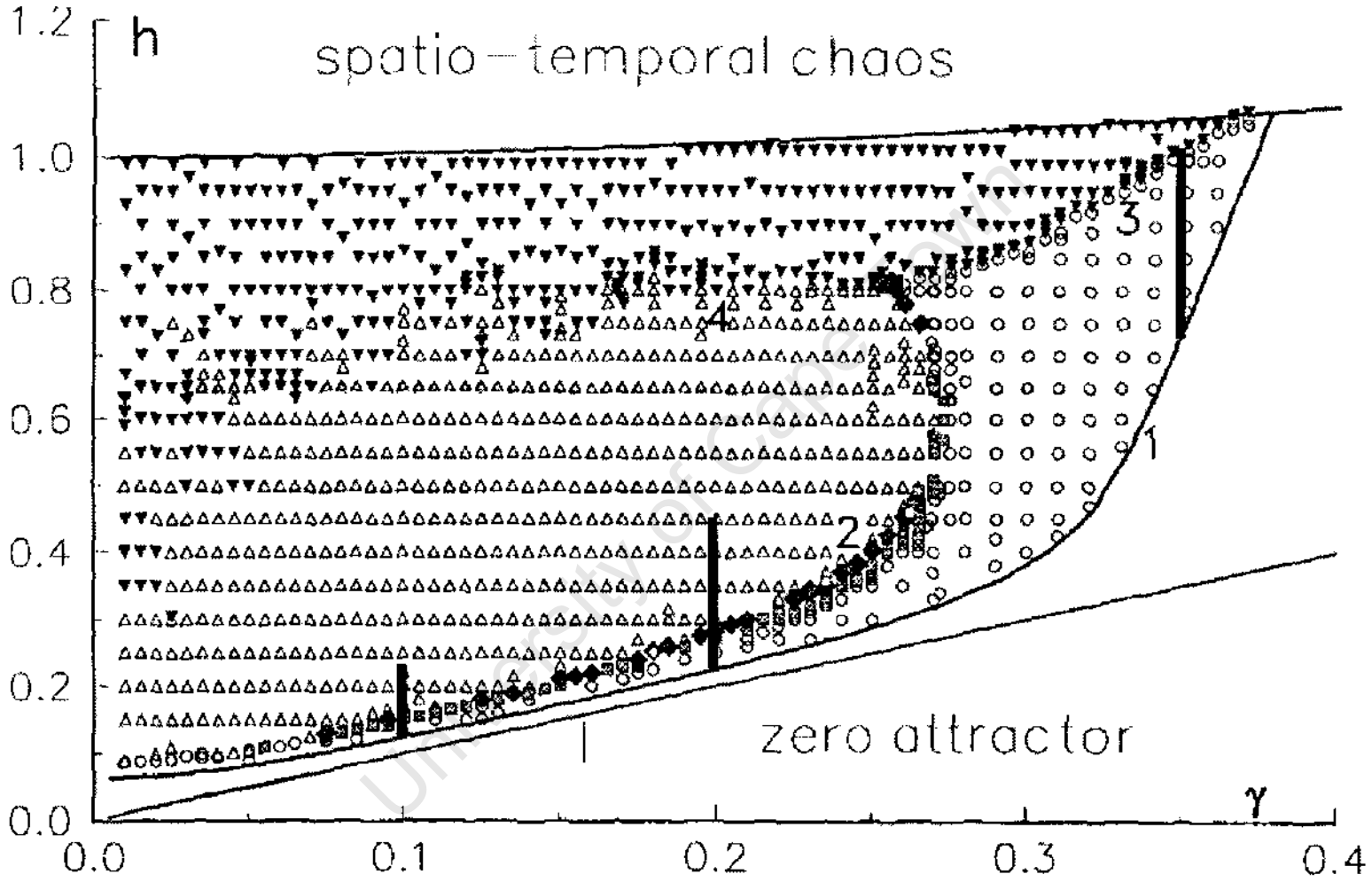

Figure 5.1: Attractor chart reproduced from Bondila *et al* [13]. We have added three vertical lines at $\gamma = 0.10$, $\gamma = 0.20$ and $\gamma = 0.35$. These indicate the three cases we investigate in sections 5.1 to 5.3 below.

5.1 Continuation of the single soliton ($\gamma = 0.35$)

In figure 5.2 we illustrate the continuation of the single 0_+ soliton past the point of Hopf bifurcation, i.e. we are continuing temporally periodic solutions which initially have just a single spatial peak. The bifurcation diagram is quite simple; as h increases the period of the solutions decrease as their energies grow. The branch undergoes a saddle-node bifurcation at $h = 1.0185$ and on the returning unstable branch the period of the solutions increase as their energies drop.

We discuss first the transformation of the characteristic multipliers along this curve, and then the change of the solution itself. At the Hopf bifurcation point, i.e. $h = 0.75$, the spectrum has three discrete eigenvalues (A1,2,3) = 1. As h increases one of the discrete eigenvalues (A_i) moves along the real axis towards the continuous spectrum. The other two discrete eigenvalues (A2,3) remain at 1 until the turning point $h = 1.0185$ is reached. As h grows beyond 0.90 additional discrete eigenvalues (A4,5,6,7,8) detach from the continuous spectrum and move along the real axis towards the unit circle.

The first of these discrete eigenvalues (A4) collides with the original eigenvalue moving inward along the real axis (A_1) as h passes 1.00 and these two form a complex conjugate pair (A1,4) that moves away from the real axis, initially increasing in both modulus and argument. This complex conjugate pair approaches the unit circle, but as the turning point is reached, they rapidly return to the real axis.

At the turning point there are five discrete eigenvalues near 1. Inside the circle there are the two eigenvalues of the complex conjugate pair ($A_{1,4}$). The discrete eigenvalue (A5) that detached from the continuous spectrum and moved unimpeded along the real axis has passed through the unit circle, as have the two original unit values (A2,3).

As h decreases and we move along the lower branch the original unit eigenvalues (A2,3) continue to move along the real axis away from the origin. The three eigenvalues near one $_{(A1,4,5)}$ remain stationary and two more of the eigenvalues (A6,7) that detached from the continuous spectrum move along the real axis until they come to rest at one when the branch ends at $h = 0.76$. The final discrete eigenvalues (A8) that detached from the continuous spectrum moves back along the real axis and rejoins it shortly after the turning point (by $h = 1.00$).

The solution also changes as we progress along the branch. Figure 5.3 shows the absolute value of the solution at representative points along the curve. The plots all show at least a full period.

It is clear that as we progress along the branch the spatial profile changes. Near the Hopf bifurcation point the solution has just one central hump; we obtained this solution by continuing from the known 0_+ soliton (Fig. 5.3.a). As we move along the branch ripples emerge from this hump (Fig. 5.3.b) and these ripples grow (Fig. 5.3.c) until at the end of the bottom branch we

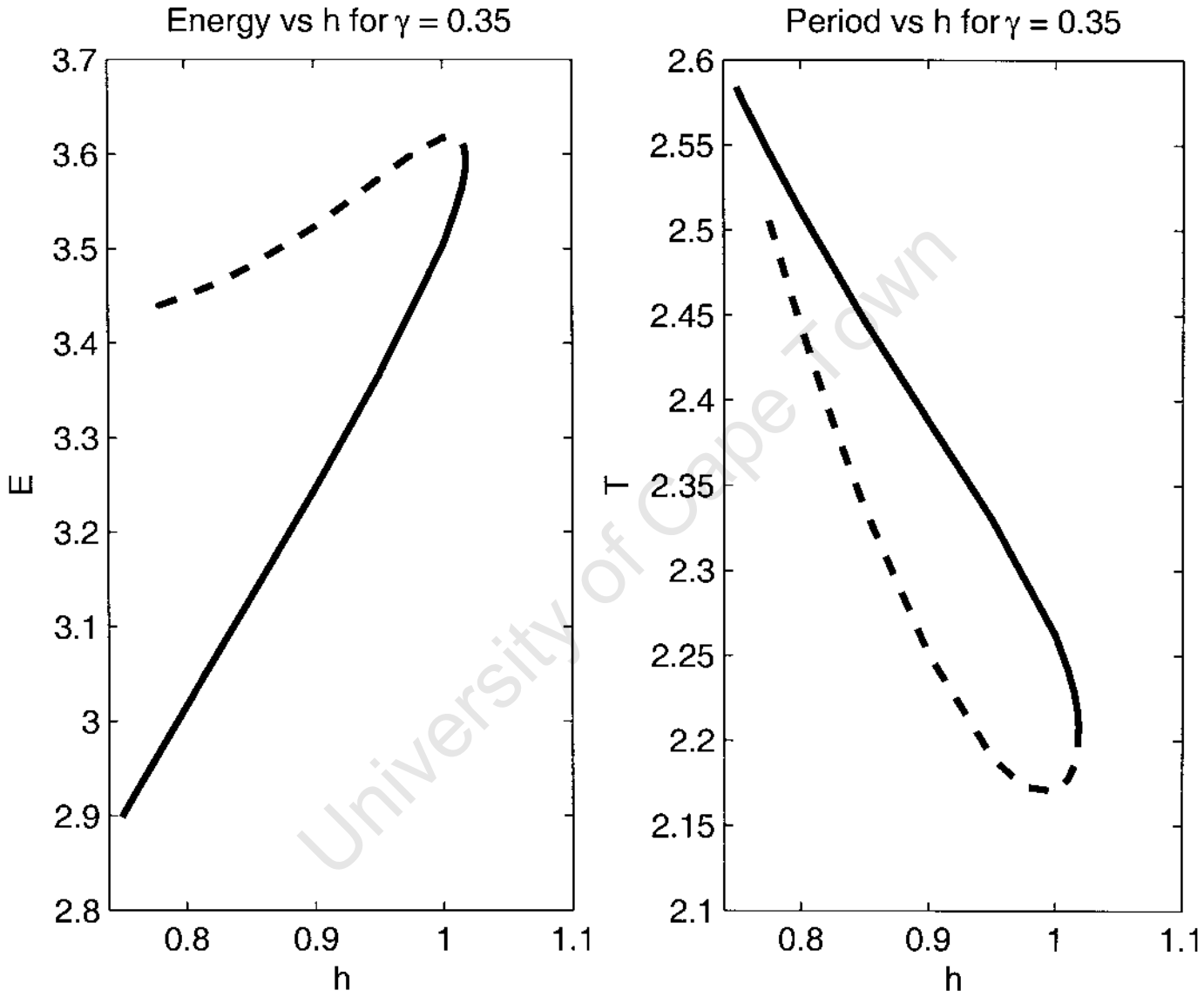

Figure 5.2: Bifurcation diagram for $\gamma = 0.35$. Solid and dashed lines indicate the existence of stable and unstable periodic solutions respectively.

have three distinct humps - the original θ_+ hump and two smaller humps which flank it (Fig. 5.3.d).

In general we can classify a soliton complex by examining its amplitude, phase and eigenvalues. If we compare the eigenvalues of the complex we've described above with the eigenvalues of the θ_+ and 0_ solitons for the same parameter values, it's easy to classify. The eigenvalues of the complex are just a superposition of the eigenvalues of the θ_+ soliton with two copies of the eigenvalues of the 0_ soliton and so it is clearly a $0_{(-+-)}$ complex. This classification was confirmed by comparing the amplitudes of the $\eta_\pm$ solitons with the amplitude of the three humps in the complex.

The correspondence between the eigenvalues of the complex and its constituent solitons, as well as of the amplitudes were in very good correspondence. This happened only because the constituents of the complex are clearly separated from each other. In most cases the agreement is not as obvious.

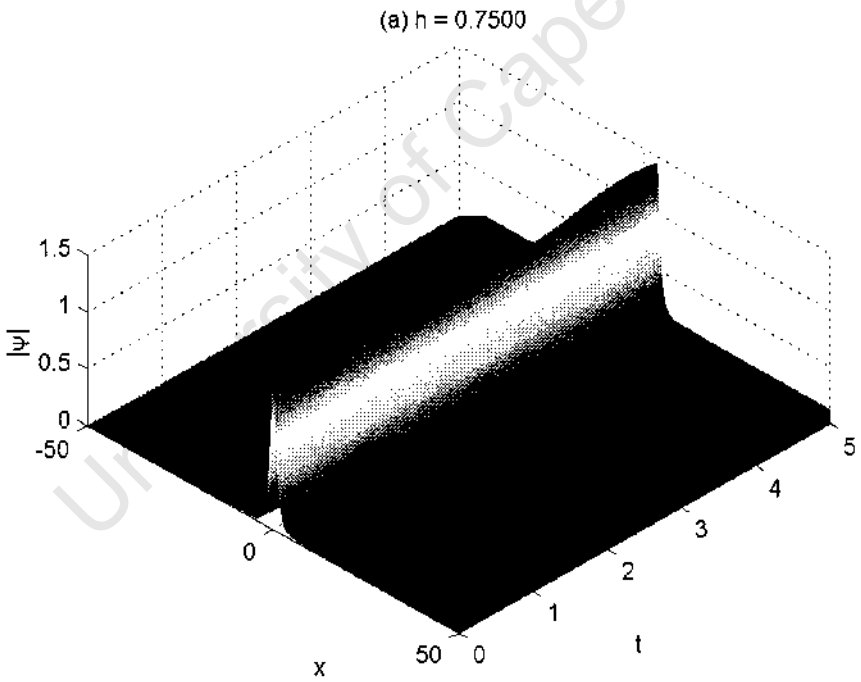

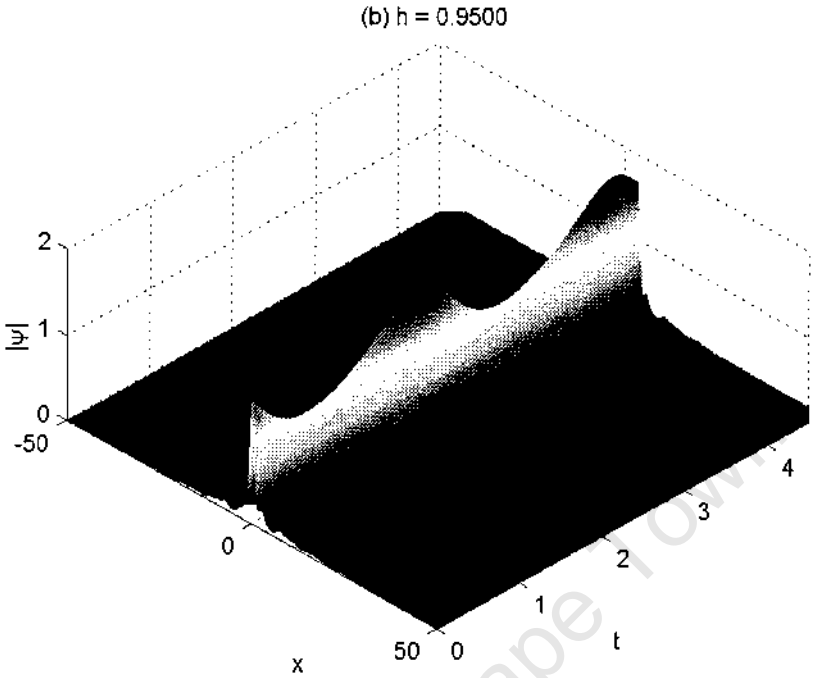

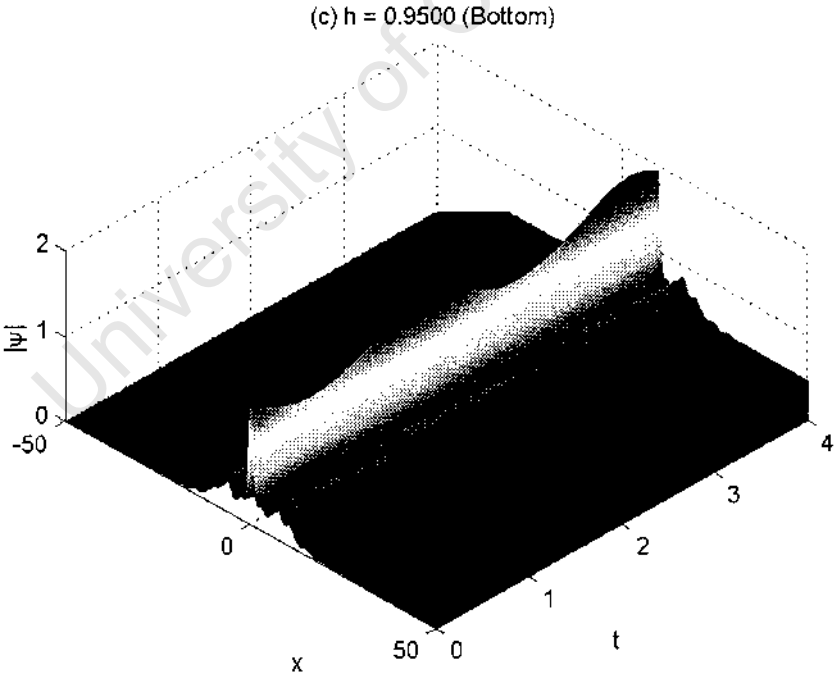

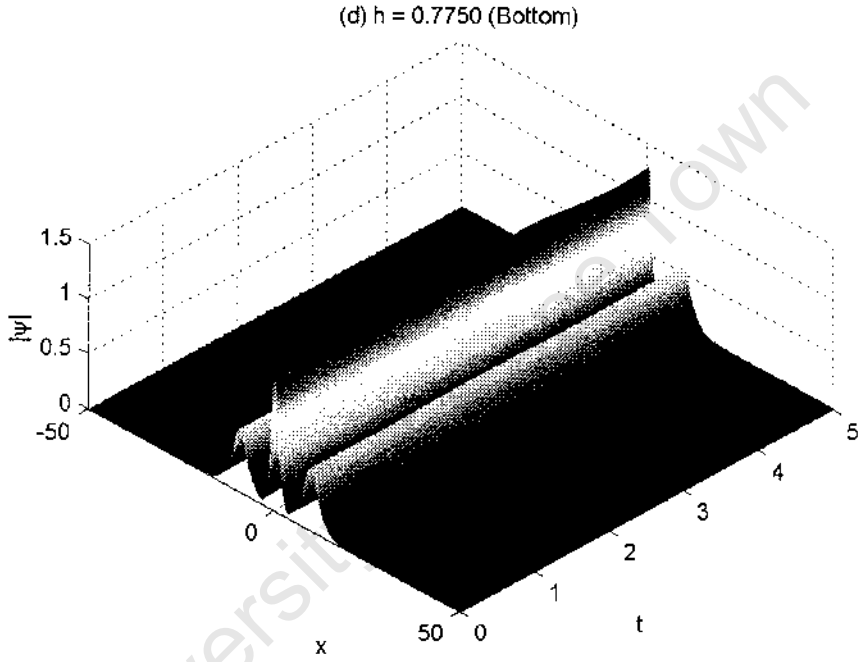

Figure 5.3: Solutions for $\gamma = 0.35$. The plots show $|\psi|$; (a) is at $h = 0.7500$, (b) $h = 0.9500$, (c) $h = 0.9500$ after the turn and (d) $h = 0.7750$ after the turn. We see ripples emerge from the central hump and by figure 5.3.d these ripples have developed into two distinct humps, well-separated from the central peak.

5.2 Continuation of the single soliton ('y = 0.20)

The continuation of the 'y = 0.20 branch from the Hopf bifurcation point is illustrated in Figure 5.4. As in section 5.1 above we are continuing periodic solutions which initially have just a single spatial peak. Note the increasing period of the solutions. As the period increases we must increase either the number, or size, of the time steps in the continuation code. Both of these options are problematic. If we increase the number of time steps the continuation calculations require more memory and time. Conversely, if we increase the size of the time steps some detail may be lost. For this reason we have not continued the solution branches beyond T = 15.

It is obvious that the behaviour for 7 = 0.20 is qualitatively very different from the behaviour for 7 = 0.35. Both branches start with a Hopf bifurcation of the stationary 0_+ soliton. While the branch for 7 = 0.35 undergoes a saddle-node bifurcation and terminates at a stationary $0(\_+\_)$ complex the branch for 7 = 0.20 undergoes a series of period doubling bifurcations before snaking upwards.

At the Hopf bifurcation point, i.e. h = 0.2275, the solution has three discrete eigenvalues (A1,2,3) at one. As h increases one of these eigenvalues, (A_i), moves along the real axis towards the continuous spectrum. It is absorbed by this spectrum, then detaches again from the other side of the continuous spectrum on the real axis, but is now negative. It continues moving along the real axis and passes through negative one at h = 0.2663. This is a period-doubling bifurcation: the original branch loses its stability and a new stable branch appears. The bifurcation is indicated by a thin vertical line in Figure 5.4.

The spectrum of the new branch is slightly more complicated. It is also born with three discrete eigenvalues ($A'_{1,2,3}$) at one. As h increases one of these eigenvalues, (M) moves along the real axis. It is absorbed by the continuous spectrum, detaches on the other side and passes through negative one at h = 0.2725. A new stable branch appears. During that same interval a complex conjugate pair of discrete eigenvalues ($Y_{4,5}$) detaches from the continuous spectrum. As they detach they have real components of zero.

Due to the limitations discussed above we have not investigated this new branch. Bondila *et al* [13] observed period-doubling to chaos by direct simulation for 7 = 0.20. While we don't have their raw data, Figure 5.1 suggests that the period-doubling cascade they observed started at h ~ 0.27. This is in agreement with our results, and so as h increases our newest branch would presumably also undergo a period-doubling bifurcation after a short interval of stability, and similarly the branches that it births would undergo a chain of period-doubling bifurcations. We shift our attention now away from the eigenvalues and to the solutions themselves.

Figure 5.5 shows some representative solutions. In Fig. 5.5.a we see a solution after the period-doubling. Notice that the interval between the

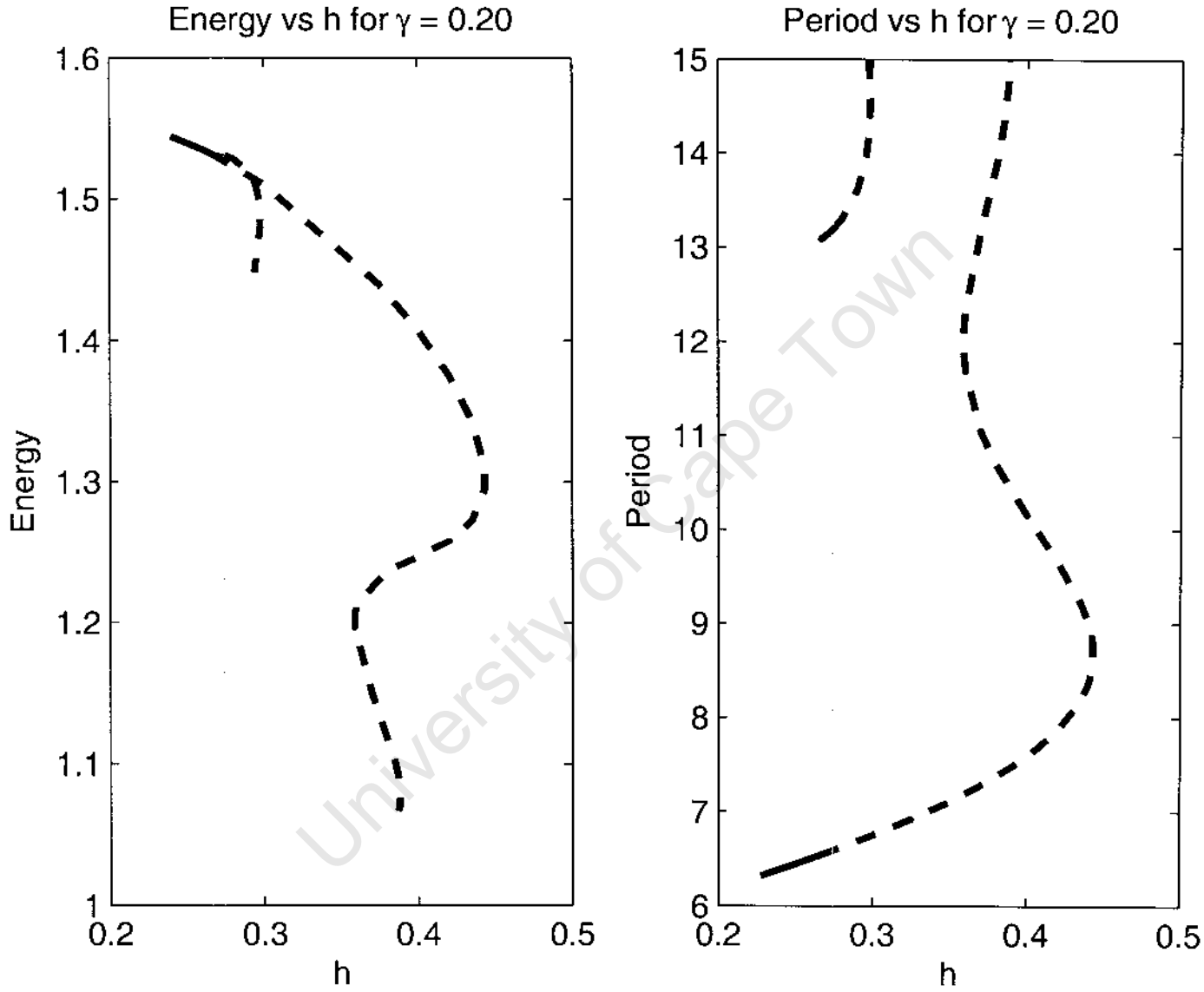

Figure 5.4: Bifurcation diagram for $\gamma = 0.20$. The thin vertical lines indicate the period-doubling bifurcations of the period-one and period-two branches.

peaks alternates; two peaks happen in quick succession before a longer gap which is followed by the same two peaks. Fig. 5.5.b shows typical behaviour for the lower branch. A sharp peak is followed by a long quasi-stationary epoch which is interrupted by the same sharp peak.

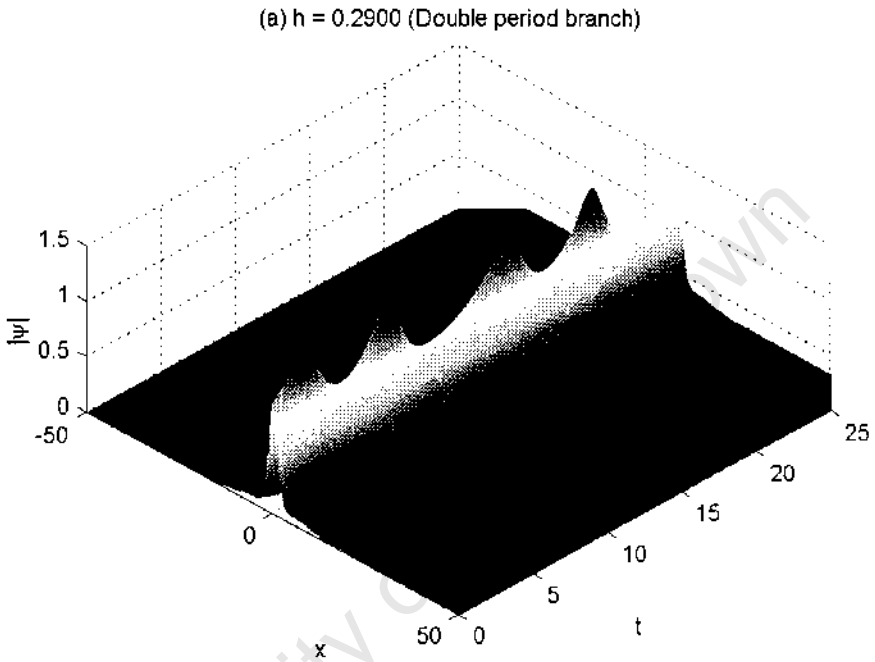

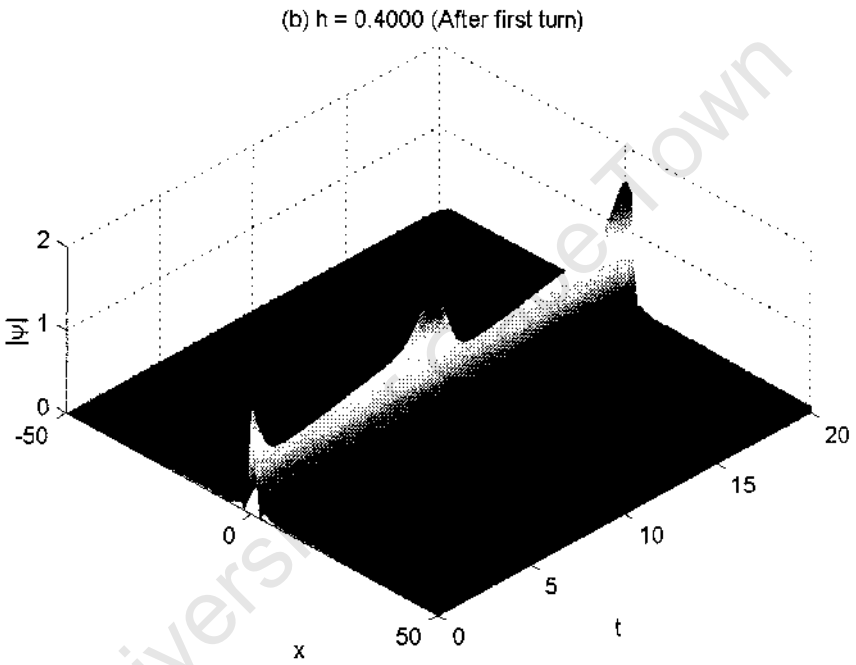

Figure 5.5: Solutions for $\gamma = 0.20$. The plots show (a) $h = 0.2900$ on the double period branch, and (b) $h = 0.4000$ on the original branch after the first turning point.

5.3 Continuation of the single soliton (Ý = 0.10)

The behaviour with 7 = 0.10 is qualitatively similar to the case with 7 = 0.20, and so instead of presenting the complete bifurcation diagram for 7 = 0.10 as we did for the previous two cases we have instead reproduced a comparison of the behaviour for these two cases in figure 5.6.

For completeness we should note that:

1. the solutions for 7 = 0.10 are qualitatively similar to the $7 = 0.20$ case, i.e. on the bottom branch a sharp peak is followed by a long quasi-stationary epoch. The length of this epoch grows as we follow the branch.

2. the first two period doublings, i.e. the bifurcation of the period-one solution to a period-two and then period-four solution, take place at $h = 0.1463$ and $h = 0.1511$. These are indicated by the thin vertical lines in Figure 5.6.

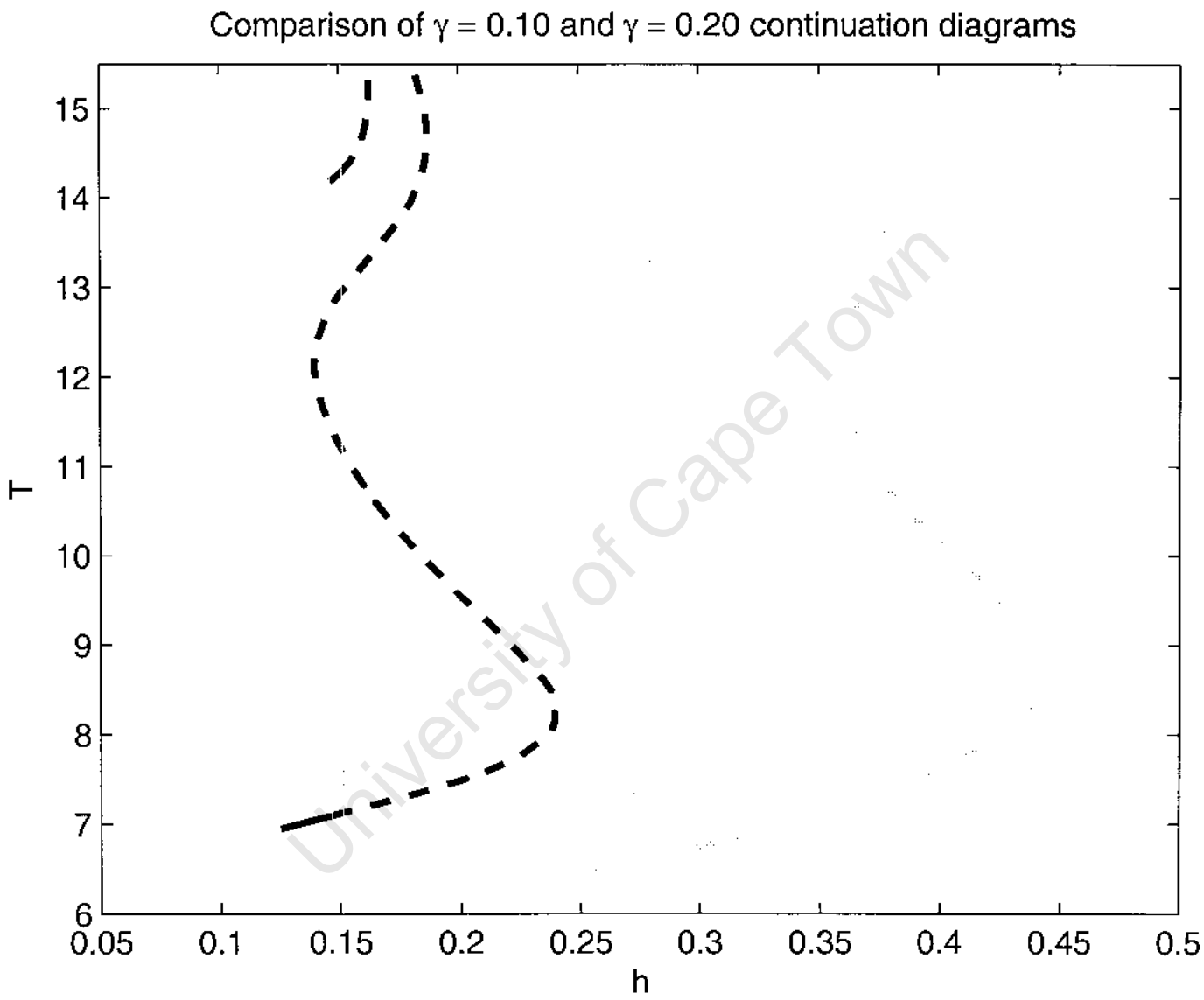

Figure 5.6: Comparison of h vs T bifurcation diagrams for $\gamma = 0.10$ (in black) and $\gamma = 0.20$ (in gray). The thin vertical lines indicate the period-doubling bifurcations of the period-one and period-two branches.

5.4 Investigation into the undamped behaviour (7 = 0)

We have seen that for 7 = 0.20 and 7 = 0.10 the periodic solution undergoes a series of period-doubling bifurcations as h increases. When 7 << 1 the behaviour is completely different. Alexeeva *et al* [4] showed that there are no periodic attractors when 7 = 0. Instead any initial conditions will evolve into either a slowly decaying breather, or a slowly growing large-amplitude soliton. They confirmed their analytical results through direct simulation.

Our own results are reproduced in figure 5.7. This figure shows the stable parts of the branches obtained by continuing a single soliton for 7 = 0.002, y = 0.004, 7 = 0.006, 7 = 0.008, and 7 = 0.010 near the Hopf bifurcation point. The dotted vertical line is at h = 0.6359, the value of the Hopf bifurcation of the 0_+ soliton with y = 0. The branches we investigated are constrained on the left by this line.

The 7 = 0.002 branch loses its stability at 0.0666, while the 7 = 0.004 branch loses its stability at 0.0675. At these points a pair of complex conjugate eigenvalues that have previously detached from the continuous spectrum pass through the unit circle, indicating the birth of a quasi-periodic solution. Figure 5.8 shows direct simulation of the 7/4 soliton for 7 = 0.002 and h = 0.0667, just after the period-one solution has lost stability. The quasi-periodic behaviour is clearly visible in this figure. The spacing between successive peaks is approximately 7.2, which agrees with the period at the end of the stable branch, but these peaks are modulated with a second, lower frequency.

The branches with 7 = 0.006, 7 = 0.008, and 7 = 0.010 all continue beyond h = 0.068 and are all still stable at that point, but their spectra of eigenvalues all include a complex conjugate pair which has detached from the continuous spectrum and is moving towards the unit cirle. We believe that these branches will also lose their stability and birth a quasi-periodic solution at a larger value of h. We have unfortunately been unable to continue our investigation of these branches due to numerical constraints. As the damping 7 becomes smaller the spatial tails of the soliton decay more slowly. This means that a broader interval must be considered to obtain results, which in turn requires both more memory and computing power.

The continuous spectrum of multipliers lies on a circle with radius $e^{-\gamma T}$. Thus as 7 decreases and the continuous spectrum of multipliers moves closer to the unit circle, the corresponding period-one solitons will lose their stability at smaller values of h. When 7 = 0 the continuous spectrum of characteristic multipliers lies *on* the unit circle and so the secondary Hopf bifurcation is immediate. This confirms that the direct simulations of Alexeeva *et al* [4] should not recover a period-one soliton, and agrees with the theoretical justification they presented.

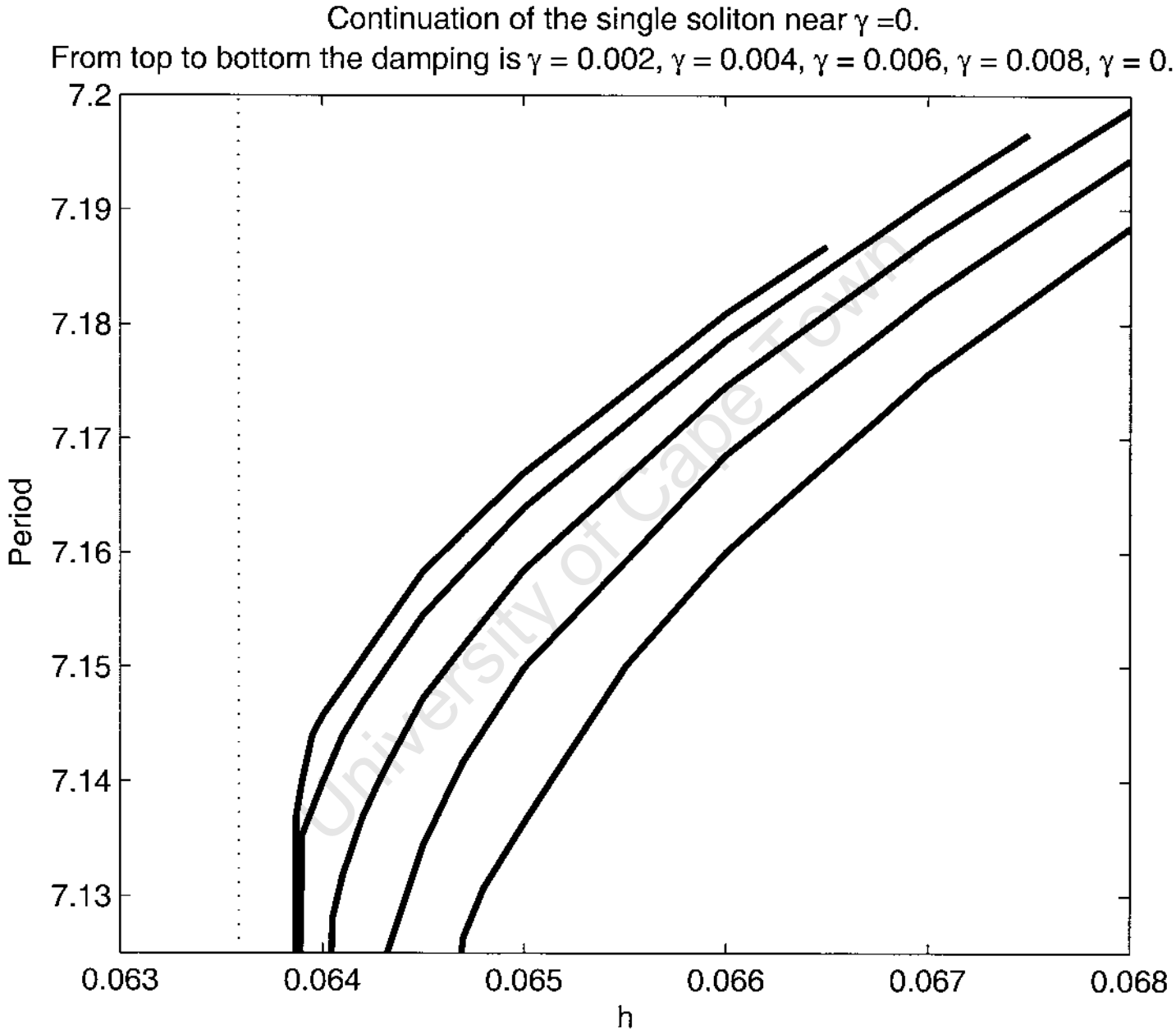

Figure 5.7: Continuation diagram showing the stable behaviour with small damping. The dotted vertical line is a t $h = 0.06359$, the Hopf bifurcation point of the ψ_0 soliton when $\gamma = 0.00$.

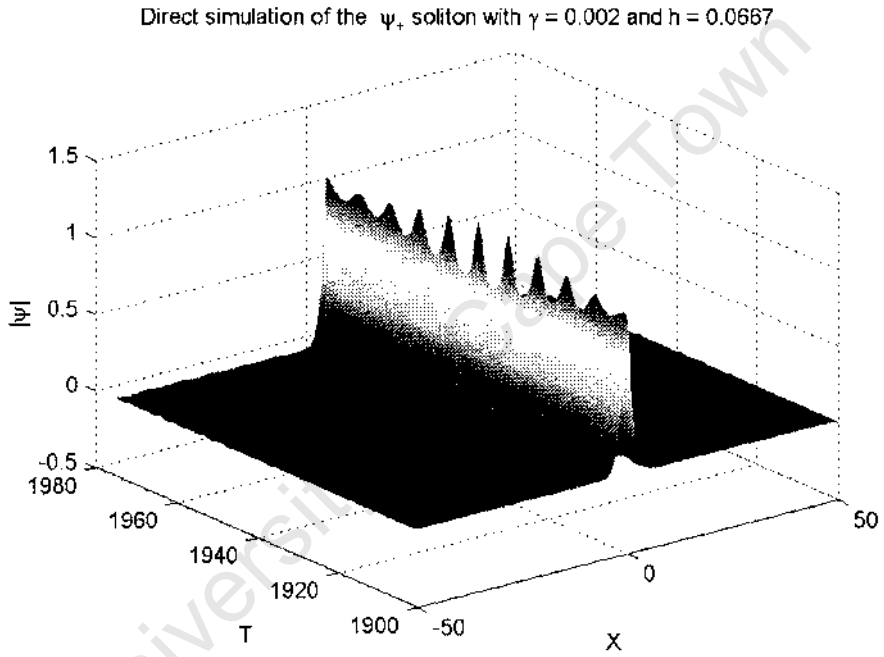

Figure 5.8: Direct simulation of the ψ_+ soliton for $\gamma = 0.002$ and $h = 0.0667$.

Chapter 6

Conclusions

In this thesis we investigated the behaviour of temporally periodic soliton solutions of the PDDNLS. We used numerical continuation with an iterative Newtonian method to solve the PDDNLS as a two-dimensional boundary value problem and examine the behaviour of the single soliton after it undergoes a Hopf bifurcation. The direct simulations of Bondila *et al* [13] found different types of behaviour as the damping strength 7 was changed. These regimes of different behaviour in ('y, *h)* parameter space meet at a tri-critical point 7, = 0.25, *h,* = 0.81. We considered a number of cases.

1. Large damping, i.e. 7 > 7,. In this case we aimed to explain how the spatio-temporal chaos observed by previous authors occurs. Large damping was exemplified by 7 = 0.35.

2. Intermediate damping, i.e. 7 < *7,.* In this case we aimed to investigate the solutions after they undergo period-doubling bifurcations. Intermediate damping was exemplified by 7 = 0.20 and 7 = 0.10.

3. Very small damping, i.e. 7 < 1. In this case we aimed to confirm that there is no periodic attractor for zero damping [4], and also to explain why a periodic solution cannot be stable for zero damping. Very small damping was exemplified by 7 = 0.002, 7 = 0.004, *7* = 0.006, 7 = 0.008, and *7* = 0.010.

The results from the large damping case ('y = 0.35) are easy to reconcile with the attractor chart produced by direct simulation [13]. Firstly, consider the previous results obtained by direct simulation. The attractor chart indicates that as we increase *h* the 0_+ soliton undergoes a Hopf bifurcation to a period-one solution which remains stable until *h c* 1. After this value any non-zero initial condition evolves chaotically.

Our own work confirms the results produced by direct simulation, and explains exactly how the chaos arises. For 7 = 0.35 we followed a stable period-one solution from *h* = 0.7500 to *h* = 1.0185. At *h* = 1.0185 the

period-one solution loses its stability as three of its characteristic multipliers pass through the unit circle. This is a compound bifurcation; two bifurcations occur simultaneously. Firstly, a saddle-node bifurcation occurs and an unstable branch turns back. Secondly, a secondary Hopf bifurcation occurs which births the chaotic behaviour we observe when $h > 1.0185$. We followed the unstable period-one solution that turned back at the saddle-node bifurcation point until it terminated as a three-soliton complex, $0_{(-+-)}$. These complexes have been observed previously for large damping [10].

The two cases with intermediate damping (7 = 0.20 and 7 = 0.10) had qualitatively different behaviour to the large damping case described above. The previous results obtained by direct simulation show that the 0_+ soliton undergoes a Hopf bifurcation to a period-one solution as h is increased. However, unlike the large damping case where the period-one solution is stable between the Hopf bifurcation and $h = 1$, in the cases with smaller damping the period-one solution undergoes a series of period-doubling bifurcations shortly after the Hopf bifurcation. We are unaware of any investigation into the (unstable) solutions after the period-doublings, and so that was the focus of our work.

In both intermediate damping cases we observed a series of period-doubling bifurcations as h was increased. This confirms the results produced by direct simulation. We also followed the unstable branches after the period-doubling bifurcations. We found that the solutions on the unstable branches were comprised of a long quasi-stationary epoch broken by a short peak. As these quasi-stationary epochs grow longer, the unstable branches snake upwards.

It is not clear whether these unstable branches snake upwards indefinitely. Numerical limitations prevented us from following the branches beyond T 15, but the steepening of the branches make it unlikely that they return.

Finally, we investigated the case of very small damping. Alexeeva *et al* [4] have shown that for zero damping the only attractors are a slowly decaying small- and a slowly growing large-amplitude breather. To confirm that these are the only attractors for zero damping, we examined the attractors for very small, but non-zero damping. In particular, we examined the branches of stable period-one solutions (i.e. attractors) when 7 = 0.002, 7 = 0.004, 7 = 0.006, 7 = 0.008, and 7 = 0.010.

We found that these branches lose their stability when they undergo a secondary Hopf bifurcation and a stable quasi-periodic solution is born. This secondary Hopf bifurcation occurs after a pair of discrete eigenvalues, or characteristic multipliers, detach from the continuous spectrum of eigenvalues and pass through the unit circle. As 7 —p 0 the continuous spectrum of eigenvalues moves closer to the unit circle, and so the secondary Hopf bifurcation occurs sooner, i.e. at smaller values of h. When 7 = 0 the continuous spectrum lies on the unit circle and so the secondary Hopf

bifurcation occurs with the same values as the primary Hopf bifurcation, $h = 0.6359$, precluding the possibility of a period-one attractor.

We have examined only the stable branches of solitons for very small damping to explain the results of Alexeeva *et al* [4]. Since we are not using direct simulation we can, in principle, also investigate the unstable branches. While the direct simulations of Bondila *et al* [13] are fairly coarsely spaced and do not indicate any interesting behaviour in this regime, the direct simulations of Robinson [67] are more careful and have uncovered alternating intervals of periodic, quasi-periodic and zero attractors for small 7. It would be interesting to track the periodic solutions through the regions where other attractors exist, and to investigate the mechanism whereby they lose, and regain, their stability.

There are two other areas that merit further investigation. Firstly, we are interested in the behaviour when the damping, 7, lies between the intermediate (7 = 0.10) and very small (7 = 0.01) cases. We have established that for very small 7 we see quasi-periodic behaviour, while at 7 = 0.10 we observe the period-doubling route to chaos. At some value of 7 < 0.10 the behaviour of the system must change. It would be enlightening to find the smallest value of 7 where we still observe the period-doubling route to chaos, to examine the transition between these two regimes and determine the underlying mechanism.

Similarly, we are interested in the change that must occur between 7 = 0.20 and 7 = 0.35. As is clear from the attractor chart, Figure 5.1, this interval includes the tri-critical point where the line separating spation-temporal chaos from the zero attractor, the line separating period-one solutions from chaos and the line tracing period-doublings meet. This behaviour, and the transformation between regimes, is currently being investigated by Elena Zemlyanaya.

Bibliography

[1] M.J. Ablowitz, D.J. Kaup, A.C. Newell, and H. Segur. The inverse scattering transform-Fourier analysis for nonlinear problems. *Studies in Applied Mathematics,* 53:249-315, 1974.

[2] G.P. Agrawal. *Nonlinear fiber optics.* Academic Press, 2001.

[3] N.N. Akhmediev and A. Ankiewicz. *Solitons: Nonlinear pulses and beams.* Chapman and Hall, 1997.

[4] N.V. Alexeeva, I.V. Barashenkov, and D.E. Pelinovsky. Dynamics of the parametrically driven NLS solitons beyond the onset of the oscillatory instability. *Nonlinearity,* 12:103-140, 1999.

[5] E.L. Allgower and K. Georg. *Introduction to numerical continuation methods.* Society for Industrial and Applied Mathematics, 2003.

[6] A.A. Andronov and L.S. Pontriagin. Robust systems. *Doklady Akad. Nauk SSSR,* 16:247-250, 1937.

[7] I.V. Barashenkov, N.V. Alexeeva, and E.V. Zemlyanaya. Two- and three-dimensional oscillons in nonlinear Faraday resonance. *Phys. Rev. Lett.,* 89:104101, Aug 2002.

[8] I.V. Barashenkov, M.M. Bogdan, and V.I. Korobov. Stability diagram of the phase-locked solitons in the parametrically driven, damped nonlinear Schrödinger equation. *Europhys. Lett.,* 15:113-118, 1991.

[9] I.V. Barashenkov and Y.S. Smirnov. Existence and stability chart for the ac-driven, damped nonlinear Schrödinger solitons. *Phys. Rev. E,* 54:5707-5725, Nov 1996.

[10] I.V. Barashenkov and E.V. Zemlyanaya. Stable complexes of parametrically driven, damped nonlinear Schrödinger solitons. *Phys. Rev. Lett.,* 83:2568-2571, Sep 1999.

[11] I.V. Barashenkov, E.V. Zemlyanaya, and M. Bar. Traveling solitons in the parametrically driven nonlinear Schrödinger equation. *Phys. Rev. E,* 64:016603, Jun 2001.

[12] L. Berge. Wave collapse in physics: principles and application to light and plasmawaves. *Physics reports,* 303:259-370, 1998.

[13] M. Bondila, I.V. Barashenkov, and M. Bogdan. Topography of attractors of the parametrically driven nonlinear Schrödinger equation. *Physica D,* 87:314-320, 1995.

[14] C.G. Broyden. A class of methods for solving nonlinear simultaneous equations. *Mathematics of Computation,* 19:577-593, 1965.

[15] C.G. Broyden. The Convergence of a Class of Double-rank Minimization Algorithms 1. General Considerations. *IMA J Appl Math,* 6:76-90, 1970.

[16] D. Cai, A.R. Bishop, N. Gronbech-Jensen, and B.A. Malomed. Bound solitons in the ac-driven, damped nonlinear Schrödinger equation. *Phys. Rev. E,* 49:1677-1679, Feb 1994.

[17] B. Charbonnier and T. Georges. Influence of power variations along a transmission line on soliton interaction. *Optics Communications,* 132:232 — 235, 1996.

[18] A.A. Coley. *Beicklund and Darboux transformations: the geometry of solitons: AARMS-CRM Workshop, June 4-9, 1999, Halifax, N.S., Canada.* AMS Bookstore, 2001.

[19] T. Dauxois and M. Peyrard. *Physics of Solitons.* Cambridge University Press, 2006.

[20] D.F. Davidenko. On a new method of numerical solution of systems of nonlinear equations. *Doklady Akad. Nauk SSSR (N.S.),* 88:601-602, 1953.

[21] W.C. Davidon. A class of methods for solving nonlinear simultaneous equations. *Mathematics of Computation,* 19:577-59, October 1965.

[22] M. Demazure. *Bifurcations and Catastrophes: Geometry of Solutions to Nonlinear Problems.* Springer-Verlag, 1989.

[23] M. Farkas. *Periodic Motions.* Springer-Verlag, 1994.

[24] M.J. Feigenbaum. Quantitative universality for a class of non-linear transformations. *J. Stat. Phys.,* 19:25-52, 1978.

[25] R. Fletcher. A new approach to variable metric algorithms. *The Computer Journal,* 13:317-322, 1970.

[26] D. Gale and M. Sotomayor. Some remarks on the stable matching problem. *Discrete Appl. Math.,* 11:223-232, 1985.

[27] C.S. Gardner, J.M. Greene, M.D. Kruskal, and R.M. Miura. Method for solving the Korteweg-de Vries equation. *Phys. Rev. Lett.,* 19:1095-1097, Nov 1967.

[28] T. Georges, B. Charbonnier, and F. Favre. Influence of filter frequency dispersion on soliton arrival time jitter. *Optical Fiber Technology,* 2:134 — 142, 1996.

[29] D. Goldfarb. A family of variable-metric methods derived by variational means. *Mathematics of Computation,* 24:23-26, 1970.

[30] J. Guckenheimer and P.J. Holmes. *Nonlinear Oscillations, Dynamical Systems and Bifurcations of Vector Fields.* Springer-Verlag, 1983.

[31] P. Hartman. *Ordinary Differential Equations.* Wiley, 1964.

[32] C.B. Haselgrove. The Solution of Non-Linear Equations and of Differential Equations with Two-Point Boundary Conditions. *The Computer Journal,* 4:255-259, 1961.

[33] J. Hecht. *City of Light.* Oxford University Press, 1999.

[34] R. Hirota. *The direct method in soliton theory.* Cambridge University Press, 2004.

[35] R. Hirota and J. Satsuma. A variety of nonlinear network equations generated from the bcklund transformation for the toda lattice. *Progress of Theoretical Physics Supplement,* 59:64-100, 1976.

[36] E. Hopf. Sabzweigung einer periodischen lösung von einer stationâren lösung eines differenetialsystems. *Ber. Verh. Sachs. Akad. Wiss.,* 95:3-22, 1942.

[37] E. Hopf. A mathematical example displaying the features of turbulence. *Comm. Pure Appl. Math.,* 1:303-322, 1948.

[38] J.D. Kafka and T. Baer. Fiber raman soliton laser pumped by a nd:yag laser. *Opt. Lett.,* 12:181-183, 1987.

[39] J.D. Kafka and T. Baer. Prism-pair dispersive delay lines in optical pulse compression. *Opt. Lett.,* 12:401-403, 1987.

[40] J.D. Kafka, T. Baer, and D.W. Hall. Mode-locked erbium-doped fiber laser with soliton pulse shaping. *Opt. Lett.,* 14:1269-1271, 1989.

[41] H.B. Keller. Numerical solution of bifurcation and nonlinear eigenvalue problems. In *Applications of bifurcation theory (Proc. Advanced Sem,., Univ. Wisconsin, Madison, Wis., 1976),* pages 359-384. Publ. Math. Res. Center, No. 38. Academic Press, New York, 1977.

[42] A. Kelley. The stable, center-stable, center, center-unstable and unstable manifolds. *J. Diff. Equ.,* 3:546-570, 1937.

[43] J.K. Kjems and M. Steiner. Evidence for soliton modes in the one-dimensional ferromagnet CsNiF3. *Phys. Rev. Lett.,* 41:1137-1140, Oct 1978.

[44] R.W. Klopfenstein. Zeros of nonlinear functions. *J. ACM,* 8:366-373, 1961.

[45] E. Knobloch and J.D. Gibbon. Coupled NLS equations for counter-propagating waves in systems with reflection symmetry. *Physics Letters A,* 154:353-356, 1991.

[46] R.L. Kraft. Chaos, cantor sets, and hyperbolicity for the logistic maps. *The American Mathematical Monthly,* 106(5):400-408, 1999.

[47] M. Kubicek. Dependence of solution on nonlinear systems on a parameter. *ACM Trans. of Math. Software,* 2:98-107, 1976.

[48] G.L. Lamb. Bäcklund transformation in nonlinear pulse propagation. *Physics Letters A,* 48:73-74, May 1974.

[49] G.L. Lamb. Bäcklund transformations for certain nonlinear evolution equations. *Journal of Mathematical Physics,* 15:2157-2165, 1974.

[50] L.D. Landau. On the problem of turbulence. *Doklady Akad. Nauk SSSR,* 44:339-342, 1948.

[51] O.E. Lanford. A copmuter-assisted proof of the feigenbaum conjectures. *Bull. Amer. Math. Soc.,* 6(3):427-434, 1982.

[52] P.D. Lax. Integrals of nonlinear equations of evolution and solitary waves. *Comm. Pure Appl. Math.,* 21:467-490, 1968.

[53] E.N. Lorenz. Deterministic nonperiodic flow. *J. Atmos. Sci.,* 20:130-141, 1963.

[54] J.E. Marsden and M. McCracken. *The Hopf Bifurcation and its Applications.* Springer-Verlag, 1976.

[55] F.M. Mitschke and L.F. Mollenauer. Discovery of the soliton self-frequency shift. *Opt. Lett.,* 11:659-661, 1986.

[56] T. Miya, Y. Terunuma, T. Hosaka, and T. Miyashita. Single-mode optical fiber cable. *Applied Optics,* 18:2232-2236, 1979.

[57] T. Miya, Y. Terunuma, T. Hosaka, and T. Miyashita. Ultimate low-loss single-mode fibre at 1.55 um. *Electron. Lett.,* 15:106-108, 1979.

[58] L.F. Mollenauer, R.H. Stolen, and J.P. Gordon. Experimental observation of picosecond pulse narrowing and solitons in optical fibers. *Phys. Rev. Lett.,* 45:1095-1098, 1980.

[59] L.F. Mollenauer, R.H. Stolen, and M.N. Islam. Experimental demonstration of soliton propagation in long fibers: loss compensated by raman gain. *Opt. Lett.,* 10:229-231, 1985.

[60] A.C. Newell. *Solitons in Mathematics and Physics.* Society for Industrial and Applied Mathematics, 1985.

[61] J.M. Ortega and W.C. Rheinboldt. *Iterative Solution of Nonlinear Equations in Several Variables.* Society for Industrial and Applied Mathematics, 1970.

[62] M.M Peixoto. On structural stability. *Annals of Mathematics,* 69:199-222, 1959.

[63] M.M Peixoto. Structural stability on two dimensional manifolds. *Topology,* 1:101-120, 1962.

[64] Y. Pomeau and P. Manneville. Intermittent transition to turbulence in dissipative dynamical systems. *Commun. Math. Phys.,* 74:189-197, 1980.

[65] M. Remoissenet. *Waves called solitons. Concepts and experiments.* Springer-Verlag, 1996.

[66] W.C. Rheinboldt. Solution fields of nonlinear equations and continuation methods. *SIAM Journal on Numerical Analysis,* 17:221-237, 1980.

[67] W. Robinson. *The attractor chart for the paramertically driven, damped nonlinear Schrödinger equation.* University of Cape Town, 2003.

[68] C. Rogers and W.K. Schief. *Bäcklund and Darboux transformations: geometry and modern applications in soliton theory.* Cambridge University Press, 2002.

[69] D. Ruelle. *Elements of Differentiable Dynamics and Bifurcation Theory.* Academic Press, 1989.

[70] D. Ruelle and F. Takens. On the nature of turbulence. *Commun. Math. Phys.,* 20(3):167-192, 1971.

[71] J.S. Russel. *Report on Waves, made to the meetings of the British Association in 1842-1843.* Richard and John E Taylor, 1845.

[72] R. Seydel. A continuation algorithm with step control. In *Numerical methods for bifurcation problems. Proceedings of a conference in Dortmund, 1983,* pages 480-494. Birkhauser Basel, 1984.

[73] R. Seydel. *Practical Bifurcation and Stability Analysis. From Equilibrium to Chaos.* Springer-Verlag, 1994.

[74] D.F. Shanno. Conditioning of quasi-newton methods for function minimization. *Mathematics of Computation,* 24:647-656, July 1970.

[75] C. Sulem and P-L. Sulem. *The Nonlinear Schrodinger Equation: Self-Focusing and Wave Collapse.* Springer-Verlag, 1999.

[76] R. Thom. *Stabilité Structurelle et Morphogénese.* Benjamin, 1972.

[77] A. Vanderbauwhede. Centre manifolds, normal forms and elementary bifurcations. In *Dynamics Reported 2.* Teuber, 1989.

[78] H. Whitney, J. Eells, and D. Toledo. *Hassler Whitney: Collected Papers.* Nelson Thornes, 1992.

[79] V.E. Zakharov. Stability of periodic waves of finite amplitude on the surface of a deep fluid. *Journal of Applied Mechanics and Technical Physics,* 9:190-194, 1968.

[80] V.E. Zakharov, V.S. L'Vov, and G. Falkovich. *Kolmogorov spectra of turbulence 1. Wave turbulence.* Springer-Verlag, 1992.

[81] V.E. Zakharov and A.B. Shabat. Exact theory of two-dimensional self-focusing and one-dimensional self-modulation of waves in nonlinear media. *Sov. Phys. JETP,* 34:62-69, 1972.

[82] V.E. Zakharov and A.B. Shabat. Interactions between solitons in a stable medium. *Soy. Phys. JETP,* 37:823-828, 1973.

[83] E.V. Zemlyanaya and I.V. Barashenkov. Traveling solitons in the damped-driven nonlinear Schrödinger equation. *SIAM Journal on Applied Mathematics,* 64:800-818, 2004.